Investigation of a Novel Application of Optically Stimulated Luminescence (OSL) for Sediment Fingerprinting

by

Taryn Hicks

A thesis submitted to the Graduate Faculty of
Auburn University
in partial fulfillment of the
requirements for the Degree of
Master of Science

Auburn, Alabama
May 8, 2023

[Provenance, Sediment Fingerprinting, OSL, Heavy Mineral Analysis, Buffalo National River]

Approved by

Dr. Stephanie Shepherd, Associate Professor, Auburn University
Dr. Ashraf Uddin, Robert B. Cook Professor, Auburn University
Dr. Kathleen Rodrigues, Assistant Research Professor, Desert Research Institute

Abstract

Optically Stimulated Luminescence (OSL) is a tool that is commonly used to measure the length of time a quartz or feldspar grain has been buried in a sediment deposit. Recently there have been advances in using OSL as a sediment fingerprinting tool. In order to test this novel application of OSL, quartz grains from three major sandstone units along the Buffalo National River (BNR) in Northwestern Arkansas have been analyzed. OSL sensitivity and linearly modulated (LM-OSL) measurements of quartz grains from the sandstones were also investigated to determine if there are noticeable OSL characteristic differences between the major sandstone units. This novel application of OSL was paired with heavy mineral analyses of the sandstones to quantify potential differences between the units. This study finds that there are noticeable differences in the OSL signals and heavy minerals, which provides a promising outlook on the applicability of OSL investigations for sediment fingerprinting and provenance. By utilizing multiple tools and analyses, the utility of OSL as a sediment fingerprinting tool has been further quantified.

Acknowledgments

I would first like to thank Dr. Stephanie Shepherd for providing an opportunity to continue my education in geosciences and constant support throughout my time as a graduate student. Her constant mentorship has provided an avenue to further refine my research skills that I will be able to take with me as I move forward with my geologic career. I would also like to thank the other members of my committee, Dr. Ashraf Uddin, and Dr. Kathleen Rodrigues. I would like to thank both people for taking time to teach me new methods and provide valuable insight for my project. A special extra thanks is for Kathleen for housing me and providing integral support for my research. I am very thankful to have been able to visit Reno and learn more about OSL! I would also like to acknowledge the immeasurable support of my fellow graduate students and friends. I would especially like to thank Ryan Brooks for assisting in my sample collection and for providing opportunities to assist in field work in our beautiful research area. Special thanks also go to the Geosciences Graduate Advisory Board for their financial contributions to my project. Finally, I would like to thank my parents and my siblings for providing never ending support and encouragement throughout my life and educational pursuits.

Table of Contents

List of Tables

List of Figures

List of Abbreviations

BNR	Buffalo National River
QFL	Quartz, feldspar, and lithic classification
OE	Ordovician Everton sandstones
MBv	Mississippian Batesville sandstones
PB	Pennsylvanian middle Bloyd sandstones
OSL	Optically Stimulated Luminescence
TL	Thermoluminescence
HM	Heavy Mineral
CW- OSL	Continuous Wave Optically Stimulated Luminescence
LM-OSL	Linearly Modulated Optically Stimulated Luminescence
Phi	Φ
TBE	Tetrabromoethane
LST	Lithium heteropolytungstate
RZi	Rutile-Zircon Index
AZi	Apatite-Zircon Index
MZi	Monazite-Zircon Index
ATi	Apatite-Tourmaline Index
Crzi	Chromium-Zircon Index
ZTR	Zircon-Rutile-Tourmaline Index
SEM	Scanning Electron Microscope
DRILL	Desert Research Institute Luminescence Laboratory
QFL	Quartz, feldspar, and Lithic classification

IR	Infrared Light
LED	Light Emitting Diode
^{o} C	Degrees Celsius
Sr	Strontium
ppl	Plane-Polarized Light
xpl	Cross-Polarized Light
Zr	Zircon
Op	Opaque mineral
R	Rutile
Tm	Tourmaline
Alt	Altered Mineral
Msc	Muscovite
Clr	Chlorite

Chapter 1: Introduction

1.1 Introduction

Provenance studies have gained a large amount of interest as they help geoscientists interpret how landscapes develop through time. Specifically, researchers have been exploring novel tools and methods to better understand source-to-sink pathways. Provenance studies are used in many disciplines of geosciences, including sedimentology, geomorphology, petrology, geochemistry, and tectonics (Caracciolo, 2020; Haughton et al., 1991). While there are theoretical and modeling approaches developed to investigate sediment provenance, there are few robust analytical tools utilized for determining sediment provenance (Caracciolo, 2020). Some of the quantitative methods that have been utilized include heavy mineral, geochemical analyses, and geochronological investigations. One of the most common geochronological metrics is Uranium/ Lead dating (U/Pb) dating of zircons (Haughton et al., 1991). Often, the most robust approach for investigating sediment provenance involves using a combination of techniques. A promising novel provenance tool utilizes optically stimulated luminescence (OSL), a common method used to determine the burial age of a sedimentary deposit (Gray et al., 2019).

Provenance studies can provide vital information on a variety of spatial scales. In smaller watersheds, provenance studies can provide information on how the sediment accumulated from the surrounding sources, while on larger scales, it can show greater patterns of sediment movement and transportation history. These transportation routes result in the landscapes that are present today and provide information about past environmental conditions. Fluvial environments provide a valuable location to investigate landscape development. Sediment erosion and deposition are primary controls on channel formation, so gaining more insight to

how rivers interact with the surrounding geology can provide further insight to processes that result in the landscapes of today.

The Buffalo National River (BNR) incised through layers of Ordovician, Mississippian, and Pennsylvanian sedimentary layers of the Ozark Plateaus Physiographic Province (Keen-Zebert et al., 2017). The BNR has been incising for at least two-million years (Rodrigues, personal communication, April 13, 2023). has created a series of strath terraces. An extensive amount of recent work has focused on understanding the terrace preservation and valley form of the BNR (Keen-Zebert et al., 2017; Heidner, 2019, Braun, 2021; Rodrigues et al. In Review). Because they document fluvial deposition over broad timescales, these terraces also create an ideal natural laboratory to study the efficacy of quartz OSL signatures as a tool for understanding sediment routing throughout the watershed.

1.2 Geologic Background of the Study Area

The BNR is an incising bedrock river located in northwestern Arkansas (Figure 1.1). As the river incises through sedimentary lithology, sediments of various sizes, predominately gravel, are introduced to the channel (Keen-Zebert et al., 2017). Sediment is deposited on the active flood plain and in gravel bars along the river. When downcutting is greater than lateral erosion, these deposits may be preserved as strath terraces, which collect sediment eroded from the rocks within the watershed (Bull, 1990).

The BNR flows throughout the southern region of the Ozark Plateaus Physiographic Province in northwestern Arkansas. This area is located in the midcontinent where Late Pre-Cambrian rifting created Laurentia and Gondwana (Poole et al., 2005; Xie et al., 2016; Xie et al., 2018; Simbo et al., 2019). This rifting allowed for the creation of a passive continental margin to the southeast of Laurentia (Xie et al., 2016; Xie et al., 2018; Simbo et al., 2019). In the middle

Pennsylvanian, the Ouachita Trough closed and formed a fold-thrust belt of the Ouachita Orogeny to the southeast of Laurentia (Xie et al., 2016; Xie et al., 2018; Simbo et al., 2019). This orogeny formed the Ozark Dome and the Arkoma Basin (Poole et al., 2005; Xie et al., 2016; Xie et al., 2018; Simbo et al.,2019).

The Ozark dome is subdivided into three plateaus: the Boston Mountains, the Springfield Plateau, and the Salem Plateau (McFarlin, 2016; Figure 1). The Ozark Dome also encompasses the St. Francois mountains, an uplift that exposes Precambrian granite and rhyolite (Kincade, 2016). The plateaus decrease in age moving away from the St. Francois mountains (McFarlin, 2016; Hudson, 2000). The stratigraphic ages of these plateaus range from Ordovician to Pennsylvanian (Figure 1.2).

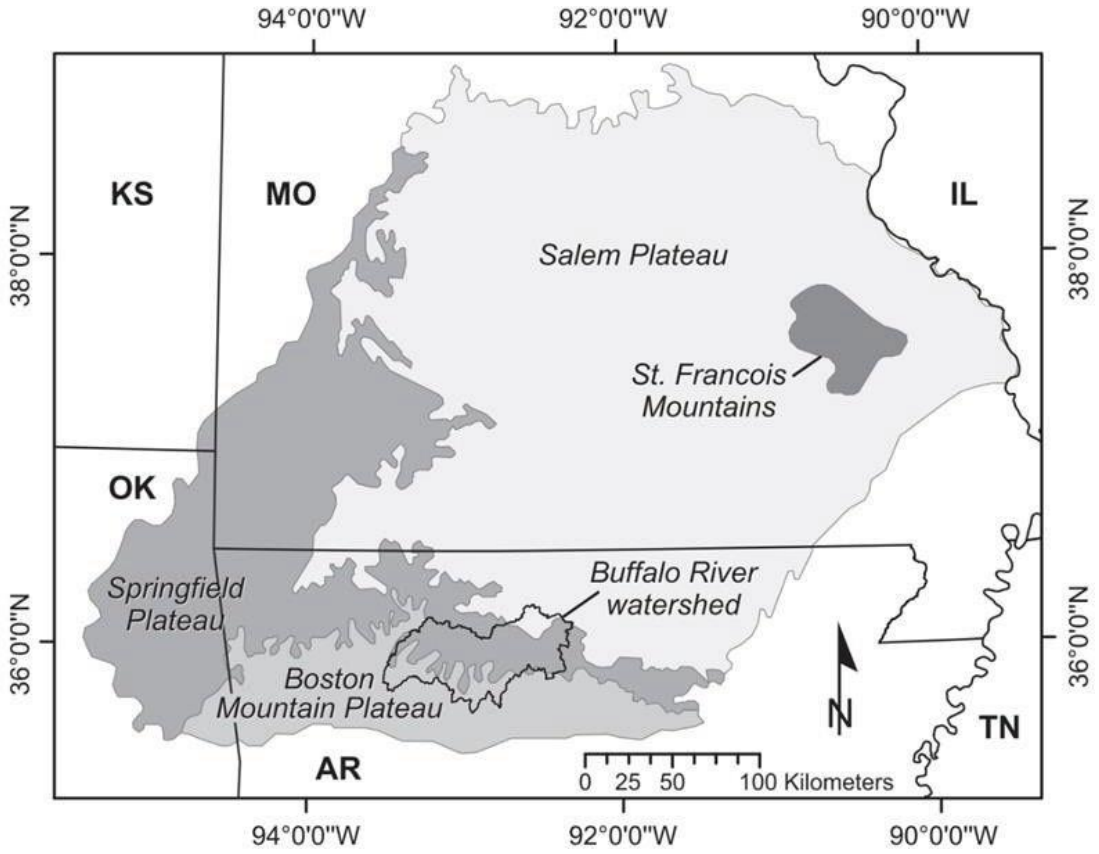

Figure 1.1: BNR watershed and its relationship to the plateaus of the Ozarks Plateau Physiographic Province (from Keen-Zebert et al., 2017).

In addition to the formation of the Ozark Dome, tectonic activity linked to the Ouachita orogeny is present. This adds to the intrigue of the sedimentary record in this watershed. Specifically, there is uplift that has deformed Mississippian rocks and creates an unusual setting for sediment transportation, creating some confusion about the orientation of the sediment movement (Hudson, 2000; Keen-Zebert et al., 2017; Caracciolo, 2020). Hudson (2000) discusses the orientation of two fault sets that have different strike directions, one striking east and the other striking northeast. These fault sets also present evidence of different tectonic mechanics. The east striking faults are overall normal faults while the other set is composed of strike-slip faults. Hudson estimates that the tectonic activity created deformation began after the Middle Mississippian (Hudson, 2000).

1.3 Lithology of the Buffalo National River

The river corridor exposes rocks of Ordovician, Mississippian, and Pennsylvanian ages. The predominate rock types include limestones, dolostones, sandstones, siltstones, and shales (Keen-Zebert et al., 2017; Figure 1.2). The majority of the lithology of the BNR falls within the stratigraphy of the Springfield Plateau. There are several unconformities present throughout the stratigraphic record (Bello, 2017).

Within the Springfield Plateau Ordovician aged rocks include the dolomites, sandstones, limestones, and shale (McFarland, 1998). The Powell Dolomite is one of the oldest units present in the watershed, and it is overlain by the Everton Formation. The Everton Formation is composed of sandstone, dolostone, and limestones. The sandstone units of the Everton include the Newton, Kings River, and Calico Rock sandstones (McFarland, 1998). The St. Peter Sandstone overlies the Everton Formation. The sandstones from these formations are

compositionally and texturally similar (Giles, 1932). The remainder of the Ordovician period is dominated by the Plattin and Fernvale limestones (McFarland, 1998; Keen-Zebert, 2017).

The stratigraphy around the BNR does not include a large amount of Silurian or Devonian units (Turner and Hudson, 2010; Hudson and Turner, 2014; Keen-Zebert et al., 2017). In the West-Central Geologic map, there is an unconformity bounded sequence of Silurian-age rocks. These rocks are described as the Lafferty Limestone, St. Clair Limestone, and Brassfield Limestone (Turner and Hudson, 2010; Hudson and Turner, 2014).

The predominant Mississippian units include limestone, sandstone, and shale (McFarland, 1998). The Chattanooga Shale Formation occurs from the late Devonian to the early Mississippian and is overlain by an unconformity. Following the Chattanooga Shale are the St. Joe and Boone Formations. McFarland (1998) describes that the upper Boone Formation contact is unconformable. The main lithologies in these units is limestone (McFarland, 1998; Bello, 2017). Following these units is the Batesville Sandstone. After the Batesville Sandstone unit is the Fayetteville Shale Formation. This formation is broken up into upper and lower units by the Wedington Sandstone (McFarland, 1998; Bello, 2017). The final unit of the Mississippian period is the Pitkin Limestone (McFarland, 1998; Bello, 2017).

The major Pennsylvanian units include the Hale Formation and Bloyd Formation (McFarland,1998). The majority of these units are composed of sandstone. The youngest of the Pennsylvanian units, the Hale Formation, overlies an unconformity. This formation is composed of the Prairie Grove and Cane Hill units. The Bloyd Formation also includes sandstones,shales and limestones (Bello, 2017). Though not shown in figure 1.2, the Atoka formation overlies the Bloyd formation (McFarland, 1998; Bello, 2017).

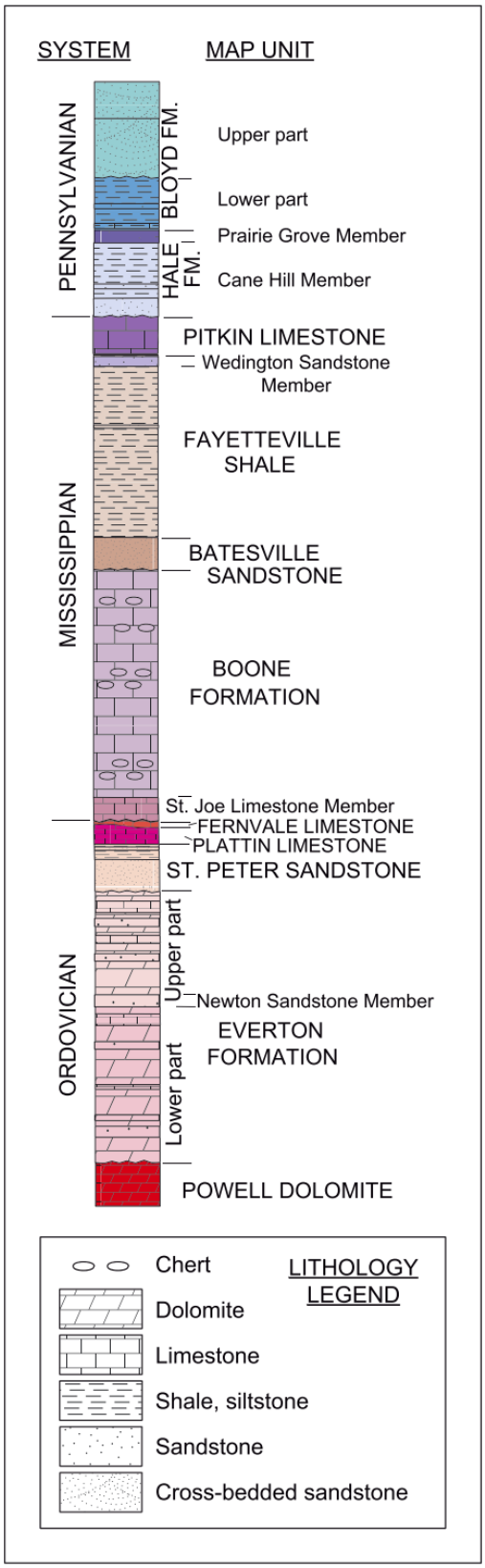

Figure 1.2: Lithostratigraphy of common Paleozoic rocks present in the BNR watershed (Modified from Keen- Zebert et al., 2017).

Some of the sandstone units of the BNR have been petrographically analyzed in previous research. These include, the Middle Bloyd, Everton, St. Peter, Wedington, and Batesville sandstones, as well as sandstone members of the Atoka and Hale formations (Bello, 2016; Figure 1.3). These units have been classified through the quartz, feldspar, and lithic fragment (QFL) ternary diagram. The St. Peter and Everton sandstones are predominately classified as quartzarenite. The Middle Bloyd often ranges from sublitharenite to quartzarenite and will occasionally fall into the subarkose range (Bello, 2016; Xie et al., 2018). The Hale Formation plots similarly to Bloyd sandstones. The Wedington plots as quartzarenite and sublitharenite. The Batesville Sandstone has been plotted as quartzarenites, subarkose, and sublitharenite, The Atoka Formation has the most varied petrographic analysis as it plots in quartzarenite, sublitharenite, subarkose, and litharenite.

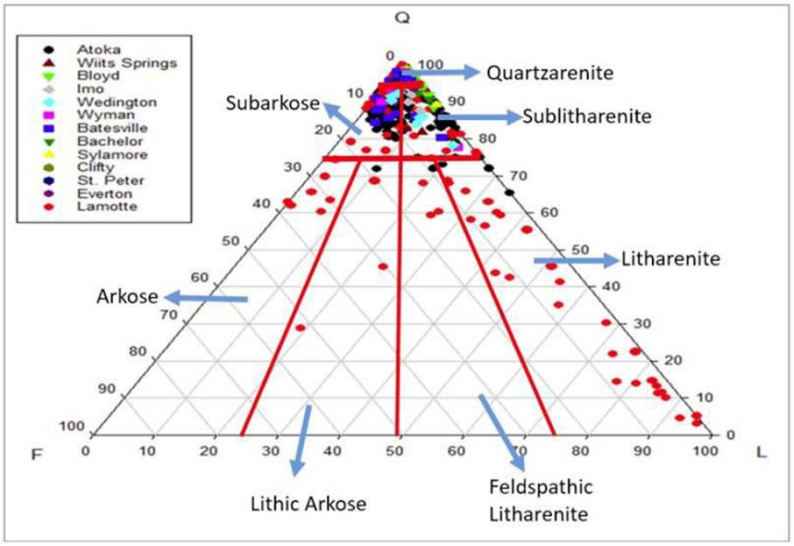

Figure 1.3: Petrographic Analysis of an assortment of sandstones present in northwestern Arkansas (from Bello, 2016).

Of the units present in the BNR, three sandstones were chosen to analyze within the scope of this project. One extensive sandstone unit from each of the major time periods was chosen for analysis. The Everton Formation sandstones (OE) were chosen as the Ordovician

sandstones. The Batesville (MBv) sandstone and the middle Bloyd (PB) sandstone were chosen as the representative Mississippian and Pennsylvanian sandstones respectively.

1.4 Optically Stimulated Luminescence

Luminesce is a phenomenon that occurs when grains in sediment deposits are exposed to environmental radiation, retain energy produced from radioactivity in their crystal lattice, and eventually release a light signal proportional to the dose of radiation exposure (Duller, 2008; Pradhan et al., 2008; Rhodes, 2011). During transport cycles, sedimentary grains are exposed to environmental radiation when buried. The exposure to environmental radiation excites electrons that then become stored in imperfections, or traps, within the crystal lattice (Duller, 2008; Pradhan et al., 2008; Rhodes, 2011; Wintle and Adamiec, 2017; Gray, 2019; Figure 1.4). The excitation of an electron leaves a net positive hole in the crystal lattice. The electrons are released from the traps when the grain is exposed to sunlight or temperatures ranging from 200 ^{o}C-400 ^{o}C (Wintle and Adamiec, 2017). After this exposure, the electron can be removed from its trap. After its release, the electron begins to move throughout the lattice until it reaches a hole that will act as a recombination center. When this occurs, a photon may be emitted creating a luminescence signal (Wintle and Adamiec, 2017; Rhodes, 2011; Gray et al., 2019; Figure 1.5). The release of light, luminescence, is used to gauge the length of time that the grain has been exposed to radiation. There are several methods that investigate this phenomenon, including optically stimulated luminescence (OSL) and thermoluminescence (TL) (Gray et al., 2019; Duller, 2008). TL refers to luminescence that is produced under exposure to heat (Gray et al., 2019). OSL is a technique that usually involves investigating the light emitted after these grains are exposed to a source of light (Duller, 2008; Gray et al., 2019). This technique works to date depositional ages up to 200,000 years (Jain et al., 2004; Rhodes, 2011).

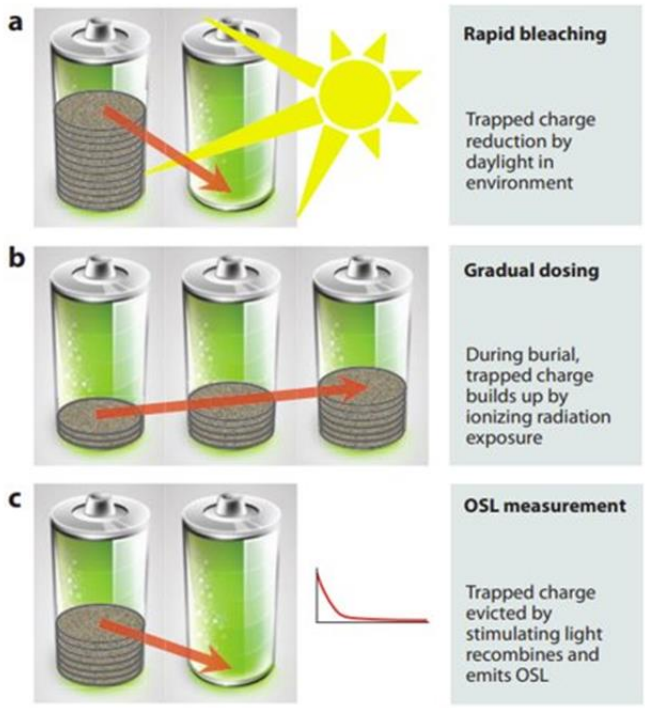

Figure 1.4: This image depicts the battery analogy for OSL measurement for a sedimentary grain (From Rhodes, 2011)

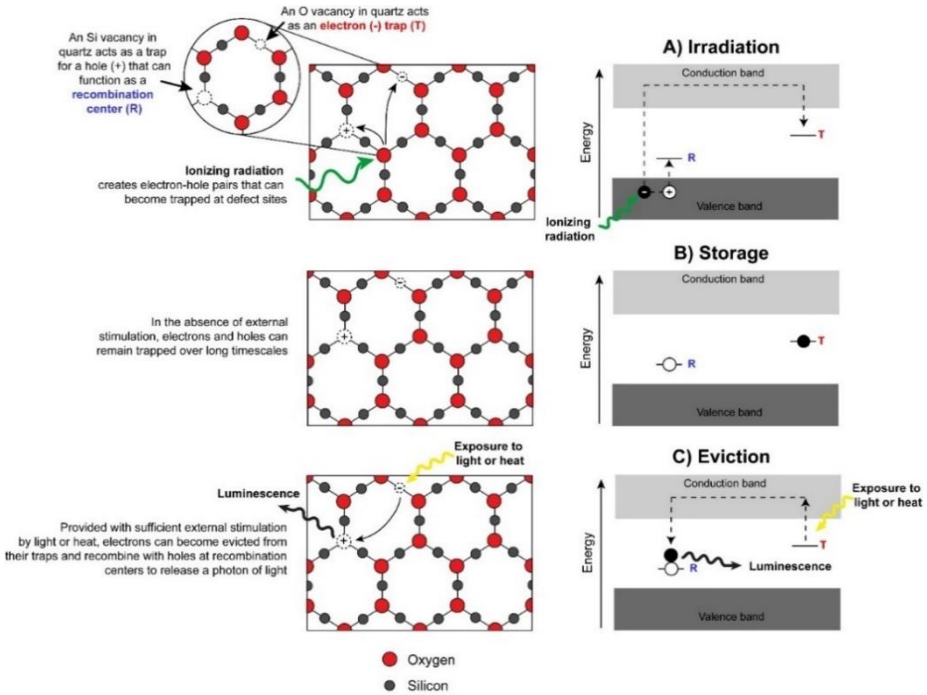

Figure 1.4: The model on the left shows a schematic of traps can store electrons within a quartz crystal lattice. The right panel depicts an energy band gap model. This schematic shows how the electron travels throughout different levels of excitement and losing energy throughout a depositional cycle (from Rodrigues, K., personal communication, April 13, 2023)

There are many methods to stimulate OSL signals of detrital grains. A common method is continuous-wave OSL (CW-OSL). In this type of analysis, there is a continuous and constant intensity of stimulation of the sample. This constant stimulation is applied to a sample that has already stored a dose of radiation (Bulur et al., 2002; Pradhan et al., 2008; Gray et al., 2019). The stimulation causes a luminescence signal to be released from the sample (Pradhan et al., 2008). Another method to analyze OSL includes linearly modulated OSL (LM-OSL). In this method, the intensity of the stimulation applied to the sample increases gradually over time (Bulur et al., 2002; Jain et al., 2003; Pradhan et al., 2008; Gray et al., 2019). Figure 1.6 shows a schematic of the difference between these two approaches for measuring OSL.

CW-OSL is often used to collect data to test the OSL sensitivity of a sample. OSL sensitivity (Counts sec^{-1} Gy^{-1} mg^{-1}) is the luminescence signal that occurs in a quartz grain in response to a dose of radiation (Rhodes, 2011; Capaldi et al., 2022). LM-OSL is utilized to determine the components that make up the traps that allow the storage of radiation. Components are largely defined by their detrapping probability (s^{-1}) which describes how the charge is released from the crystal lattice (Wintle and Adamiec, 2017; Gray et al., 2019). Investigations using CW-OSL have identified of up to four components, and LM-OSL have shown up to five components (Jain et al., 2003).

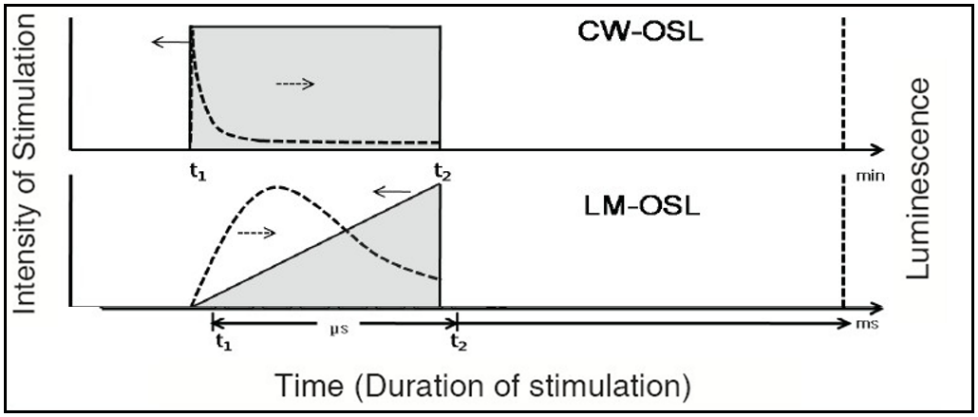

Figure 1.6: Schematic showing the intensity and time differences between CW-OSL and LM-OSL (modified from Pradhan et al., 2008)

1.5 Objectives

The main objective of this research is to investigate the utility of OSL as a sediment fingerprinting tool in the BNR. We believe that the novel application of OSL can be used to gain insight to provenance of the sediment in the terraces along the river. Previous research has revealed that there are varied OSL signatures from quartz grains in strath terraces along the river channel. This variation is believed to be linked to differences in quartz sources in the watershed. This novel application has the potential to model the transportation history of sediment in the BNR and identify the provenance of these sediments within different rock units.

This observation has been further explored by comparing the luminescence signatures from quartz grains from the lithology of the BNR. To further categorize differences between the quartz bearing lithologic units that may be linked to the varied OSL signatures, heavy mineral analysis has been completed on the sandstone source rocks. In addition, the OSL signatures were compared to those of quartz grains from a strath terrace as a preliminary investigation of this novel approach in the BNR. This is to gain further insight into the varied quartz signatures that have been found, and to investigate if the detrital quartz can be linked to a source rock in the stratigraphy of the BNR.

Chapter 2: Sediment Fingerprinting and Provenance Background

2.1 Introduction

Provenance and sediment fingerprinting studies are utilized to gain a better understanding of the travel histories of grains in sedimentary rocks and deposits. It is expected that the depositional histories of the sandstones likely affect the properties of the sand grains within the rock unit. If the quartz grains form the major sandstone units have different luminescence characteristics, then it is possible to gain insight into how each unit contributes to sediment production as well as what is preserved within the terrace units. Luminescence characteristics can be studied in tandem to more established fingerprinting tools to explore provenance. Some common methods for sediment fingerprinting and investigating provenance that have been completed in the BNR include U-Pb dating on detrital zircon grains from sandstone units, heavy mineral analysis, and mineralogical investigations.

2.2 Previous Provenance Studies in Northwestern Arkansas

There is limited research dedicated to provenance in the BNR and the surrounding Ozark Plateaus. The majority of this work utilizes U-Pb dating of detrital zircon grains. The units that have previously undergone U-Pb dating include the Atoka, Bloyd, Wedington, Cane Hill, and Batesville sandstones (Figure 2.1; Thomas et al., 2021). The studies of detrital zircons from the Bloyd sandstones found that there are major peaks at Grenville age (~ 900-1350 Ma) (Xie et al., 2018). While the studies focused on the Wedington sandstone reported having two dominant peaks from the Grenville (~900-1350 Ma) and the Yavapai-Mazatzal terrane (~1600-1800 Ma) (Xie et al., 2016). Both the Wedington sandstone and the Bloyd sandstone are projected to have some influence from Appalachian sources. The Batesville sandstone detrital zircons range between ~339-488 Ma with a secondary abundance with Grenville ages. The zircon age range for

the Cane Hill member has a dominant age group from the Grenville Province (935-1265 Ma) with other prominent age groups ranging from Taconic and Acadian ages (380-487 Ma) and Granite and Rhyolite Province (1295-1935 Ma) (Xie et al., 2018; Thomas et al., 2021). The Batesville Sandstone is reported to have detrital zircon ages predominately within the range of Appalachian age (339-488 Ma). The Batesville sandstone zircons also record Grenville ages (942-1210 Ma) (Thomas et al., 2021). U-Pb age dates of Atokan Sandstones have been investigated in Oklahoma. The Atokan sandstones studied are subdivided into two categories based on the dispersal direction (Sharrah, 2006; Thomas et al., 2021). A distinction is made due to the difference in the characterization of the sandstones (Sharrah, 2006). Atokan sandstones with a south and westward dispersal contain zircons with a prevalent group of Grenville age (934-1295 Ma) (Sharrah, 2006; Thomas et al, 2021). Atokan sandstones with a Northeastward dispersal have a dominant detrital zircon age range of 937-1195 Ma. These sandstones also have secondary age groups of 354- 492 Ma and 505-799 Ma (Sharrah, 2006; Thomas et al, 2021). Previous geochronology research indicates that the sandstones in the BNR have a majority of both Grenville and Appalachian age influence.

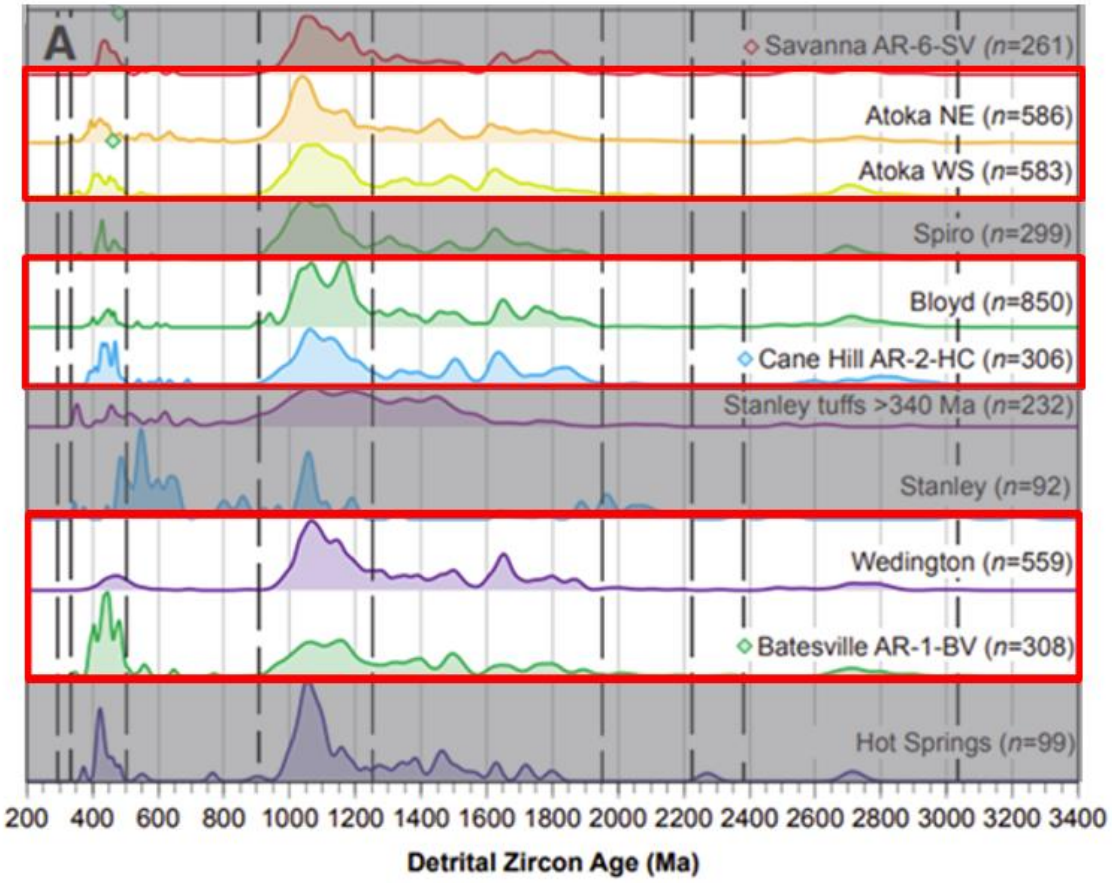

Figure 2.1: Ages of detrital zircons from sandstones present in the BNR (Modified from Thomas et al., 2019)

Other studies have investigated heavy mineral abundance in sandstones present in the BNR. Minimal Heavy Mineral (HM) analysis work has been completed for the Wyman, Wedington, and Batesville sandstones (Allen, 2010). This investigation discovered that the Wyman sandstone has a higher abundance of heavy minerals than the two other sandstones analyzed. Most of the found minerals are zircon and tourmaline (Allen, 2010). Another study that investigates heavy minerals in the Missouri Ozarks. The sandstones analyzed in this study are the Roubidoux, Lamotte, St. Peter, and unnamed Pennsylvanian and unknown sandstones. Of the sandstones studied, the heavy minerals found include zircon, tourmaline, and leucoxene (Cordry, 1929), This analysis concludes that these sandstones have similar assemblages of heavy

minerals. While this study is focused on Ozark Region sandstones, many of the sandstone units are not prevalent in the BNR. A lack of in-depth analysis of heavy mineral assemblages of prevalent sandstones of northwestern Arkansas and the BNR watershed is a critical gap in our knowledge about the lithologies of interest in this research.

2.3 Heavy Minerals as a Provenance Tool

HM analysis has been utilized as a provenance tool because the assemblage of heavy minerals provides insight to source areas and travel histories due to the variable stability of accessory minerals (Morton, 1991). Common heavy minerals include pyroxene, amphibole, spinel, amphibole, staurolite, garnet, tourmaline, apatite, zircon, and rutile (Morton, 1991). Of these, zircon, tourmaline, and rutile are often present due to their stability (Hubert, 1962; Monami et al., 2022). Even though heavy mineral analysis is often used, it is important to consider factors altering the detrital minerals. Sedimentation cycles of transport, deposition, and diagenesis can influence the abundance of heavy minerals in a sample (Hubert, 1962; Morton and Hallsworth, 1994; Morton and Hallsworth, 1999, Knox et al., 2007).

The mineral assemblages present in a sample can be used to investigate provenance in diverse ways. Mineral indexes of the heavy mineral assemblage are often used to compare percentages of minerals present in each sample (Knox et al., 2007; Monami et al, 2022). Some commonly used indices include the Rutile-Zircon Index (RZi) the Apatite-Zircon index (Azi), Monazite- zircon index (Mzi), and Apatite-Tourmaline index (Ati) (Morton and Hallsworth, 1994; Knox et al., 2007; Monami et al., 2022). The use of an electron microprobe of heavy mineral grains can be used to study the mineral chemistry of detrital grains to determine potential sources of the rocks (Monami et al., 2022).

In addition, heavy minerals like zircon can also be used for age dating. Detrital zircons ages are often investigated through U -Pb age dating (Xie et al., 2016; Xie et al., 2018; Joshi et al., 2021). The age of detrital grains, such as zircon, are also used to interpret different source terranes (Thomas et al., 2019). These applications of heavy mineral analysis are an integral to the study of provenance, because they provide additional information on the possible source terrains and context to the extent of travel or sedimentary processes of the mineral grains that form sandstones.

2.4 Luminescence as a Provenance Tool

Because quartz grains can display different OSL signals, there is a possibility for this unique property of quartz to be utilized to decipher provenance of sediment (Gray et al., 2019). Several studies specifically investigate the applicability of luminescence to determine the depositional history or source of quartz grains (Capaldi et al., 2022). These studies work to determine whether the number of depositional cycles or sediment source has a larger influence on the OSL sensitivity and predominate type of components of the quartz grains.

Luminescence properties have been utilized to investigate sediment source in a variety of settings, including fluvial, aeolian, and marine environments (Olley et al., 2004).

In recent years, there has been an increased interest in investigating the use of OSL as a provenance tool (Gray et al., 2019). This has been completed in environmental settings ranging from fluvial, marine, and aeolian sediment deposits. There is precedent of comparing OSL components from quartz grains found in both sediment deposits and from rock samples (Tsukamoto et al., 2011; Gray et al., 2019; Figure 2.2). This method for investigating provenance

is also often compared to more established methods such as heavy mineral analysis, composition, and grain size analysis (Zular et al., 2015; Tsukamoto et al., 2011). These studies have shown promise in utilizing OSL as a provenance tool. While previous research is available for using OSL as a sediment tracer tool in a fluvial system, the literature is not extensive (Gray et al., 2019; Bartyik et al., 2021). Investigating the utility of OSL as a novel sediment provenance tool would provide foundational work and be beneficial to the broader study of source to sink relationships.

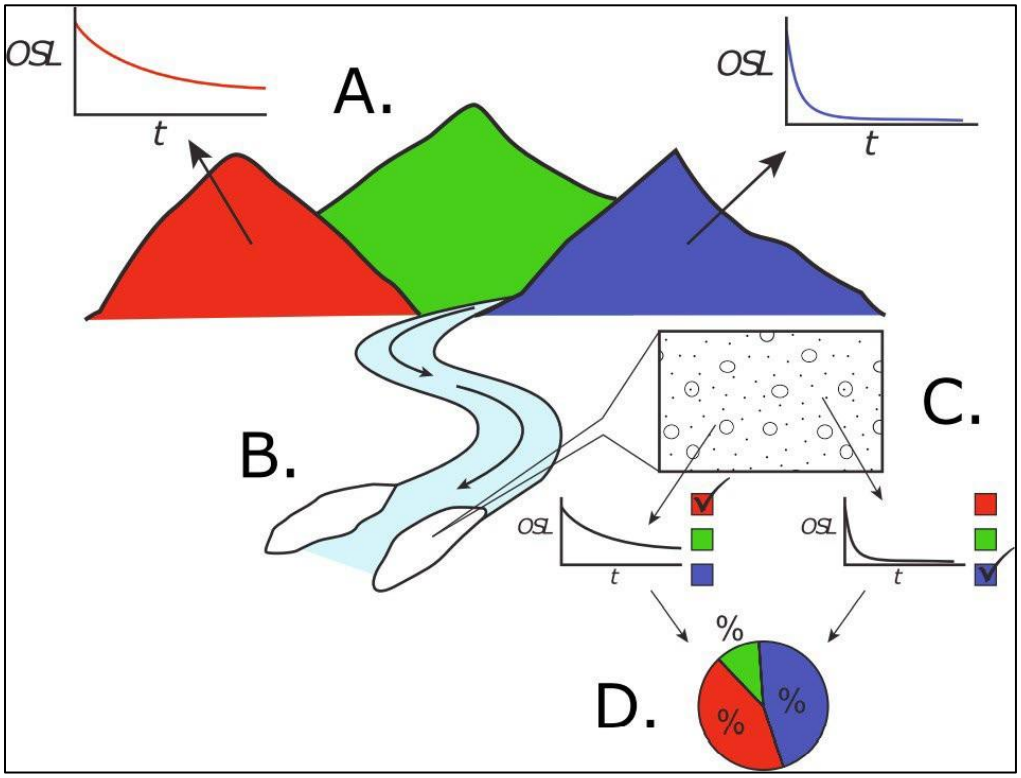

Figure 2.2: Schematic showing different source rock OSL signatures being found in a sediment deposit (Gray et al., 2019)

Chapter 3: Methods

3.1 Introduction and Sample Collection

To test the utility of OSL as a provenance tool, the luminescence signatures and sensitivity of quartz grains from major sandstones will be analyzed and compared to the heavy mineral assemblage within the sandstones. These analyses will be used to investigate differences between the sandstones that may provide clues into which strata are contributing quartz grains to the terrace deposits. The samples being collected and tested include the Pennsylvanian middle Bloyd sandstone (PB), the Mississippian Batesville Sandstone (MBv), and the Ordovician sandstones of the Everton Formation (OE) within the BNR watershed. These samples were chosen to include a sandstone unit from each of the major time periods. Three samples from each of these geologic units will be analyzed.

The sandstone samples were collected using geologic maps to determine where outcrops of the targeted rock units are located (Hudson and Murray, 2003; Hudson and Turner, 2006; Turner and Hudson, 2010; Hudson and Turner, 2014). Samples were taken from three different locations throughout the BNR watershed. The samples were mostly collected in the upper portion of the watershed in Harrison, Marshall, and Newton counties of Arkansas. Due to laws prohibiting removing natural materials from federal property, the samples were not taken within the park boundary.

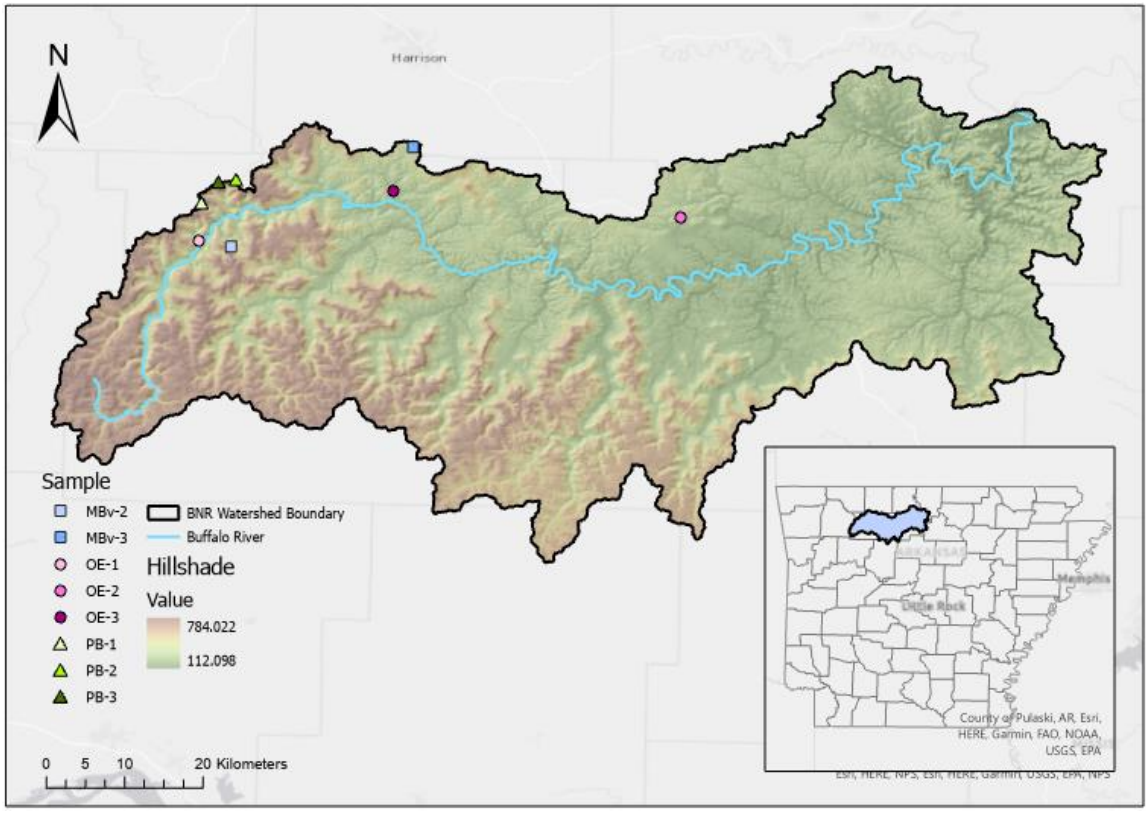

Figure 3.1: Sample locations of the sandstones used in this study. The inlet map shows the location of the watershed in the state of Arkansas. (Data used for the map from (Arkansas GIS Office, 2006; Arkansas GIS Office, 2020; National Weather Service, 2023; USDA, 2023).

From each collected sandstone sample, between 200-300 grams of sample was crushed with a rock hammer and then fully disaggregated using a mortar and pestle to isolate individual grains. The disaggregated sub-sample was sieved using mesh sizes of 250 µm, 125µm, 63µm. The target size fraction for both the heavy mineral separation and OSL analysis includes the 3 – 4 phi (Φ) (125-63µm) size fraction (Knox et al., 2007; Caracciolo et al., 2015; Liu et al., 2015, Uddin et al., 2016). The target sample weight in the 3-4 Φ fraction was 50 grams, but not all samples reached this goal., notably the final analysis for samples Mbv-1, OE-1, OE-2, and OE-3. These sample weights were between 8.826 g and 19.682 g. This is due to a lack of sample resulting from multiple trials of heavy mineral separations to account for potential errors. Additional trials were conducted for these with a gentler disaggregation of grains so that there

was a smaller contribution of grains that had been altered in the preparation process.

3.2 Heavy Mineral Separation

The nine disaggregated samples were weighed and added to a separation funnel with the heavy liquid tetrabromoethane (TBE, $C_2B_2Br_4$, density 2.96 g/cm^3). The sample remained immersed in the heavy liquid for 24 hours, which was enough time for complete separation, where the heavier minerals remain at the bottom of the funnel, while the lighter portion rises to the top of the TBE (Figure 3.2). The heavy mineral samples were then drained from the funnel into filter paper and washed with acetone. This step was repeated for the lighter minerals. After being washed with acetone, the heavy mineral and light mineral portion were placed in an oven to dry. When the samples were completely dry, the heavy mineral sample was weighed to determine the weight percentage of heavy minerals (Uddin et al., 2016; Monami et al., 2022).

The heavy mineral assemblage was analyzed using a petrographic microscope and smear slides (Uddin and Lundberg, 1998). Smear slides were prepared using Cargille type A non-drying immersion oil with a refractive index of 1.518 (R.I. = 1.518 $\pm$ 0.0002). A drop of this oil was added to a microscope slide. Following this step, heavy mineral grains were added to the slide. The samples were analysed under both plane-polarized light (ppl) and cross-polarized light (xpl). This method was used as a preliminary investigation of the heavy minerals present in each of the samples.

After determining the heavy mineral assemblage of the nine sandstones, the rutile-zircon index (RZi) and the zircon-rutile-tourmaline (ZTR) index were calculated. The opaque minerals and altered minerals were included in these calculations. The RZi was calculated using Equation 1, and the ZTR index was calculated using Equation 2 (Knox et al., 2007; Ayofe and Anthony, 2020; Appendix A).

$$\text{Rutile Index} = \frac{Rutile \times 100}{Rutile + Zircon} \qquad \text{Equation 1}$$

$$\text{ZTR Index} = \frac{(Zircon + Tourmaline + Rutile)}{Total\ number\ of\ grains\ on\ slide} \times 100 \qquad \text{Equation 2}$$

In addition, the heavy mineral assemblages of eight samples were analyzed using a Hitachi TM4000 Plus table top Scanning Electron Microscope (SEM) at the Desert Research Institute. Using Aztec 1 software, general elemental maps were created for a portion of the heavy minerals of each sample.

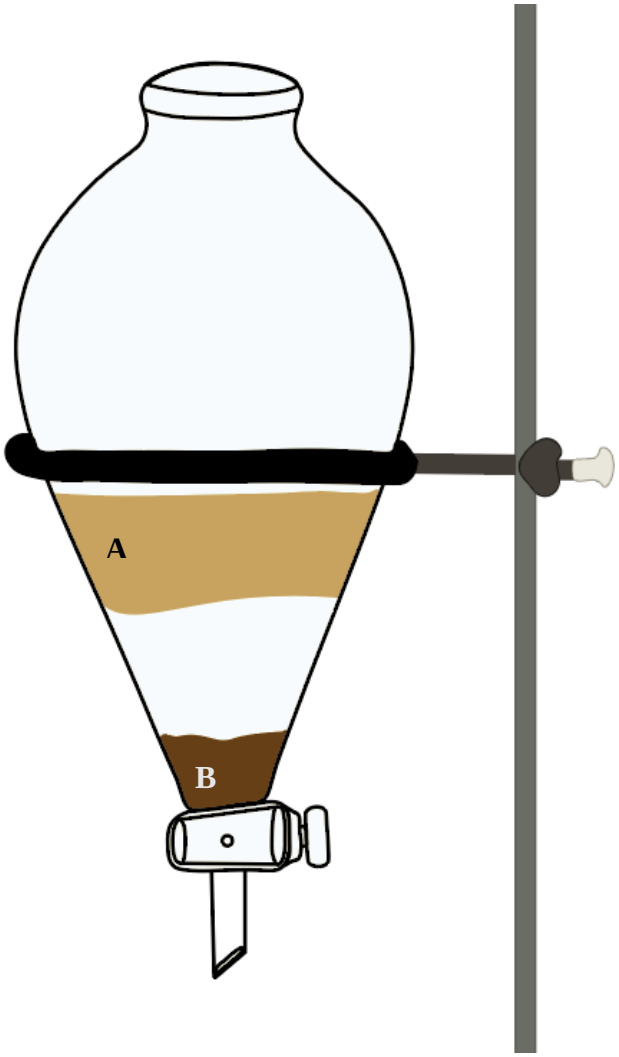

Figure 3.2: Schematic diagram of separation funnel. A) the lighter weight fraction floats above the separation liquid. B) The heavy minerals settle to the bottom of the separation funnel

3.3 Optically Stimulated Luminescence Methods

Two samples from each of the sandstone units were used for OSL analysis. Approximately 25 grams of the light fraction from the initial heavy mineral separation samples was sent to the Desert Research Institute Luminescence Lab (DRILL). After arriving to the DRILL, the samples were treated with a 10% HCl solution to remove carbonates from the sample and a 30% H_2O_2 to remove organic material (Aitken, 1998). In addition, the quartz grains were isolated by completing another density separation was carried out to further separate the 2.62-2.68 g/cm^3 grains using lithium heteropolytungstate (LST) (Rodrigues et al., 2016).

After the quartz grains were isolated, 6 mm diameter multi-grain aliquots were prepared by placing a fixed amount of silicon oil on 10 mm steel discs. The oil adheres the quartz grains to the discs. The weight of the quartz grains was recorded using a high precision scale in order to calculate a weight normalized luminescence sensitivity for each aliquot. Each Aliquot contained approximately 2648 grains with an assumed packing density of 0.65. After ten multi-grain aliquots were prepared for each of the six samples, the discs were added to the TL/OSL DA-20 Risø Reader at the DRILL (Figure 3.3).

The first analysis was completed using continuous wave OSL (CW-OSL). The experiment was set up so that each aliquot was 'bleached' using blue LED's (458 nm) for 500 s and subsequently heated to 450 °C at a rate of 5 °C/s to remove any residual luminescence signal. Bleaching the aliquots in this way removes any residual radiation dose that may have been trapped in the grains, effectively resetting the luminescence clock. To measure OSL sensitivity, the aliquots were then given a 40 Gy beta dose using a calibrated Strontium-90 (^{90}Sr) source integrated into the OSL reader. After irradiation, each aliquot was heated to 220^o C for 60 seconds in order to remove trapped charge from secondary and less stable traps. The aliquots

were then stimulated with 850 nm infrared (IR) LED's and simultaneously heated to 50 °C for 200 seconds, which removed any luminescence contribution from feldspar grains that may have not been removed during heavy liquid separation. The aliquots were stimulated with Blue LED's (458 nm) for 100 seconds at 125° C and subsequently heated to 450 °C to remove any residual signal. For thermally stimulated luminescence (TL) sensitivity measurements, all aliquots were exposed to a 40 Gy beta dose, stimulated with 850 nm IR LED's to remove any unwanted luminescence contribution from feldspars, and TL glow curves were measured by detecting photon counts while heating the aliquots to 450C at a rate of 5 °C/s. All TL glow curves were background-subtracted to determine a net TL signal used for sensitivity calculations. These steps are also presented in table 3.1. After the OSL and TL signals were collected, the intensities were normalized to the mass of the sample (Nian et al., 2019).

Step	Treatment
1	Sample is bleached (458 nm, 50° C for 500sec)
2	Sample heated to 450 C at 5° C/sec
3	Beta irradiation (40 Gy)
4	Stimulated with IR light (850 nm for 200 secs)
5	Sample preheat (220° C for 60 seconds)
6	OSL signal measured using blue LED's (458 nm) ay 125° C for
7	heat sample to 450° C
8	Beta Irradiation (40 Gy)
9	Stimulated with IR light (850 nm for 200 secs)
10	TL measurement to 450° C at 5C/s
11	Background TL measurement to 450° C at 5C/s

Table 3.1: outline of methods for measuring OSL and TL sensitivity.

An additional analysis using the OSL reader to determine the LM-OSL characteristics of the sandstone quartz. This analysis was completed to categorize what components are contributing to the Luminescence signal. Four of the ten multigrain aliquots used for the previous analysis were used in this analysis (Table 3.2). The experiment design follows that outlined in

Jain et al., 2003. The aliquots were first bleached using blue LED stimulation for 500 s and heated to 450C to remove any residual signal. A 60 Gy beta dose was administered to each of the aliquots and subsequently preheated to 220 C for 60 s to remove trapped charge from unstable traps. An LM-OSL signal was recorded for each aliquot by ramping Blue LED stimulation power from 0 to 47 $mWcm^{-2}$ over 3,500 s. This experimental design was also applied to 3 multigrain aliquots of sediment from a terrace deposit in the BNR as a preliminary comparison of relative component contributions of the detrital and source sediment in the BNR watershed.

The components of the LM-OSL curves were completed for four aliquots per sample. The data was processed using the Luminescence package and RStudio (Kreutzer et al., 2012; Kreutzer et al., 2022). The number of components was determined through an iterative process to determine the best fit of the model. This was completed by starting at 3 components and then increasing the number by one until the best fit of the model was found. Identification of the components of each sample was completed using the classification scheme of Jain et al., 2003.

Step	Treatment
1	Sample is bleached (458 nm, 50^{o} C for 500sec)
2	Sample heated to 450 C at 5^{o} C/sec
3	Beta irradiation (60 Gy)
4	Stimulated with IR light (850 nm for 200 secs)
6	Ramped stimulation blue LED intensity from 0-47 mW^{-1} over 3500 s at 125^{o} C/sec

Table 3.2: outline of methods for measuring LM-OSL

Figure 3.3: DA-20 Risø TL/OSL Reader at the E.L. Cord Luminescence Laboratory at Desert Research Institute (From Keen-Zebert, 2013)

Chapter 4: Heavy Mineral Results

4.1 Heavy Mineral Assemblage

There are noticeable differences between the HM weight percentages (Table 4.1). The PB sandstones have the highest percentages of heavy minerals. OE has an intermediate amount of heavy minerals, and the MBv sandstones have the least amount of heavy mineral weight percentage. In addition to differences of weight percentages, the HM assemblages of the different sandstone units also have significant differences (Figure 4.1). The most common phases present include zircon(Zr), rutile (R), tourmaline (Trm), opaques (Op), and altered minerals (Alt) (Appendix A).

The OE samples exhibit a high percentage of zircon grains, with additional secondary amounts of rutile and tourmaline. OE samples also have a slight presence of opaque minerals and altered phases (Figure 4.2). Muscovite (Msc) was identified in these samples by petrographic properties. Muscovite has a low relief compared to many other heavy minerals and has a visible crystal habit (Mange and Maurer, 2012). MBv sandstones contain mostly altered minerals (Figure 4.3). The altered phases often have a reddish tint to the grains or opaque inclusions. After altered phases, MBv samples contain a large amount of opaque minerals. These sandstones also have muscovite grains present. The PB samples have a majority of opaque minerals present and lesser amounts of translucent and easily identifiable heavy minerals (Figure 4.4). In addition, the PB samples have some chlorite (Chl) grains. Of the more common heavy minerals, these samples exhibited larger amounts of zircon with even smaller appearance of rutile and tourmaline.

SEM data of the initial trial of heavy minerals show a large amount of silicate minerals that have small amounts of Aluminum present in the MBv and OE samples. The SEM data show that the OE samples have a higher portion of zircon and titanium oxides than the MBv and PB

samples. The PB samples have a large amount of chromium oxides, magnesium oxides, and iron oxides compared to the other sandstone samples (Appendix A).

Sample	3-4 Φ Sample Weight	Heavy Mineral Weight	Heavy Mineral Weight Percent
Oe-1	8.8260	0.0092	0.1042
Oe-2	10.5605	0.0030	0.0284
Oe-3	19.6820	0.0099	0.0503
MBv-1	9.5780	0.0007	0.0073
MBv-2	49.6753	0.0145	0.0292
MBv-3	50.8920	0.0024	0.0047
PB-1	49.5522	0.1412	0.2850
PB-2	50.7564	0.0982	0.1935
PB-3	50.7996	0.0340	0.0669

Table 4.1: The original sample weight and heavy mineral weight that were used to calculate the heavy mineral percentage.

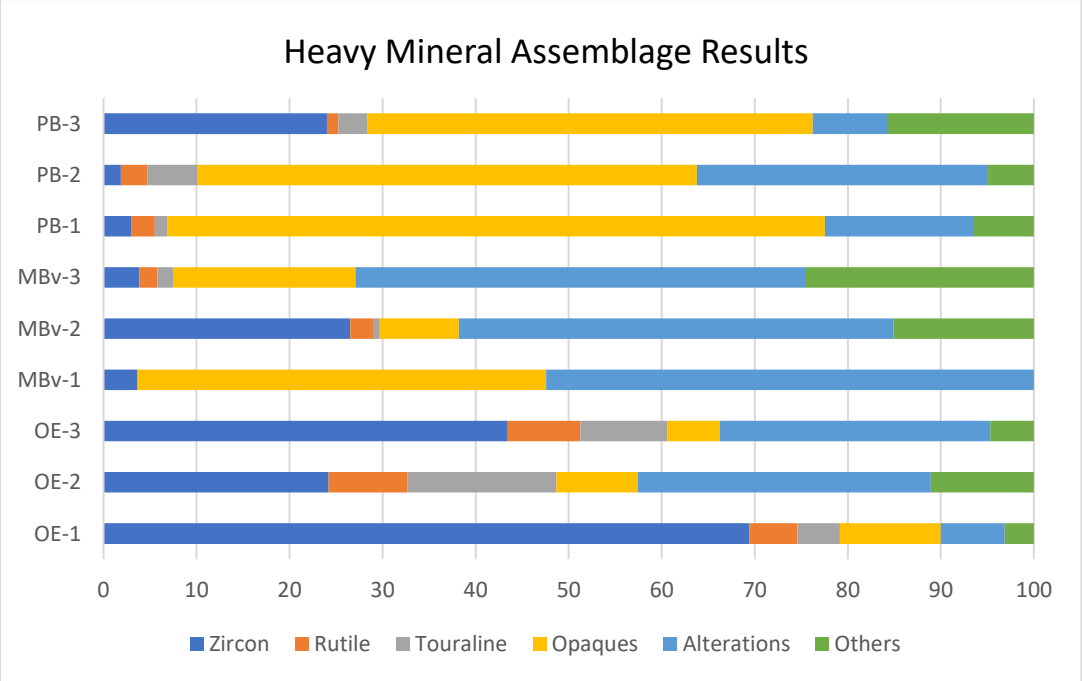

Figure 4.1: Heavy mineral assemblage between all nine sandstone units.

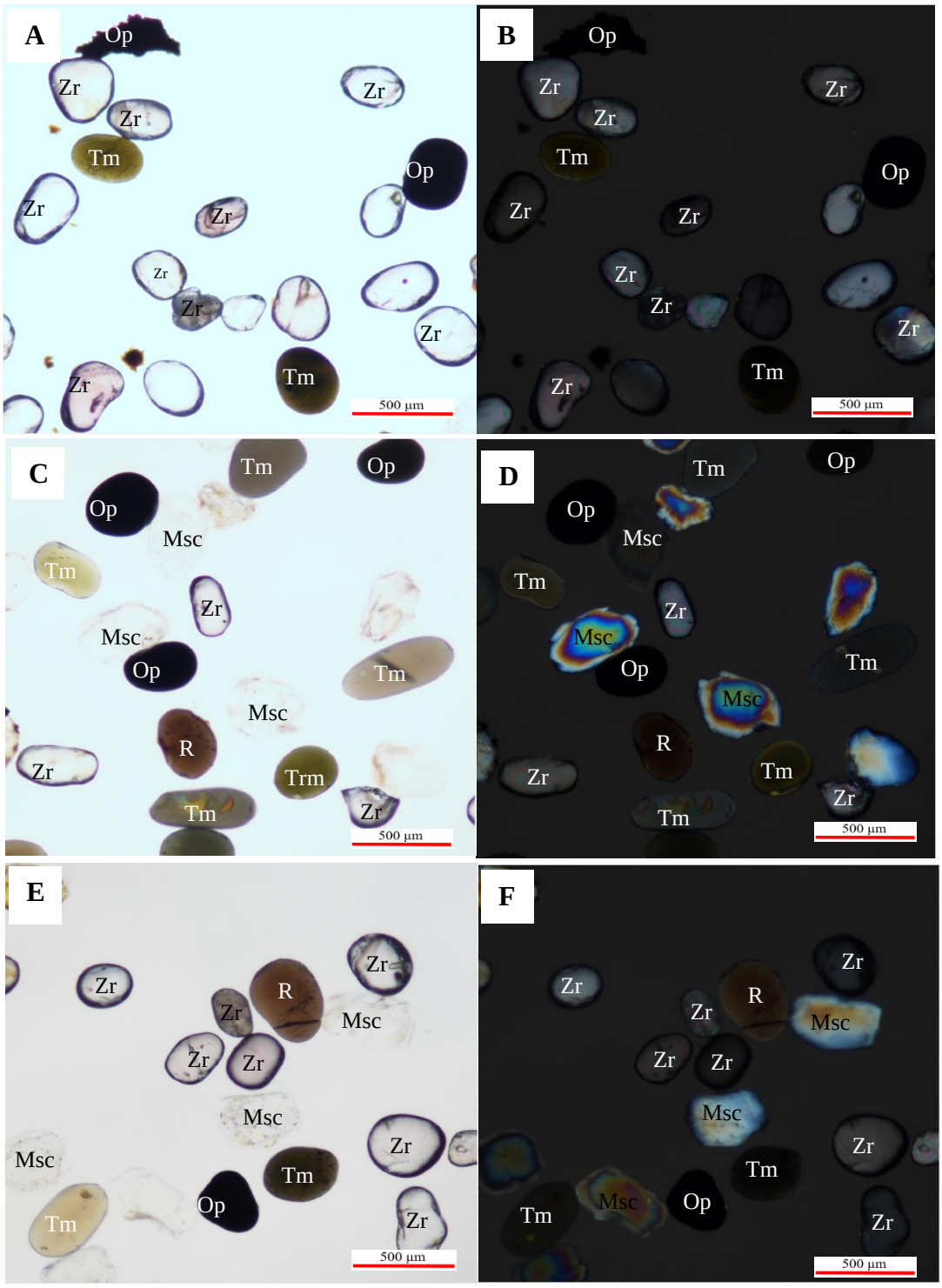

Figure 4.2: Representative photomicrographs of the heavy minerals for the OE samples. A) OE-1 ppl, B) OE-1 xpl, C) OE-2 ppl, D) OE-2 xpl, E) OE-3 ppl, F) OE-3 xpl

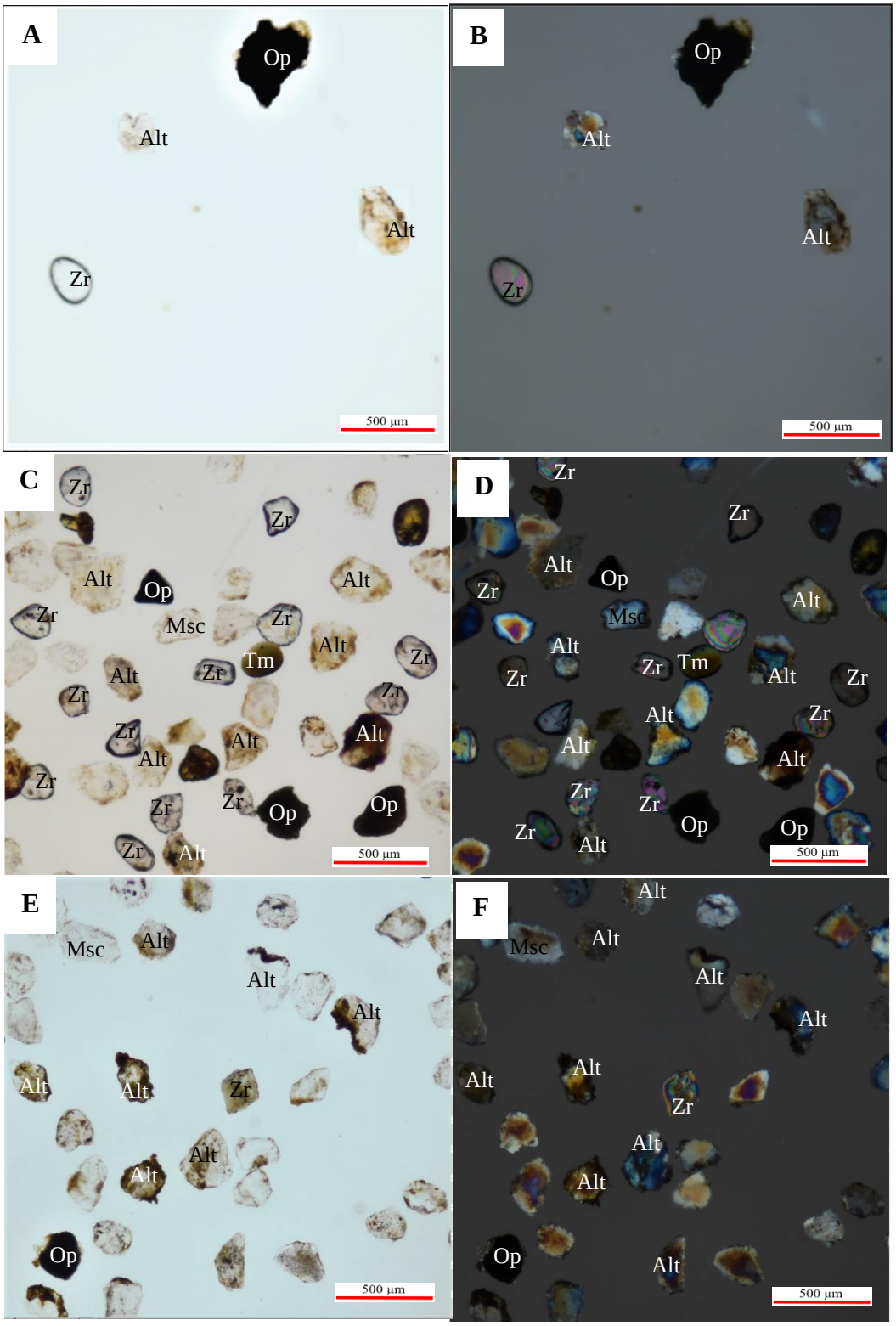

Figure 4. 3: Representative photomicrographs of the heavy minerals for the MBv samples. A) MBv-1 ppl, B) MBv-1 xpl, C) MBv-2 ppl, D) MBv-2 xpl, E) MBv-3 ppl, F) MBv-3 xpl

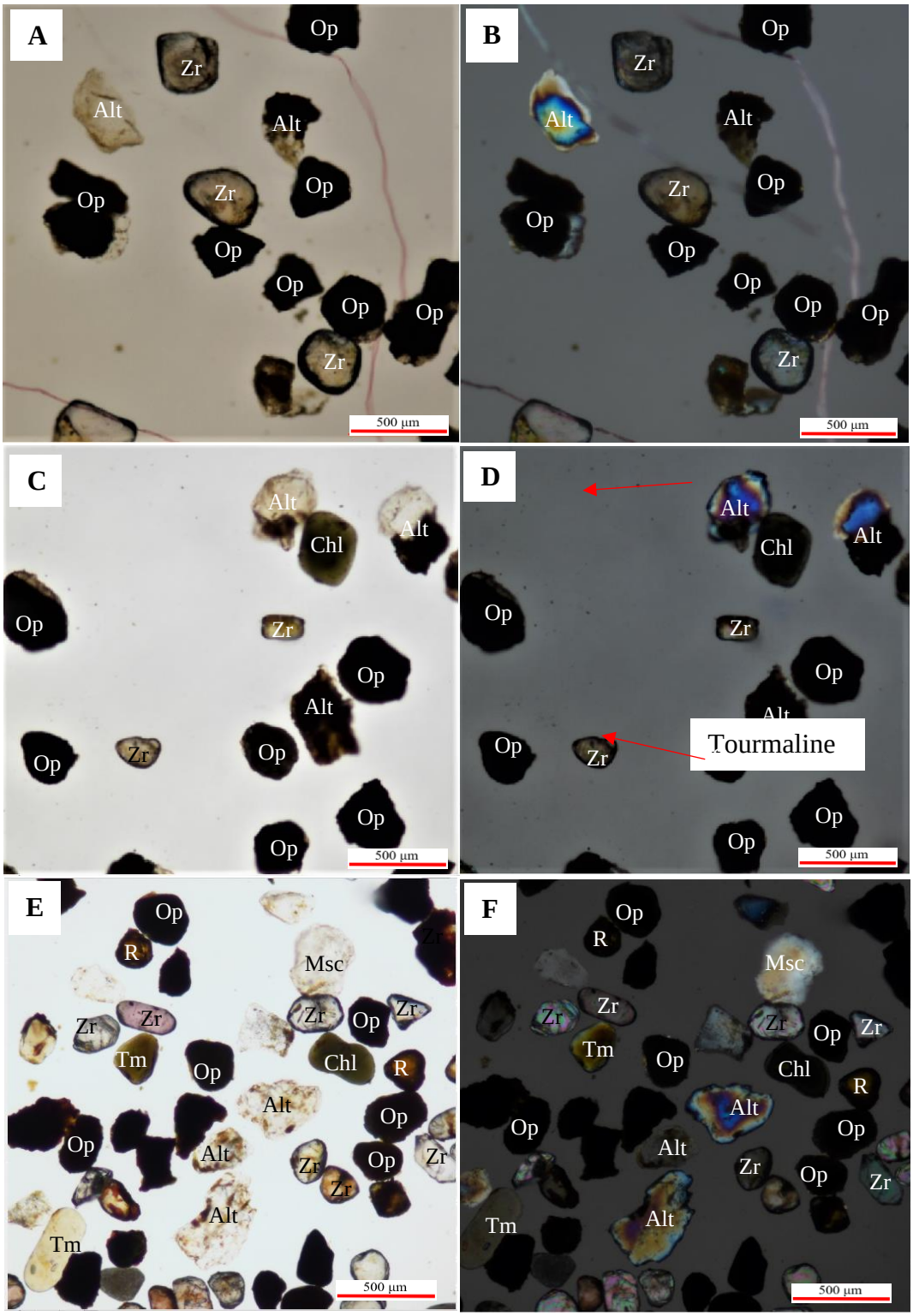

Figure 4.4: Representative photomicrographs of the heavy minerals for the PB samples. A) PB-1 ppl, B) PB-1 xpl, C) PB-2 ppl, D) PB-2 xpl, E) PB-3 ppl, F) O-3 xpl

4.2 Heavy Mineral Indices

All sandstone units have a high variance of RZi between their samples (figure 4.5 A). The OE samples RZi range from 7-26%. The MBv samples range from 0-33%. The PB samples have an RZi index ranging from 5-60%. The ZTR index for the OE samples display a statistical difference from that of the other samples. The ZTR index for the OE samples ranges from 53-89% (Figure 4.5 B). The MBv sandstones have a ZTR index ranging from 4-30 % and the PB samples have a range from 7-28 %. While the index range for the MBv and PB samples are similar, the MBv has a slightly lower average ZTR average. The ZTR index for the OE samples display a statistical difference from that of the other samples. The p-value of a two-tailed t-test comparing OE ZTR indices to the MBv sample indices is 0.0149 and 0.0127 for the PB samples.

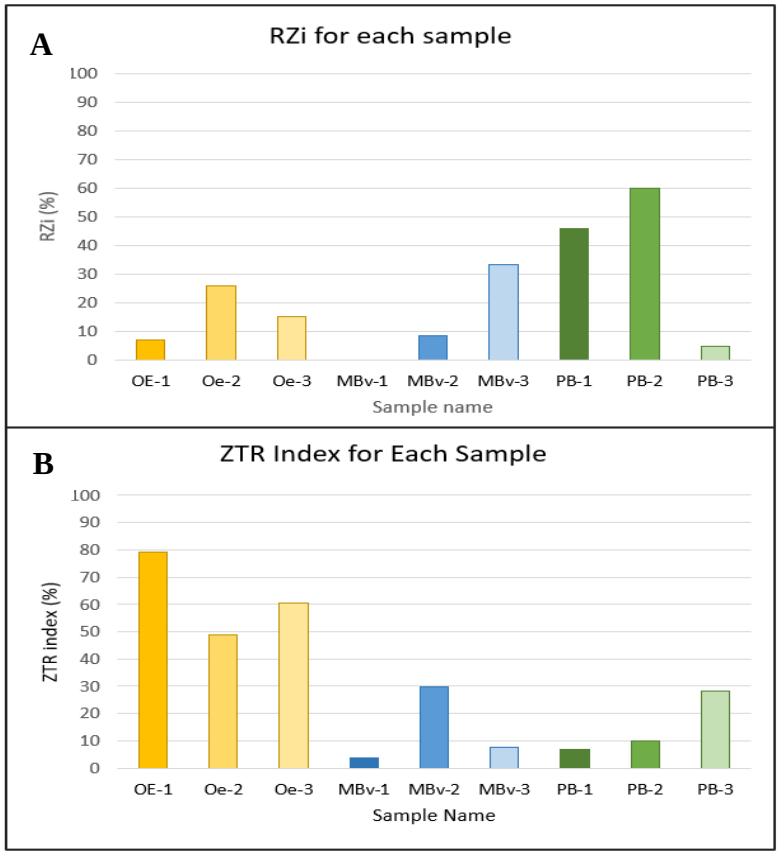

Figure 4.5: Plot of the RZi (A) and ZTR (B) of the sandstone sample

Chapter 5: Optically Stimulated Luminescence Results

5.1 Luminescence Sensitivity

OSL and TL sensitivity were calculated for the six sandstone samples (Appendix B). A two-sample t-test was completed between the sensitivity measurements of the sandstones to determine if there is significant difference between the sandstones of the BNR. The samples display a statistical difference between the weight normalized OSL sensitivity. All of the sandstones have average OSL sensitivity values that are statistically different from each other. The p-value for the difference between the OE and MBv sensitivity is 0.0001. The p-values for differences between MBv and PB samples and OE and PB samples are 0.0019 and 0.0012 respectively. The weight normalized TL sensitivity of the different sandstones displays a significant difference between the OE sandstones and the MBv sandstones (p-value = 0.0013) and the MBv and PB sandstones (p-value = 0.005). There is no statistical difference between the OE and the PB sandstones (p-value = 0.0761). (Figure 5.1). The OE and PB sandstones have an average TL sensitivity value that is an order of magnitude greater than the MBv samples. Within the sandstone units, there are noticeable differences between the aliquots within the MBv and PB sandstone units (Figure 5.2 B-C). The MBv sensitivity plots do not display strong fit. The R^2 values for MBv 1 is 0.23 and for 0.18 MBv-2. Both PB 1 and PB 2 have an R^2 value greater than 0.8. The OE samples plot more similarly than the other two samples, but still have two identifiable populations (Figure 5.2 A).

The CW-OSL decay curves all display an exponential decrease of OSL signal over time. (Figure 5.3 D-F). There is not noticeable variation between the OSL decay curves. The TL sensitivity of all samples have a defined peak at 100^{o} C (Figure 5.2 A-C, Appendix B).

There are no strong relationships between TL sensitivity with the heavy mineral weight

percentage (Figure 5.4). The RZi also does not display strong relationships to the TL sensitivity. There is some weak clustering with the sandstone samples OSL sensitivity and the HM weight percent and the RZi (Figure 5.5).

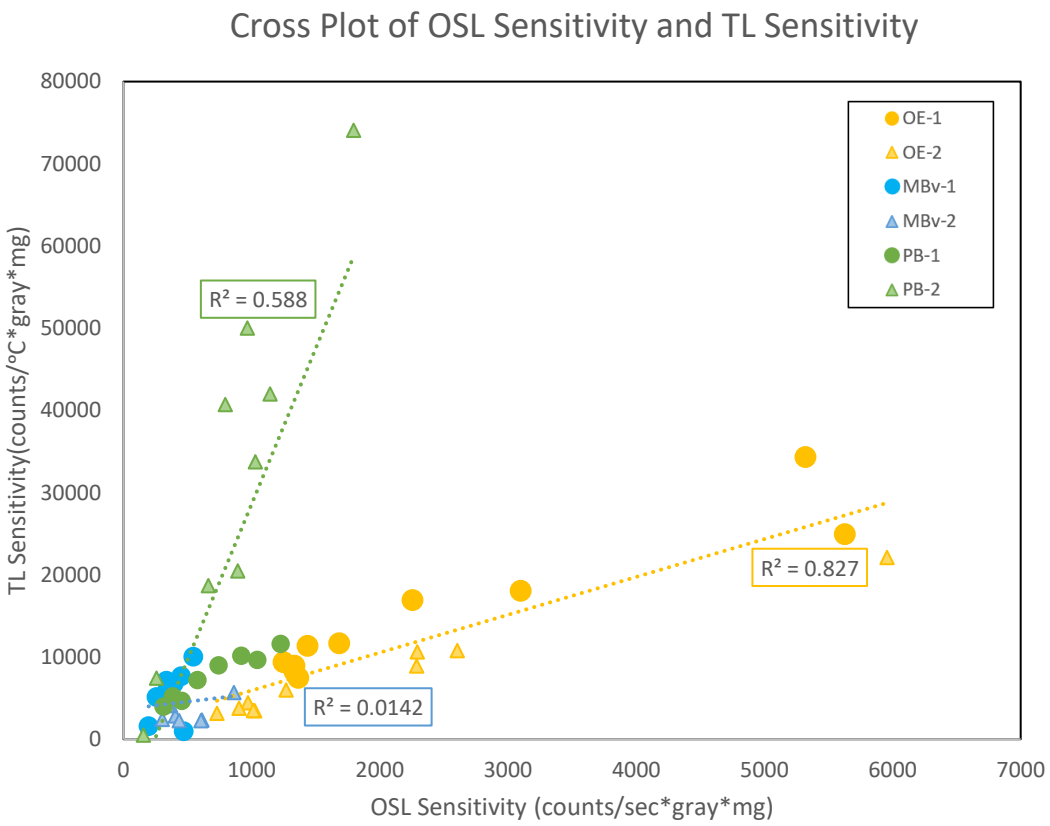

Figure 5.1: Cross-plot of OSL sensitivity and TL sensitivity for all sandstone aliquots

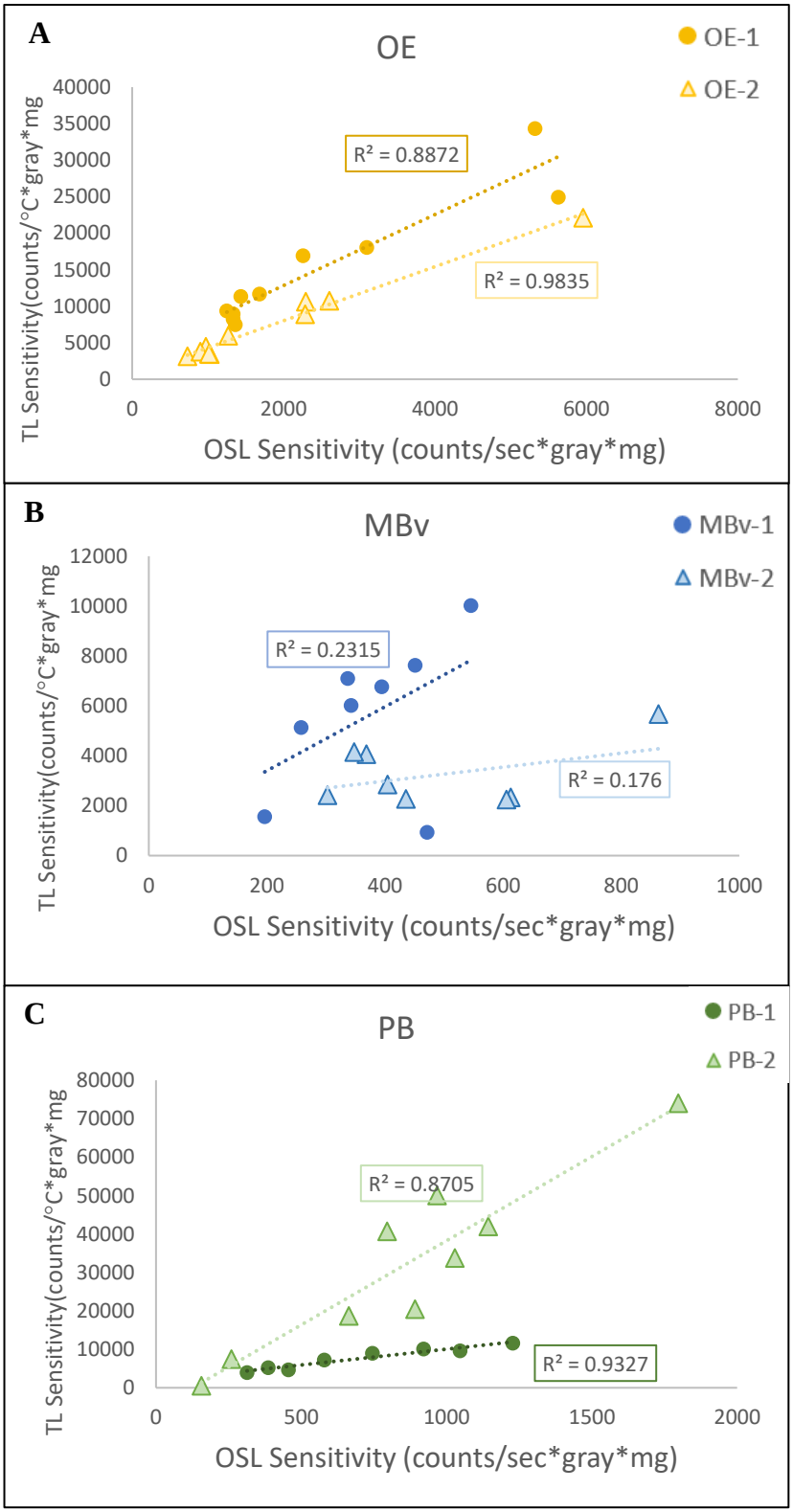

Figure 5.2: Cross-plot of OSL sensitivity and TL sensitivity for each sandstone units A) OE, B) MBv), and C) PB

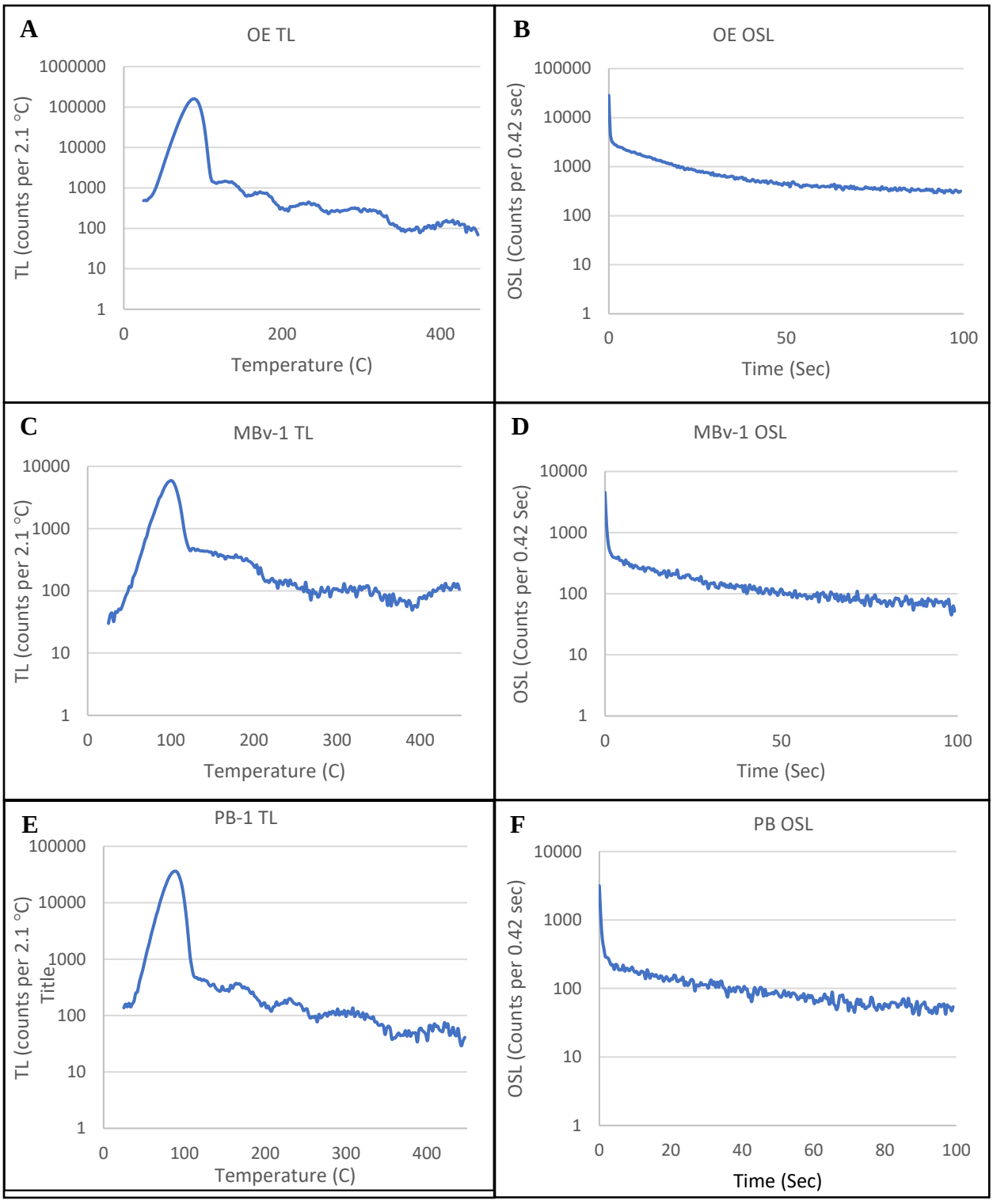

Figure 5.3: TL glow curves for sample OE (A), MBv (C), PB (E). OSL decay curvevs for samples OE (B), MBv (D) and PB (F)

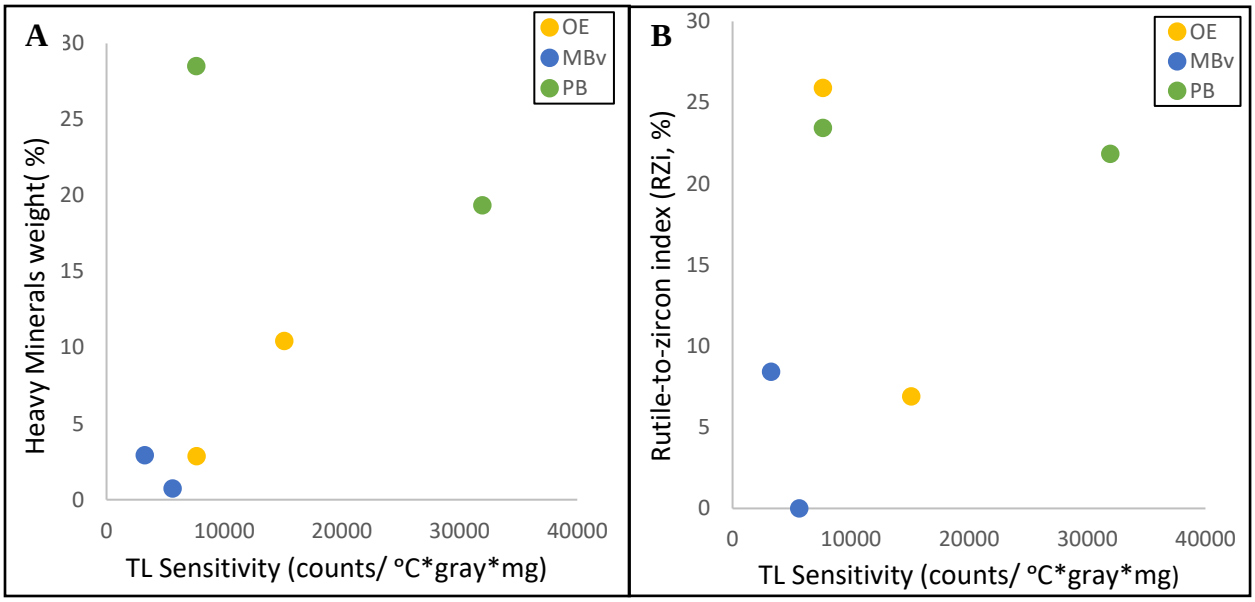

Figure 5.4: Plot of TL sensitivity comparing the heavy mineral wt% (A) and the RZi (B)

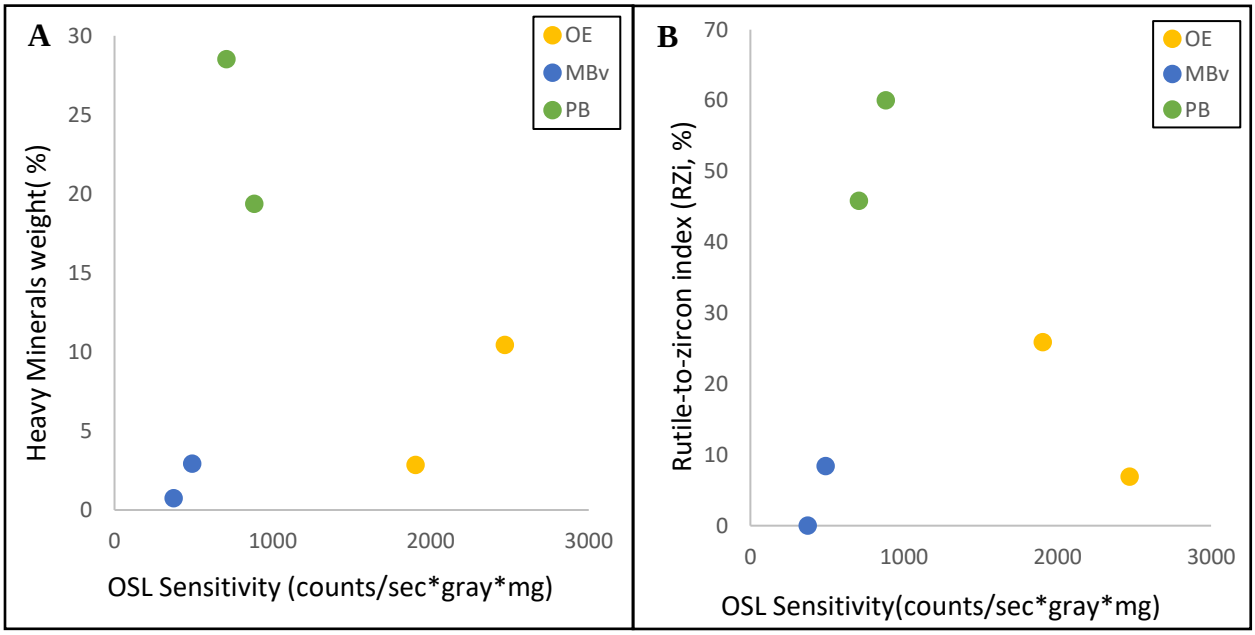

Figure 5.5: Plot of OSL sensitivity comparing the heavy mineral wt% (A) and the RZi (B)

5.2 LM-OSL

Components were analyzed for all six aliquots (Appendix C). All OE samples contained four or five components. For all OE samples, the fast trap (component 1) dominates the initial signal (Table 5.1, Figure 5.5). The R^2 values for the OE sandstones range from 0.87 – 9.5. The second component is either Medium, Slow1 or Slow2. All OE samples contain traps Slow3 and Slow 4. The fast component of the OE samples contributes the most. The relative cross-section of the Slow4 components to the Fast is 0.0002.

The MBv samples contain more components than the OE samples. The number of components recorded for these samples range from 4 to 6 with R^2 values ranging from 0.27-0.83. The first components in MBv samples are either the Fast or Ultrafast components. These components contribute to a large portion of the curve (Figure 5.6). MBv sandstones also tend to have Medium or Slow1 traps. In addition, MBv samples also contain Slow2, Slow3, and Slow4 components.

The PB samples also have more components present. Most samples have five components. The fit of these curves range from 0.22 – 0.91. These samples mostly contain the Ultrafast, Fast, Slow2, Slow3, and Slow4 components. The Slow4 components of the PB samples have a higher relative cross section to the first component than the MBv and OE sandstones.

The terrace sediment analyzed included a fast component. None of the terrace aliquots contain a medium component, but all aliquots record a Slow3 trap component. The LM-OSL curve produced for these samples fits the expected model well. The R^2 values for the three aliquots range from 0.86-0.95.

Sample	OSL Components	Detrapping Probability	Photoionization Cross Section (cm2)	Relative Cross Section to First Component
OE-1	Fast	2.7	$2.495*10^{-17}$	1
	Slow2	0.031	$2.834*10^{-19}$	0.0114
	Slow3	0.004	$3.9*10^{-20}$	0.0016
	Slow4	0.0001	$4.714*10^{-21}$	0.0002
OE-2	Fast	2.6	$2.457*10^{-17}$	1
	Slow2	0.032	$2.914*10^{-19}$	0.0119
	Slow3	0.005	$5.043*10^{-20}$	0.0021
	Slow4	0.0004	$3.725*10^{-21}$	0.0002
MBv-1	Ultrafast	17	$1.613*10^{-16}$	1
	Fast	1.5	$1.39*10^{-17}$	0.0862
	Slow1	0.14	$1.249*10^{-18}$	0.0077
	Slow2	0.022	$2.056*10^{-19}$	0.0013
	Slow3	0.004	$3.552*10^{-20}$	0.0004
	Slow4	0.00004	$2.767*10^{-21}$	0
MBv-2	Ultrafast	12	$1.099*10^{-16}$	1
	Fast	1.5	$1.394*10^{-17}$	0.1268
	Slow1	0.15	$1.41*10^{-18}$	0.0128
	Slow2	0.022	$2.048*10^{-19}$	0.0019
	Slow3	0.005	$4.937*10^{-20}$	0.0004
	Slow4	0.0004	$4.937*10^{-21}$	0
PB-1	Fast	2.7	$2.517*10^{-17}$	1
	Medium	0.85	$7.87*10^{-18}$	0.3127
	Slow2	0.028	$2.615*10^{-19}$	0.0104
	Slow3	0.007	$6.961*10^{-20}$	0.0028
	Slow4	0.0004	$3.977*10^{-21}$	0.0002
PB-2	Ultrafast	9.9	$9.20*10^{-17}$	1
	Fast	1.3	$1.24 *10^{-17}$	0.1346
	Slow2	0.042	$3.86*10^{-19}$	0.0042
	Slow3	0.009	$8.21*10^{-20}$	0.0009
	Slow4	0.0005	$4.70*10^{-21}$	0.0001
Terrace-3	Fast	4.954	$4.57*10^{-17}$	1
	Slow2	0.0123	$1.14*10^{-19}$	0.0025
	Slow3	0.0015	$1.35*10^{-20}$	3.00E-04

Table 5.1: Representative LM-OSL components of sandstone and terrace aliquots included in this study

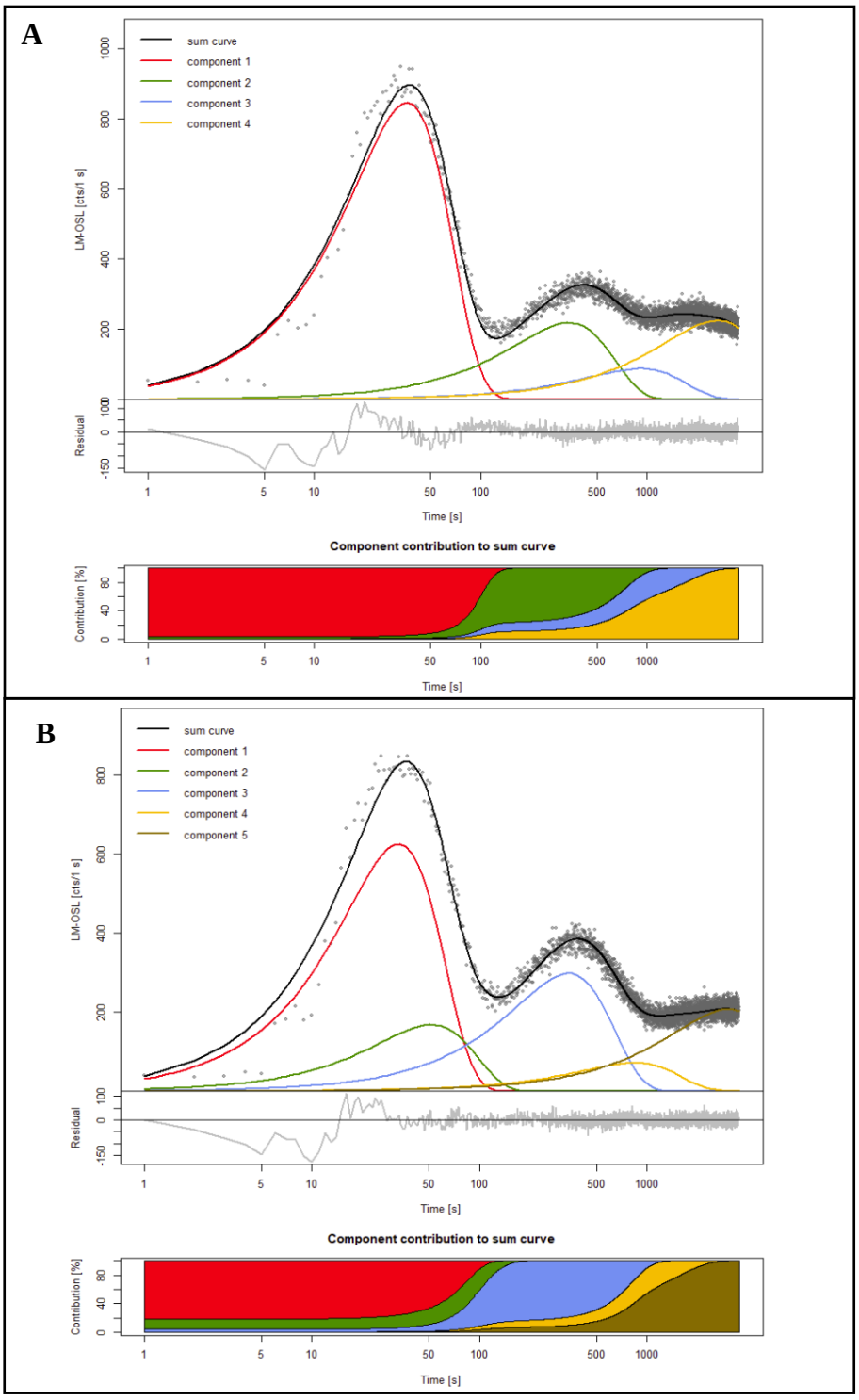

Figure 5.6: Representative LM-OSL curve for sandstones OE-1 (A) and OE-2 (B)

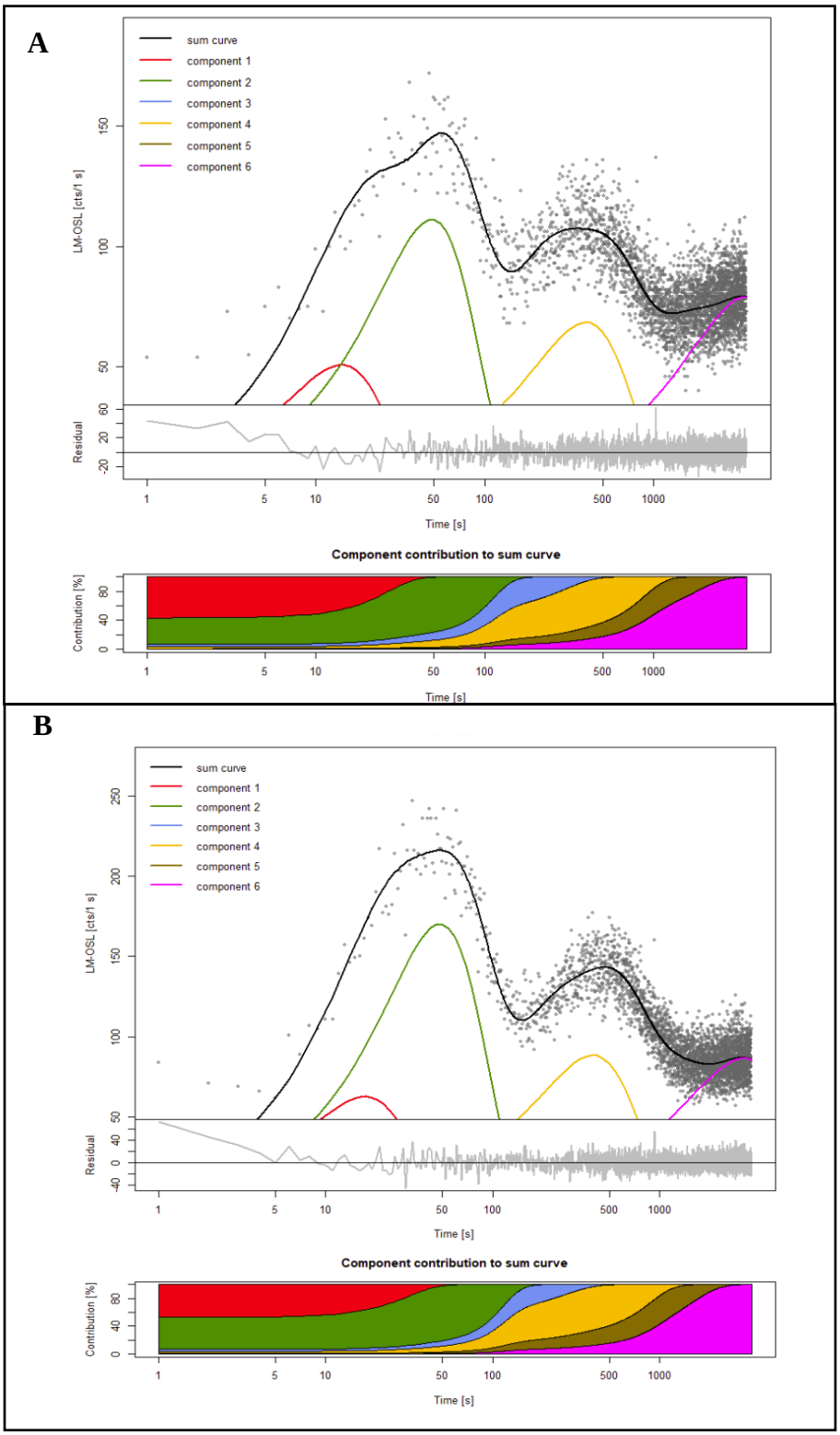

Figure 5.7: Representative LM-OSL curve for sandstone samples MBv-1 (A) and MBv-2 (B)

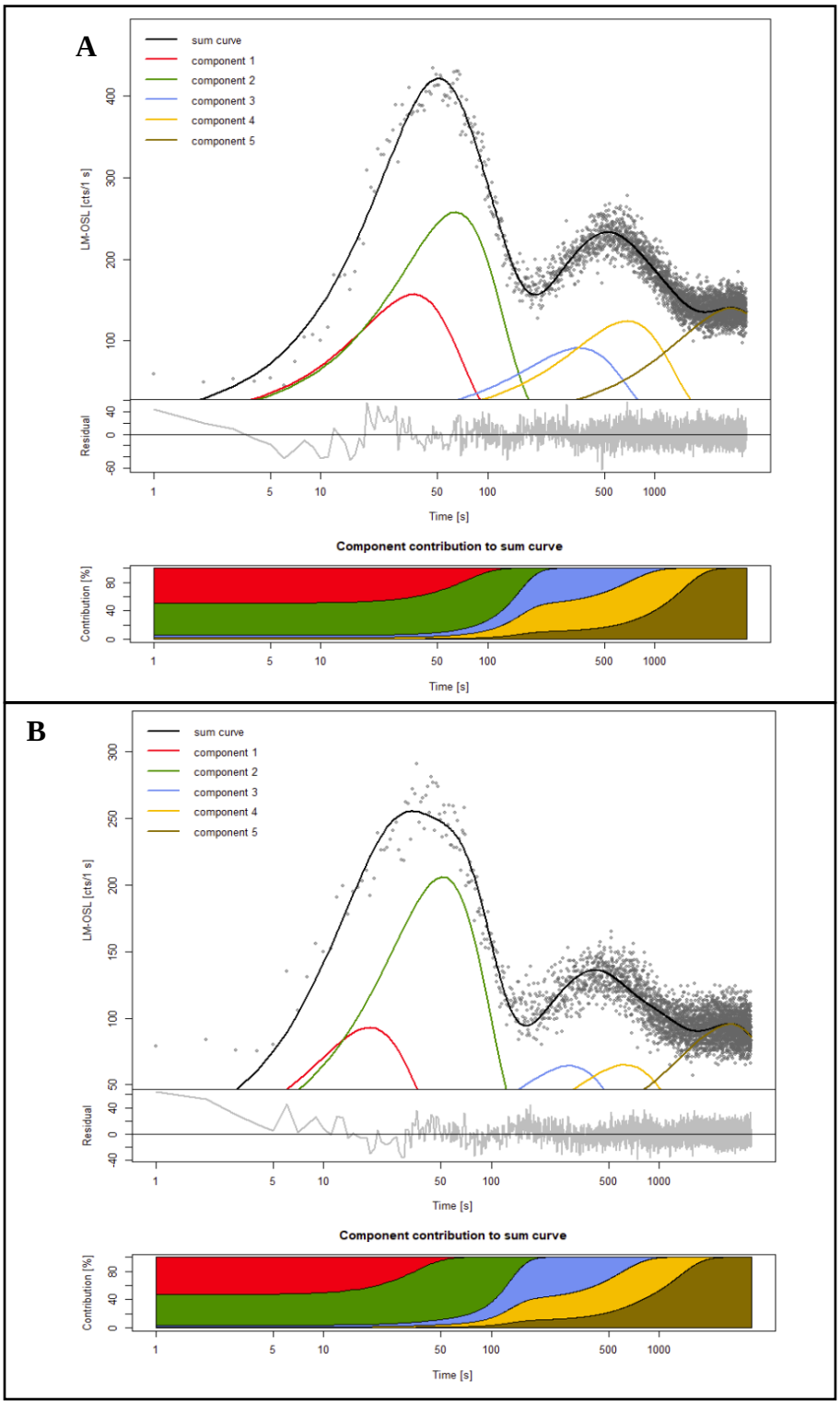

Figure 5.8: Representative LM-OSL curve for sandstone samples PB-1 (A) and PB-2 (B)

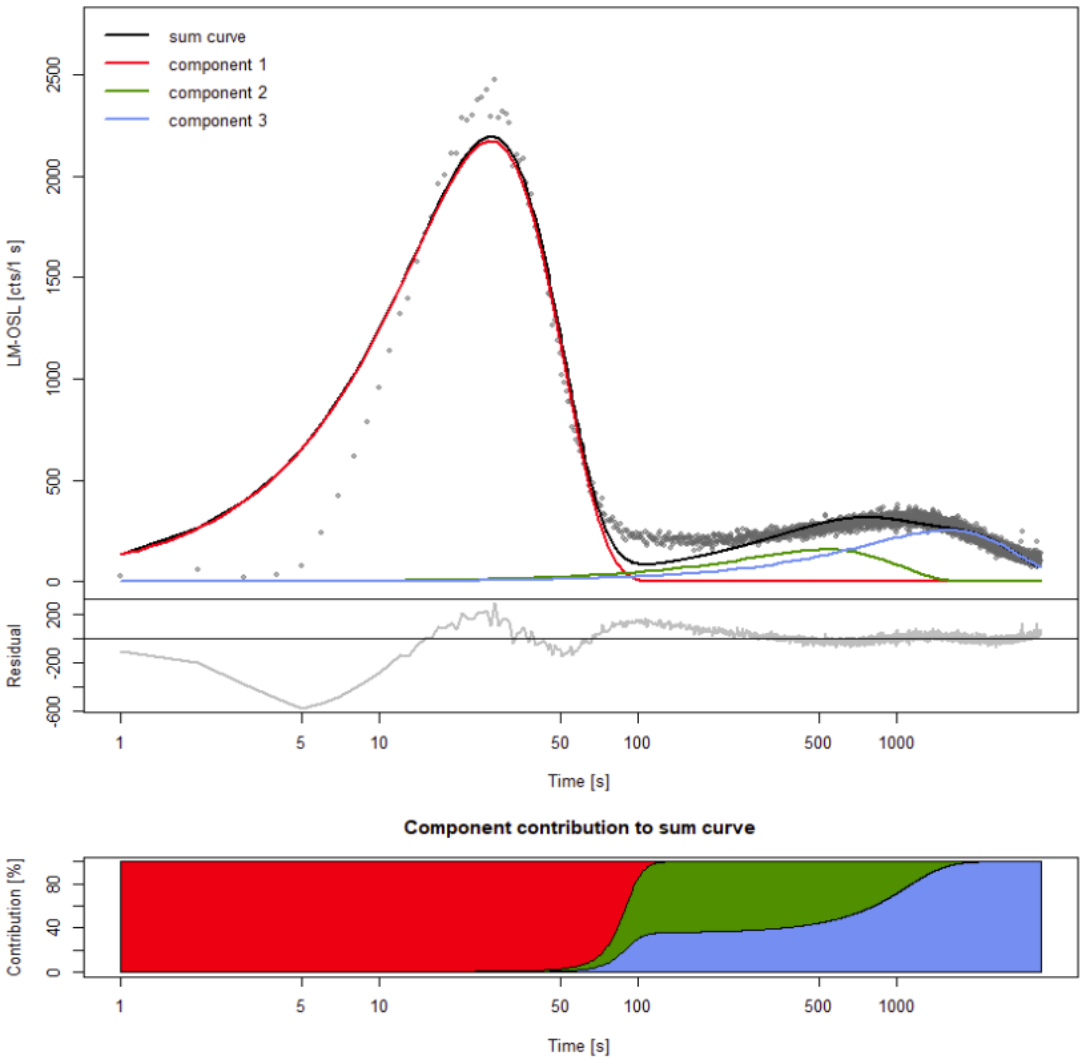

Figure 5.9: Representative LM-OSL curve for terrace 1

Chapter 6: Discussion and Conclusions

6.1 Heavy Minerals Discussion

The ZTR index of the OE samples indicate that these sandstones are very mature (Hubert 1962). This is also supported by the sandstone category of quartzarenites (Bello, 2016). Because these sandstones are super mature, it is reasonable for these samples to have a limited assemblage of heavy minerals. Because zircon, rutile, and tourmaline are among the most stable of minerals, their abundance in the heavy mineral assemblage is not surprising. These minerals are resistant to the processes that control the presence of less stable minerals. The ZTR indices for the MBv and PB samples are lower than that of the OE samples. For the MBv samples, there is a higher percentage of translucent minerals and altered phases than the OE samples. This indicates that the heavy minerals in these rocks have either not undergone weathering to completely remove less stable heavy minerals or to alter lighter minerals. The PB samples have a majority of opaque minerals and alteration phases that appear to result from weathering and oxidation

In addition to the assemblage differences of the various sandstone units, there are also differences between the morphology of the heavy minerals of the sandstones. Several of the zircon grains in the OE samples are rounded to subrounded, while the PB samples have a mixture of elongated and subrounded zircon grains. These differences in texture also support the fact that these are super mature sandstones. These textures can provide some insight to the processes that have influenced these sandstones. This sediment must have gone through several processes that have rounded these grains and resulted in the lack of other heavy mineral phases. Therefore, it is reasonable to conclude that these grains have travelled long distances from their igneous or metamorphic sources or that they had undergone intense chemical weathering that results in the sediment maturity.

Some of the altered grains also have opaque inclusions. These grains have relatively low relief and tend to have first order birefringence. In addition, there appears to be a reddish-brown staining on all of the grains in plane-polarized light. This staining could be due to an authigenic alteration of the quartz grains. These grains also are angular compared to the zircon grains that are present in the sample. This would indicate that these grains are not from the same source area as the other heavy minerals in the sample. It is unlikely that there was an error in the separation process, because the OE and MBv samples had two trials for each of the samples in the respective units. In addition, it is unlikely for the samples to have not come into contact with the heavy liquid during the separation process due to the limited amount of heavy minerals within these samples.

Additional SEM, electron microprobe, or other compositional work quantifying the nature of the opaque minerals may also provide more information on the heavy mineral assemblages of these sandstones. For example, comparing the heavy mineral assemblages from the trials would provide more robust identification of the heavy minerals that are present in each of the sandstones and allow additional comparison of the minerals. Additional compositional analysis would also assist in better quantifying the opaque minerals and altered grains.

6.2 OSL Sensitivity Discussion

There are two main interpretations as to what could potentially influence the OSL sensitivity. The first relates to the number of transportation cycles of a grain, and the other relates to the geology of the source areas (Capaldi et al., 2022). The OSL sensitivity of the different sandstones in the BNR have significant differences between the three populations of sandstones. These data support that OSL sensitivity can provide some insight to provenance and has further potential to be used as a tool for sediment fingerprinting. Even if the sensitivity is not directly

indicative of the source rock of a quartz grain, it can at least provide information on different transportation histories of a grain, which can further isolate populations of quartz grains in a sediment deposit.

While there is some vague clustering of the HM weight percentages and the RZi plotted against OSL sensitivity, there is no strong relationship between the sandstone samples heavy mineral data and the OSL sensitivities. This is also true for the TL sensitivities. It is likely, with the limited sample size in this study, that correlations would not be displayed.

6.3 LM-OSL Discussion

There are some noticeable differences in the OSL components that were detected through LM-OSL analysis. The number of components varies between the sandstone samples. The different number of components and their characteristics and the type of components can act as a provenance indicator. However, there are still challenges when investigating the components present in a terrace deposit.

The terrace deposit in this study exclusively had a Fast component recorded as the initial signal and did not record an Ultrafast component. While all of the samples have a fast component, the detrapping probability of Fast component in the terrace is more similar to that of the OE samples, but there are no exact matches. This indicates that the detrapping probability of the components in the terrace cannot be positively linked to a sandstone included in this study. This indicates that the quartz in the terrace deposit originated from a different source quartz, or there is some alteration in OSL characteristics that potentially occur over several repeated cycles of erosion and deposition.

6.4 Significance

Provenance studies have changed from being primarily the purview of sedimentologist to now be considered across a variety of disciplines, including sedimentology, structural geology, and geomorphology (Caracciolo, 2020). Many researchers are developing new methods to figure out source-to-sink pathways for sediment. For example, Thomas (2011) mentions that there have been strides in interpreting provenance, particularly focusing on detrital zircon geochronology. Improving the methodology and working toward the creation of new tools to assist in the determination of provenance is a critical need. There is also much to be learned from understanding source-to-sink pathways. This research can provide further insight into what mechanisms lead to the channel development in river channels and fluvial landscape evolution. By gaining more information about sediment transportation, this research has the potential to greatly expand our ability to understand depositional histories in the BNR watershed.

Gaining more information about the lithology of the BNR will also provide insight to sediment transport on a continental scale. There are questions around the origins of the rocks of the BNR. If the provenance of the sediment present in the strath terraces can be extrapolated, there may be a possibility to use this method to further the understanding of the source to-sink relationships for the lithologic units that comprise the Ozark stratigraphy. By investigating the sedimentary rocks present in the BNR, the sediment transportation history of the continental system may be better understood. Sediment transport on the continental scale through time is poorly understood and a critical avenue of new research, and exploring new research tools will provide additional avenues to collect information to better understand the geologic history of the current landscapes and to increase scientific understanding broader scale sediment transport patterns.

6.5 Future Directions for This Study

While the research that was completed for this thesis begins to explore using OSL as a provenance tool in the BNR, there is still more work that can be accomplished. There are many future avenues for this study. For example, the OSL sensitivity and LM-OSL of other sandstone units in the Buffalo National River watershed are yet to be quantified. Analyzing additional samples as well as additional terrace deposit quartz may be able to provide further insight into how the incising river transports sediment throughout the watershed. More analysis of the sandstone lithologies and more terrace deposits will further quantify the utility of OSL as a potential provenance tool.

Another future study that can be done is to potentially look at the microtextures of the quartz grains using an SEM and investigate the crystallographic index of the quartz grains using X-ray Diffraction (XRD). There have been previous studies that have investigated using the microtextures of quartz grains as a new technique for investigating provenance of quartz grains (Pan et al., 2016). I believe that this would be interesting to include in future studies of BNR provenance to see if there are textural differences in the quartz grains of the various sandstones present. While there have not been as many investigations using the crystallographic index of quartz in relation to OSL and sediment provenance, this additional analysis may further differentiate the quartz grains in the BNR. These additional analyses may be useful in investigating why different sandstone quartz grains have different sensitivity. Because OSL is influenced by the crystal lattice and available traps in the quartz grains, the texture of quartz grains could play a significant role in how the grains trap radiation.

In addition, there is also more work that can be completed about the provenance of the sandstones of the BNR. Additional investigations of the OSL properties of other sandstone units

will provide a more complete understanding of the quartz sources that can contribute to the terrace deposits within the watershed. Another investigation that would provide more clarity to this project moving forward would be to sample and analyze additional terrace deposits for OSL analysis and compare these to those of the sandstone data. Having data from multiple terrace deposits will determine if there are noticeable differences of quartz OSL characteristics across the BNR watershed boundary. Additionally, a study could be conducted to investigate how the number of depositional cycles influence the OSL measurements. This could be mimicked in the lab by running the OSL protocols on the same aliquot multiple times to determine if the number of cycles changes the OSL properties. All of these potential studies would further categorize the utility of using OSL as a provenance tool.

By further studying the provenance in the sandstones of the BNR, there is potential to increase scientific understanding broader scale sediment transport patterns. This is especially intriguing due to the location of the BNR and its proximity to the Ouachita mountains. There have been questions regarding the transcontinental transportation histories of the sandstone units in this region. If the OSL characteristics are further quantified for the quartz samples in this region, they could potentially be used to further investigate provenance on larger spatial scales and potentially in different settings.

6.5 Conclusions

The sandstone units that were analyzed in this study have some critical differences that support differences in provenance. The three sandstones have different heavy mineral weight percentages and assemblages, which indicate variations in transportation histories and provenance of the sediment comprising the sandstones. These travel and depositional histories of the sediment may influence the OSL characteristics of the quartz grains. Previous research

shows that repeated deposition cycles may contribute to more established traps to store environmental radiation during transport (Nian et al., 2019; Alexanderson, 2022).

There are distinct differences between the OSL sensitivities, but the TL sensitivities of the sandstone units do not have distinct differences between all three of the sandstone samples. There are some distinctions between the components of the sandstones in the BNR that can potentially be linked to signals from a depositional terrace. This study has provided more information for using OSL properties of quartz as a sediment fingerprinting tool in the BNR. The advances in this study investigating OSL sensitivity and the contributing components of the sandstones selected for this study provide more foundation for OSL being a usable tool for sediment fingerprinting. However, additional work must be completed to further extrapolate the utility of this novel application of this tool.

References

Allen, D. E., 2010, A comparative petrographic study of three Upper Mississippian (Chesterian) sandstones in northern Arkansas [M.S. Thesis]: University of Arkansas, 143 p.

Aitken, M. J., 1998, Introduction to optical dating: the dating of Quaternary sediments by the use of photon-stimulated luminescence. Clarendon Press, 267 p.

Alexanderson, H., 2022, Luminescence characteristics of Scandinavian quartz, their connection to bedrock provenance and influence on dating results: Quaternary Geochronology, v. 69, 101272.

Arkansas GIS Office, 2006, 2006 Five Meter Resolution Digital Elevation Model (Raster), https://gis.arkansas.gov/product/2006-five-meter-resolution-digital-elevation-model-raster-new/.

Arkansas GIS Office, 2020, County Boundary (Polygons), https://gis.arkansas.gov/product/county-boundary-polygons/

Ayofe, A. J. and Anthony, I. R., 2020, Application of ZTR index in the assessment of maturity of stream sediments in Akinmorin Area, Southwestern Nigeria. Iconic Research and Engineering Journal, v. 3, p. 98-107.

Bartyik, T., Floca, C., Pál-Molnár, E., Urdea, P., Hamed, D. E., and Sipos, G, 2021, The Potential Use of Osl Properties of Quartz in Investigating Fluvial Processes on the Catchment of River Mureş, Romania: Journal of Environmental Geography, v. 14, p. 58-67, DOI: 10.2478/jengeo-2021- 0006.

Bello, E. C., 2016, Lithologic Character of the Paleozoic Sandstone Succession, Southern Ozark Region, Arkansas, and Missouri. Journal of the Arkansas Academy of Science, v. 70, p. 40-44, https://doi.org/10.54119/jaas.2016.7002.

Bello, E. C., 2017, Sequence Stratigraphic and Tectono-Stratigraphic Successions, Ozark Shelf, Tri- State Region, Southern Midcontinent: Journal of the Arkansas Academy of Science, v. 71, p. 173-179, https://doi.org/10.54119/jaas.2017.7129.

Braun, J., 2021, Using Ground-Based LIDAR to Analyze Fracture Characteristics as Possible Controls on the Variability of Valley Morphology in the Buffalo River Watershed, Arkansas [M.S. Thesis]: Auburn University, 83 p.

Bull, W. B., 1990, Stream-terrace genesis: implications for soil development: Geomorphology, v. 3, p. 351-367, https://doi.org/10.1016/0169-555X(90)90011-E.

Bulur, E., Duller, G. A. T., Solongo, S., Bøtter-Jensen, L., and Murray, A. S., 2002, LM-OSL from single grains of quartz: a preliminary study: Radiation Measurements, v. 35, p. 79-85. https://doi.org/10.1016/S1350-4487(01)00256-6

Capaldi, T. N., Rittenour, T. M., and Nelson, M. S., 2022, Downstream changes in quartz OSL sensitivity in modern river sand reflects sediment source variability: Case studies from Rocky Mountain and Andean rivers: Quaternary Geochronology, v. 71, DOI: 101317.

Caracciolo, L., Critelli, S., Cavazza, W., Meinhold, G., von Eynatten, H., and Manetti, P., 2015, The Rhodope Zone as a primary sediment source of the southern Thrace basin (NE Greece and NW Turkey): evidence from detrital heavy minerals and implications for central-eastern Mediterranean palaeogeography: International Journal of Earth Sciences, v. 104, p. 815-832, 10.1007/s00531-014-1111-9.

Caracciolo, L., 2020, Sediment generation and sediment routing systems from a quantitative provenance analysis perspective: Review, application and future development: Earth-Science Reviews, v. 209, p. 1-28, https://doi.org/10.1016/j.earscirev.2020.103226.

Cordry, C. D., 1929, Heavy minerals in the Roubidoux and other sandstones of the Ozark region, Missouri: Journal of Paleontology, v. 3 p. 59-85, https://www.jstor.org/stable/1298047.

Duller, G. A., 2008, Luminescence Dating: guidelines on using luminescence dating in archaeology.

Giles, A. W., 1932, Textural features of the Ordovician sandstones of Arkansas: The Journal of Geology, v. 40, p. 97-118.

Gray, H. J., Jain, M., Sawakuchi, A. O., Mahan, S. A., and Tucker, G. E., 2019, Luminescence as a sediment tracer and provenance tool: Reviews of Geophysics, v. 57, p. 987-1017, https://doi.org/10.1029/2019RG000646.

Haughton, P. D. W., Todd, S. P., and Morton, A. C., 1991, Sedimentary provenance studies: Geological Society, London, Special Publications, v. 57, p. 1-11, https://doi.org/10.1144/GSL.SP.1991.057.01.01.

Heidner, N., 2019, Testing Erosion Potential of Heterogeneous Lithologies to Understand Atypical Valley Morphology in the Buffalo National River Watershed, Arkansas [Master's Thesis]: Auburn University, 64 p.

Hubert, J. F., 1962, A zircon-tourmaline-rutile maturity index and the interdependence of the composition of heavy mineral assemblages with the gross composition and texture of sandstones: Journal of Sedimentary Research, v. 32, p. 440-450, https://doi.org/10.1306/74D70CE5-2B21-11D7-8648000102C1865D.

Hudson, M. R., 2000, Coordinated strike-slip and normal faulting in the southern Ozark dome of northern Arkansas: Deformation in a late Paleozoic foreland: Geology, v. 28, p. 511-514, https://doi.org/10.1130/0091-7613(2000)28<511:CSANFI>2.0.CO;2.

Hudson, M. R., and Murray, K. E., 2003, Geologic Map of the Ponca Quadrangle, Newton, Boone, and Carroll Counties, Arkansas: U.S. Geologic Survey, No. 2412, scale 1:24,000.

Hudson, M. R., Turner, K. J., and Repetski, J. E., 2006, Geologic map of the Western Grove quadrangle, northwestern Arkansas: U.S. Geologic Survey, No. 2921, scale 1:24,000.

Hudson, M. R., and Turner, K. J., 2014, Geologic Map of the West-Central Buffalo National River Region, Northern Arkansas: US Geoogical Survey. Sci. Invest, No.3314 scale 1:24000, DOI: 10.3133/sim3314.

Jain, M., Murray, A. S., and Bøtter-Jensen, L., 2003, Characterization of blue-light stimulated luminescence components in different quartz samples: implications for dose

measurement. Radiation Measurements, v. 37, p. 441-449. https://doi.org/10.1016/S1350-4487(03)00052-0.

Jain, M., Murray, A. S., and Botter-Jensen, L., 2004, Optically stimulated luminescence dating: how significant is incomplete light exposure in fluvial environments: Quaternary, v. 15, p. 143-157, https://doi.org/10.3406/quate.2004.1762.

Joshi, K. B., Banerji, U. S., Dubey, C. P., and Oliveira, E. P., 2021, Heavy minerals in provenance studies: an overview. Arabian Journal of Geosciences, v. 14, p. 1-16, https://doi.org/10.1007/s12517-021-07687-y.

Keen-Zebert, Desert Research Institute, 2013, E.L. Cord Luminescence Laboratory: https://www.dri.edu/wp-content/uploads/DRILL_Fact_Sheet_Final_November2014_2.pdf.

Keen-Zebert, A., Hudson, M. R., Shepherd, S. L., and Thaler, E. A., 2017, The effect of lithology on valley width, terrace distribution, and bedload provenance in a tectonically stable catchment with flat- lying stratigraphy: Earth Surface Processes and Landforms, v. 42, p. 1573-1587, DOI: 10.1002/esp.4116.

Kincade, S. C., 2016, Sequence Stratigraphy of the St. Joe and Boone Formations, Lower Mississippian (Kinderhookian-Osagean), Southern Ozark Region: Journal of the Arkansas Academy of Science, v. 70, p. 122-125, https://doi.org/10.54119/jaas.2016.7014.

Knox, R. W. O. B., Franks, S. G., and Cocker, J. D., 2007, Stratigraphic evolution of heavy-mineral provenance signatures in the sandstones of the Wajid Group (Cambrian to Permian), southwestern Saudi Arabia: GeoArabia, v. 12, p. 65-96, https://doi.org/10.2113/geoarabia120465.

Kreutzer S., Schmidt C., Fuchs M.C., Dietze M., Fischer M., Fuchs M., 2012, Introducing an R package for luminescence dating analysis: Ancient TL, v. 30, 1-8.

Kreutzer S., Burow C. Dietze M., Fuchs M., Schmidt C., Fischer M., Friedrich J., Mercier N., Philippe A. Riedesel S., Autzen M. Mittelstrass D., Gray H., and Galharret, J., 2022, Luminescence: Comprehensive Luminescence Dating Data Analysis. R package version 0.9.20, https://CRAN.R-project.org/package=Luminescence.

Liu, X., Zhang, D., Zhai, S., Liu, X., Chen, H., Luo, W., ... and Xiu, C., 2015, A heavy mineral viewpoint on sediment provenance and environment in the Qiongdongnan Basin: Acta Oceanologica Sinica, v. 34, p. 41-55. DOI: 10.1007/s13131-015-0648-1.

Mange, M. A., and Maurer, H., 2012, Heavy minerals in colour. Springer Science & Business Media, 151 p.

McFarland, J. D., 1998, Stratigraphic summary of Arkansas: Little Rock: Arkansas Geological Commission, v. 36, p 1-44.

McFarlin, F., 2016, Lithostratigraphic Succession and Depositional Dynamics of the Lower Mississippian, Southern Ozarks, Northern Arkansas and Adjacent Areas: Journal of the Arkansas Academy of Science, v. 70(1), p. 161-166, https://doi.org/10.54119/jaas.2016.7019.

Monami, S. J., Uddin, A., and Hames, W. E., 2022, Multi-proxy provenance of the lower Pennsylvanian Pottsville sandstone of the northern Appalachian basin in Pennsylvania, USA: Paleodrainage, sources, and detrital history: Journal of Sedimentary Research, v. 92, p.304-319, doi: 10.2110/jsr.2020.189.

Morton, A. C., 1991, Geochemical studies of detrital heavy minerals and their application to provenance research: Geological Society, London, Special Publications, v. 57, p. 31-45. https://doi.org/10.1144/GSL.SP.1991.057.01.04.

Morton, A. C., and Hallsworth, C., 1994, Identifying provenance-specific features of detrital heavy mineral assemblages in sandstones: Sedimentary Geology, v. 90, p. 241-256, https://doi.org/10.1016/0037-0738(94)90041-8.

Morton, A. C., and Hallsworth, C. R., 1999, Processes controlling the composition of heavy mineral assemblages in sandstones: Sedimentary geology, v. 124, p. 3-29.

National Weather Service, 2023, Rivers of the U.S. https://www.weather.gov/gis/Rivers.

Nian, X., Zhang, W., Qiu, F., Qin, J., Wang, Z., Sun, Q., ... and Liu, N., 2019, Luminescence characteristics of quartz from Holocene delta deposits of the Yangtze River and their provenance implications. Quaternary Geochronology, v. 49, p. 131-137. https://doi.org/10.1016/j.quageo.2018.04.010.

Olley, J. M., Pietsch, T., and Roberts, R. G., 2004, Optical dating of Holocene sediments from a variety of geomorphic settings using single grains of quartz: Geomorphology, v. 60, p. 337-358, https://doi.org/10.1016/j.geomorph.2003.09.020.

Pan, B., Pang, H., Gao, H., Garzanti, E., Zou, Y., Liu, X., ... and Jia, Y., 2016, Heavy-mineral analysis and provenance of Yellow River sediments around the China Loess Plateau. Journal of Asian Earth Sciences, v. 127, p. 1-11. https://doi.org/10.1016/j.jseaes.2016.06.006.

Poole, F. G., Perry, W. J., Madrid, R. J., and Amaya-Martínez, R.,2005, Tectonic synthesis of the Ouachita-Marathon-Sonora orogenic margin of southern Laurentia: Stratigraphic and structural implications for timing of deformational events and plate-tectonic model:Geological Society of America Special Paper 393, 54 p. https://doi.org/10.1130/0-8137-2393-0.543.

Pradhan, A. S., Lee, J. I., and Kim, J. L., 2008, Recent developments of optically stimulated luminescence materials and techniques for radiation dosimetry and clinical applications: Journal of medical physics/Association of Medical Physicists of India, v. 33(3), 85.

Rhodes, E. J., 2011, Optically stimulated luminescence dating of sediments over the past 200,000 years: Annual Review of Earth and Planetary Sciences, v. 39, p. 461-488, doi: 10.1146/annurev- earth-040610-133425.

Rodrigues, K., Keen-Zebert, A., Shepherd, S.L., Hudson, M.R., Bitting, C.J., Johnson, B.G., Langston, A. In Prep. The role of lithology and climate on bedrock river incision and terrace development along the Buffalo National River, Arkansas.

Rodrigues, K., Rink, W. J., Collins, M. B., Williams, T. J., Keen-Zebert, A., and López, G. I., 2016, OSL ages of the Clovis, Late Paleoindian, and Archaic components at Area 15 of

the Gault site, central Texas, USA: Journal of Archaeological Science: Reports, v. 7, p. 94-103, https://doi.org/10.1016/j.jasrep.2016.03.014.

Sharrah, K. L., 2006, Comparative study of the sedimentology and provenance of the Atoka Formation in the frontal Ouachita thrust belt, Oklahoma [Ph.D. thesis]: The University of Tulsa, 268 p.

Simbo, C. W., Potra, A., and Samuelsen, J. R., 2019, A geochemical evaluation of the genetic relationship between Ouachita Mountains Paleozoic rocks and the Mississippi Valley-type mineralization in the southern Ozark Region, USA: Ore Geology Reviews, v. 112, p. 1-18. DOI: 103029.

Thomas, W. A., 2011, Detital-zircon geochronology and sedimentary provenance: Lithosphere, v. 3, p.304-308. https://doi.org/10.1130/RF.L001.1.

Thomas, W. A., Gehrels, G. E., Sundell, K. E., and Romero, M. C., 2021, Detrital-zircon analyses, provenance, and late Paleozoic sediment dispersal in the context of tectonic evolution of the Ouachita orogen: Geosphere, v. 17, p. 1214-1247. https://doi.org/10.1130/GES02288.1.

Tsukamoto, S., Nagashima, K., Murray, A. S., and Tada, R., 2011, Variations in OSL components from quartz from Japan sea sediments and the possibility of reconstructing provenance. Quaternary International, v. 23, p. 182-189, https://doi.org/10.1016/j.quaint.2010.09.003.

Turner, K. J., and Hudson, M. R., 2010, Geologic map of the Maumee Quadrangle, Searcy and Marion Counties, Arkansas: US Geological Survey Scientific Investigations Map, No. 3134(1), scale 1:24,000, DOI: 10.3133/sim3134.

Uddin, A., & Lundberg, N., 1998, Unroofing history of the eastern Himalaya and the Indo-Burman ranges; heavy-mineral study of Cenozoic sediments from the Bengal Basin, Bangladesh. *Journal of Sedimentary Research*, v. *68*, p. 465-472. https://doi.org/10.2110/jsr.68.465.

Uddin, A., Hames, W. E., Peavy, T., and Pashin, J. C., 2016, Detrital history of the Lower Pennsylvanian Pottsville Formation in the Cahaba synclinorium of Alabama, USA: Journal of Sedimentary Research, v. 86, p.1287-1297. https://doi.org/10.2110/jsr.2016.76.

USDA, Geospatial Data Gateway, 2023, Direct Data/ NAIP Download. https://datagateway.nrcs.usda.gov/GDGHome_DirectDownLoad.aspx.

Wintle, A. G., and Adamiec, G., 2017, Optically stimulated luminescence signals from quartz: A review: *Radiation Measurements*, v. *98*, p. 10-33. https://doi.org/10.1016/j.radmeas.2017.02.003

Xie, X., Cains, W., and Manger, W. L., 2016, U–Pb detrital zircon evidence of transcontinental sediment dispersal: provenance of Late Mississippian Wedington Sandstone member, NW Arkansas: International Geology Review, v. 58, p. 1951-1966, https://doi.org/10.1080/00206814.2016.1193775.

Xie, X., Buratowski, G., Manger, W. L., and Zachry, D., 2018, U-Pb detrital-zircon geochronology of the middle Bloyd sandstone (Morrowan) of northern Arkansas (USA):

Implications for Early Pennsylvanian sediment dispersal in the Laurentian foreland: Journal of Sedimentary Research, v. 88, p. 795-810, https://doi.org/10.2110/jsr.2018.47.

Zular, A., Sawakuchi, A. O., Guedes, C. C., and Giannini, P. C., 2015, Attaining provenance proxies from OSL and TL sensitivities: Coupling with grain size and heavy minerals data from southern Brazilian coastal sediments: Radiation Measurements, v. 81, p. 39-45, https://doi.org/10.1016/j.radmeas.2015.04.010.

Appendix A:

Heavy Mineral SEM Analysis**:**

This section includes representative SEM data from the initial heavy mineral separation of the sandstone samples. These elemental maps were collected at the Desert Research Institute with the TM4000 tabletop SEM. Elemental analysis was completed for eight of the nine heavy mineral samples. SEM analysis was not completed for sample MBv-1 due to a loss of sample prior to the analysis. OE and MBv samples have a more consistent assigned color scheme of minerals while the elemental maps for the PB samples were created prior to assigning colors to common elements.

Figure A.1: Elemental maps of heavy minerals from sandstones in the BNR. A-C) Everton heavy minerals, D-E) Batesville Heavy Minerals, and F-I) Bloyd sandstone heavy minerals assemblage

A) OE-1

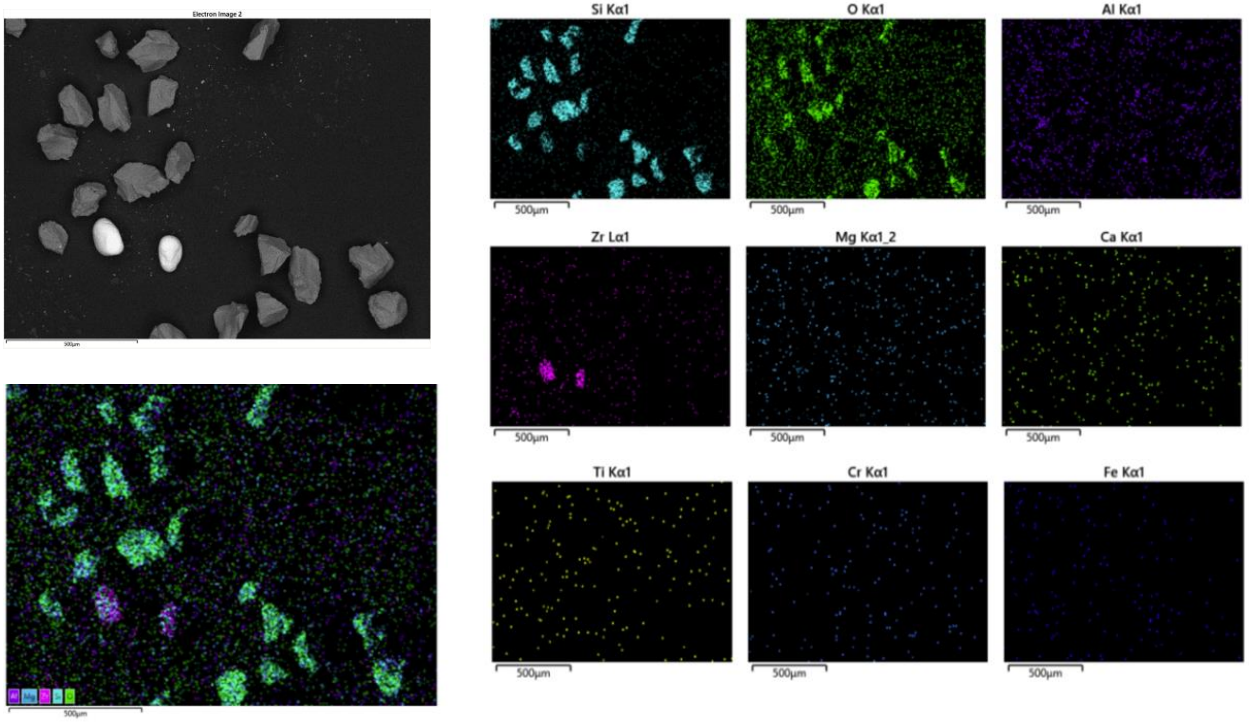

B) OE-2

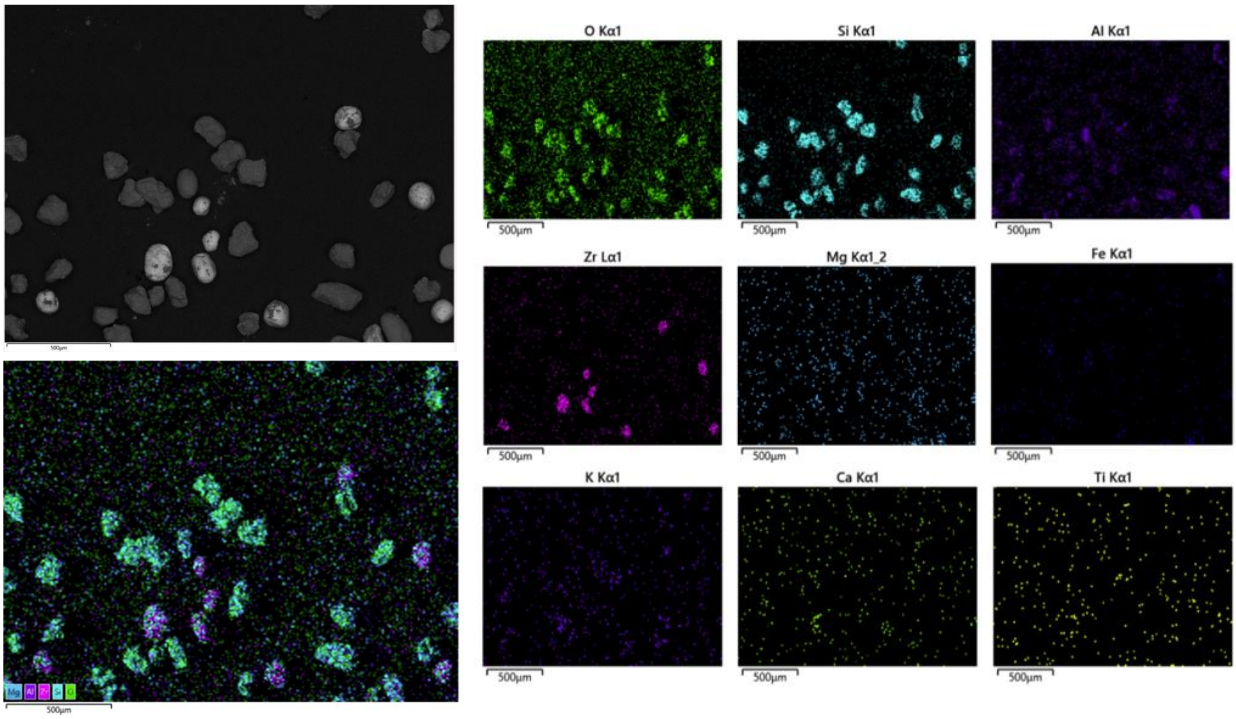
O Kα1
Si Kα1
Al Kα1
Zr Lα1
Mg Kα1_2
Fe Kα1
K Kα1
Ca Kα1
Ti Kα1
500µm

C) OE-3

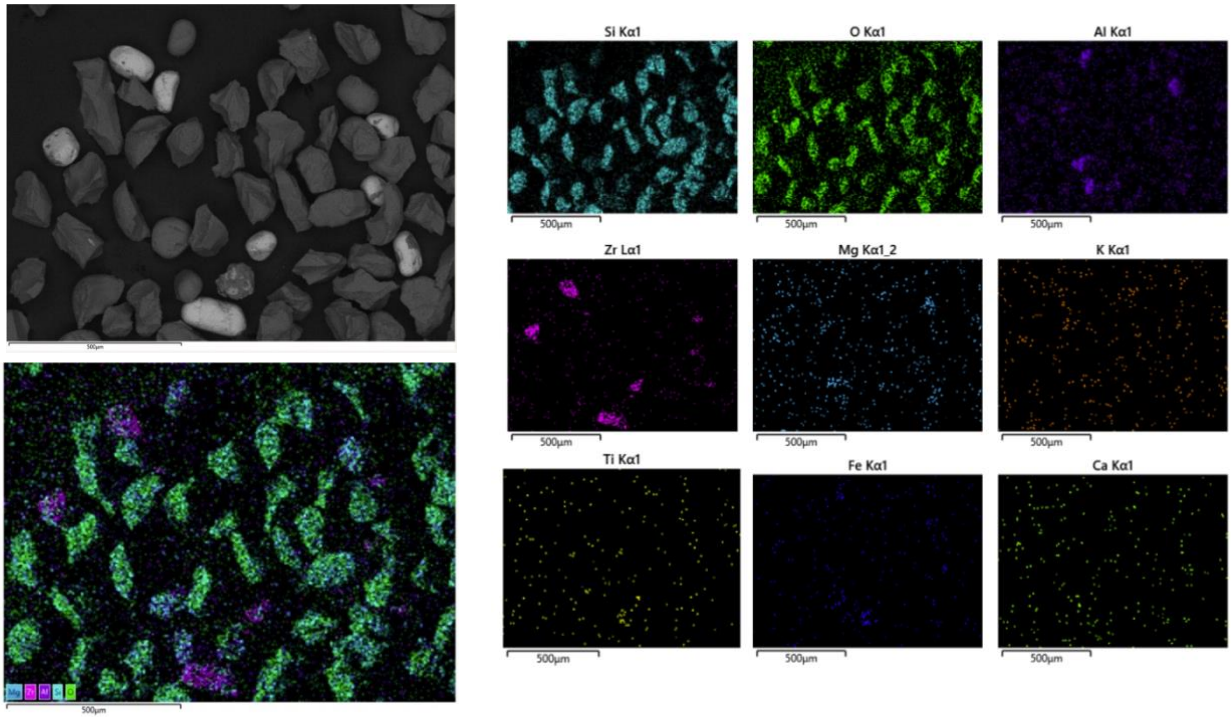
Si Kα1
O Kα1
Al Kα1
Zr Lα1
Mg Kα1_2
K Kα1
Ti Kα1
Fe Kα1
Ca Kα1
500µm

D) MBv-2

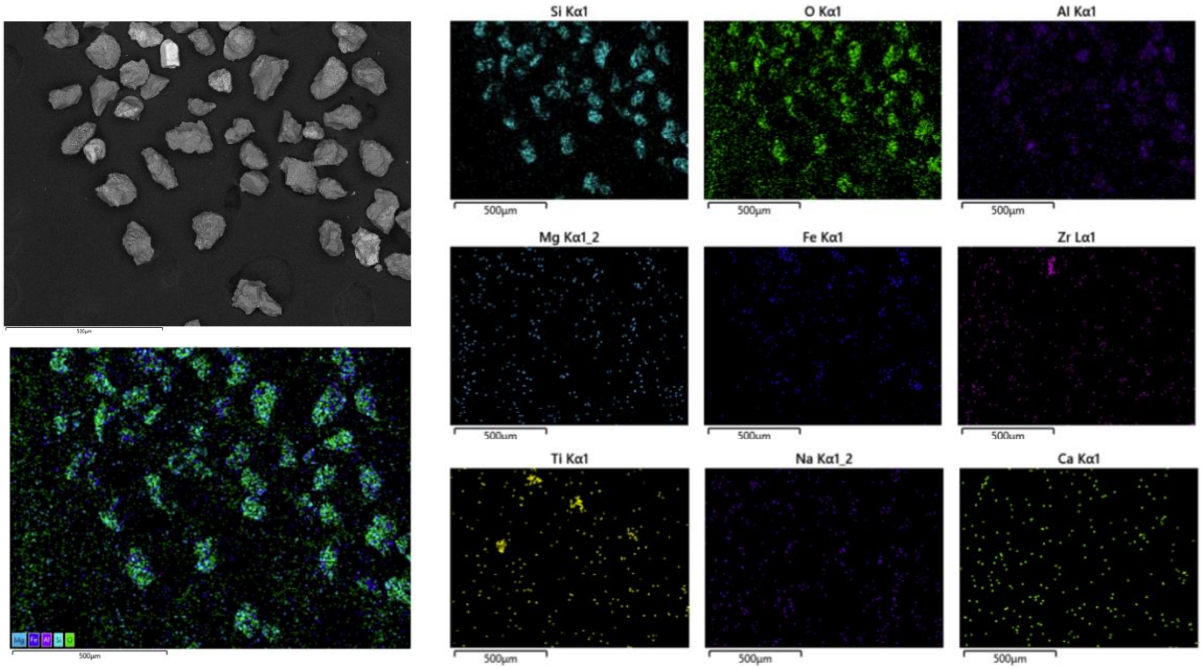
Si Kα1
O Kα1
Al Kα1
Mg Kα1_2
Fe Kα1
Zr Lα1
Ti Kα1
Na Kα1_2
Ca Kα1
500µm

E) MBv-3

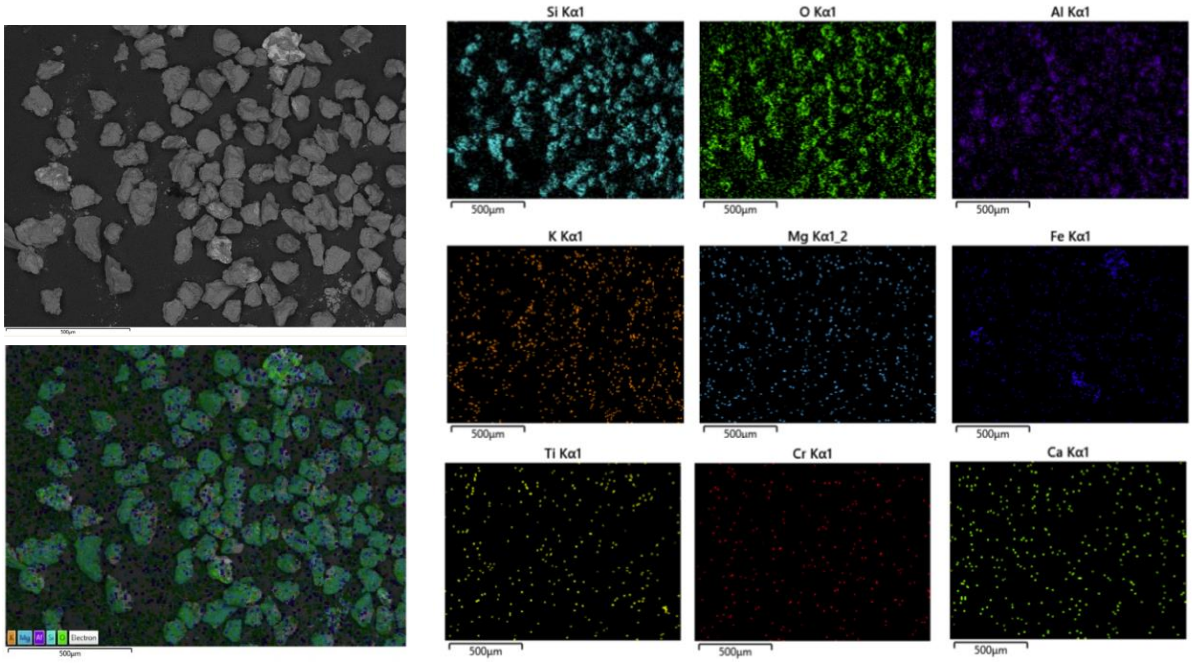
Si Kα1
O Kα1
Al Kα1
K Kα1
Mg Kα1_2
Fe Kα1
Ti Kα1
Cr Kα1
Ca Kα1
500µm

F) PB-1

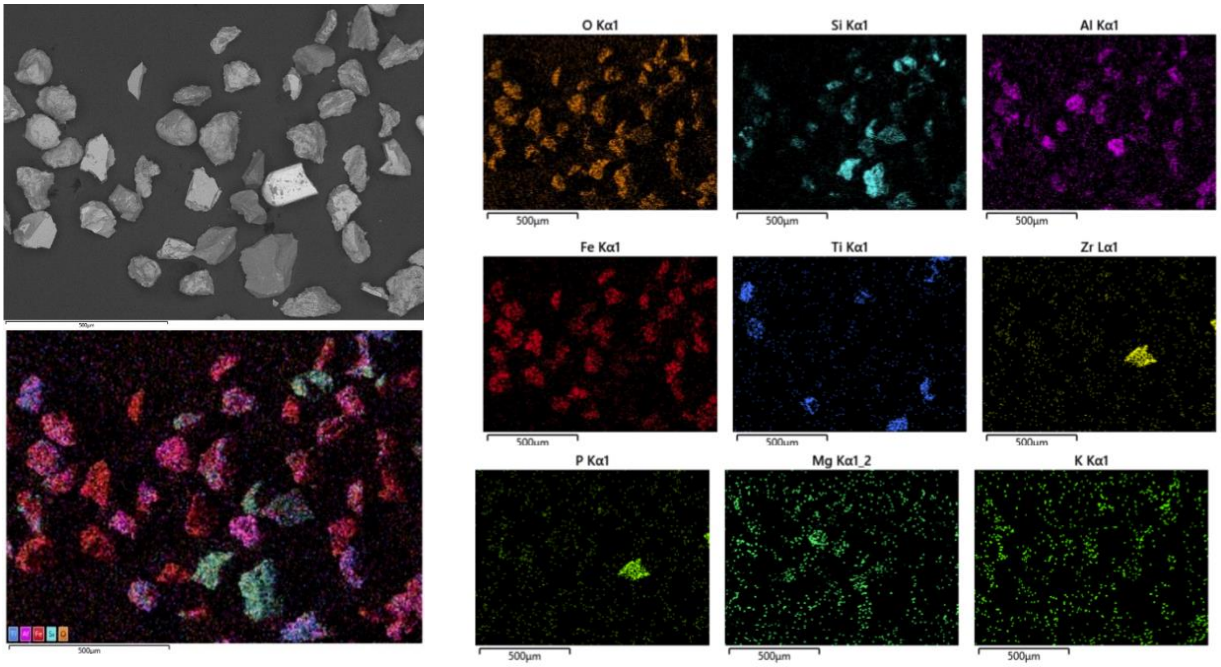
O Kα1
Si Kα1
Al Kα1
Fe Kα1
Ti Kα1
Zr Lα1
P Kα1
Mg Kα1_2
K Kα1
500µm

H) PB-2

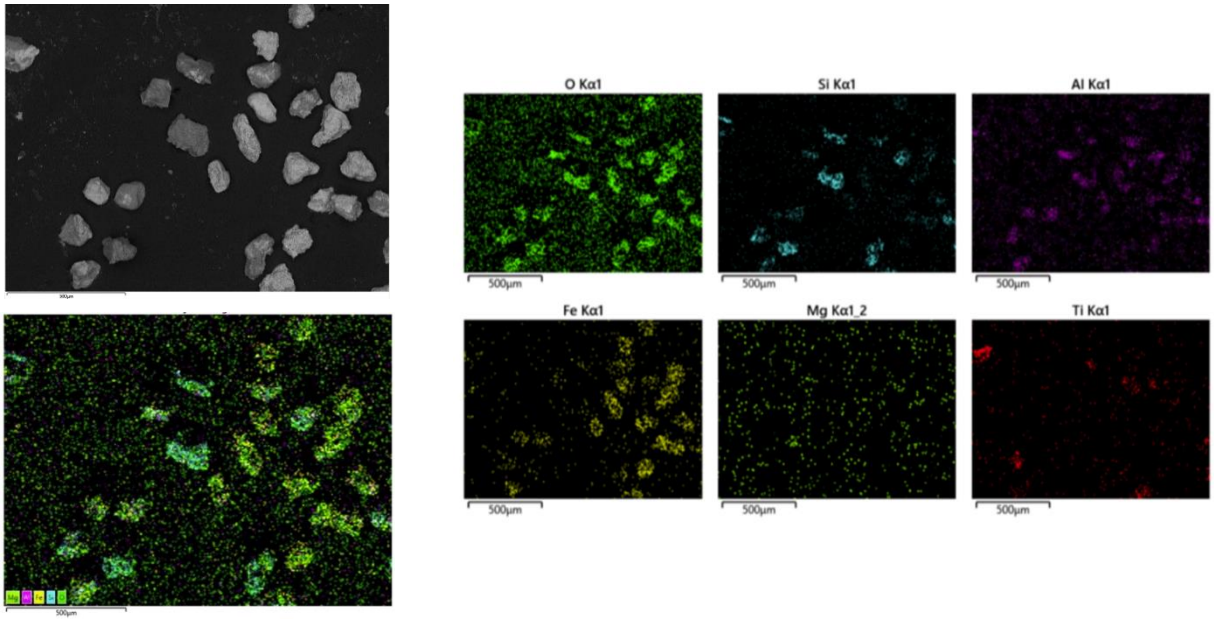
O Kα1
Si Kα1
Al Kα1
Fe Kα1
Mg Kα1_2
Ti Kα1
500µm

I) PB-3

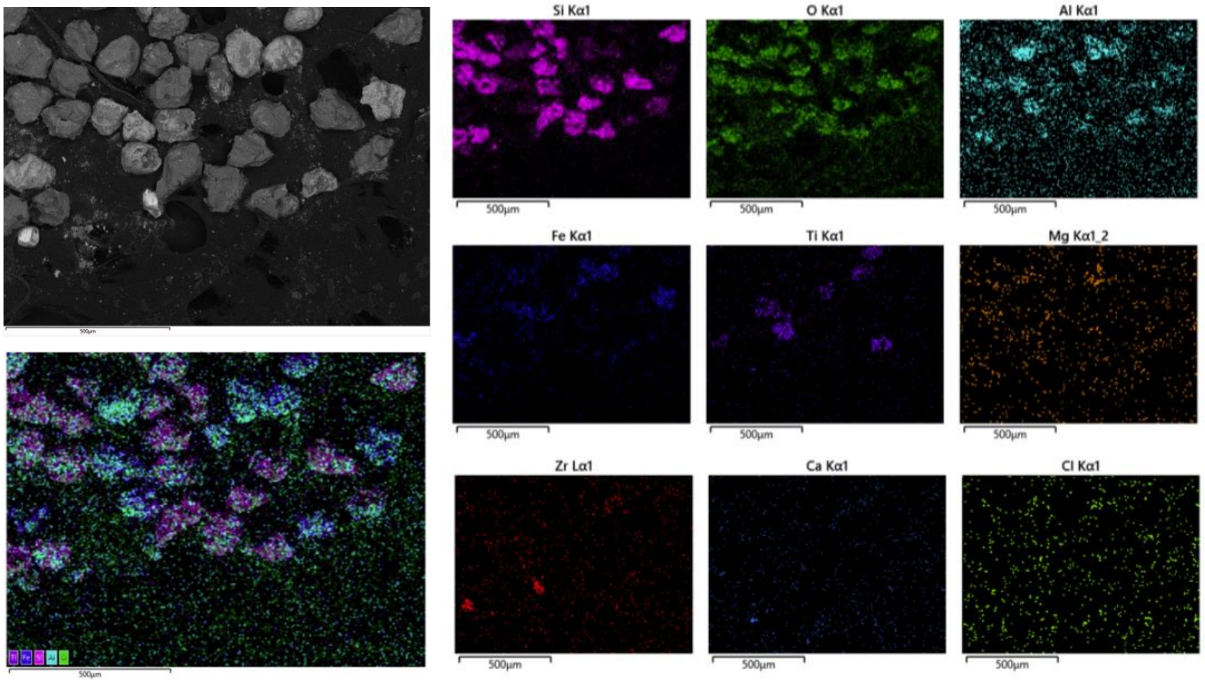

Sample	Zircon	Rutile	Touraline	Opaques	Alterations	Others	total	RZi	ZTR-Index
OE-1	243	18	16	38	24	11	350	6.896551724	79.14285714
Oe-2	83	29	55	30	108	38	343	25.89285714	48.68804665
Oe-3	139	25	30	18	93	15	320	15.24390244	60.625
MBv-1	3			36	43		82	0	3.658536585
MBv-2	109	10	3	35	192	62	411	8.403361345	29.6836983
MBv-3	14	7	6	71	175	89	362	33.33333333	7.458563536
PB-1	13	11	6	308	70	28	436	45.83333333	6.880733945
PB-2	8	12	23	228	133	21	425	60	10.11764706
PB-3	99	5	13	197	33	65	412	4.807692308	28.39805825

Table A.1 Heavy mineral smear slide count

Appendix B: CW-OSL data

This appendix contains the data used to calculate the OSL (Table B.1) and TL (Table B.2) sensitivity measurements. The resulting OSL decay curves (Figure B.1) and TL glow curves (Figure B.2).

Table B.1 depicts the calculation for OSL Sensitivity of the BNR sandstones.

	Int 1	Int 2	Background normalize	Net signal	weight(mg)	Sensitivity (counts/sec*gray*mg)
OE1						
1	12032	5181	117.75	11914.25	0.52	1363.810668
2	57949	32123	730.0681818	57218.93	0.64	5321.701248
3	14506	7379	167.7045455	14338.3	0.64	1333.546824
4	27864	11810	268.4090909	27595.59	0.53	3099.235277
5	11927	7831	177.9772727	11749.02	0.31	2255.956745
6	20889	10543	239.6136364	20649.39	0.73	1683.739919
7	15899	9484	215.5454545	15683.45	0.7	1333.627087
8	80923	23821	541.3863636	80381.61	0.85	5628.96454
9	17349	9280	210.9090909	17138.09	0.71	1436.795012
10	13620	7851	178.4318182	13441.57	0.64	1250.14585
Average						2470.752317
Standard Deviation						1684.34915
Relative Standard error						68.17150947
Standard Error						532.6379688
OE2						
1	10695	6618	150.4090909	10544.59	0.86	729.8304893
2	33034	13076	297.1818182	32736.82	0.85	2292.49427
3	33165	14854	337.5909091	32827.41	0.75	2605.349928
4	21930	8580	195	21735	1.02	1268.382353
5	9031	3350	76.13636364	8954.864	0.52	1025.053072
6	12728	6254	142.1363636	12585.86	0.77	972.9331815
7	14456	9119	207.25	14248.75	0.94	902.2764691
8	41837	14898	338.5909091	41498.41	1.08	2287.169813
9	64667	26449	601.1136364	64065.89	0.64	5958.508776
10	11899	5600	127.2727273	11771.73	0.69	1015.504423
Average						1905.750278
Standard Deviation						1579.157328
Relative Standard error						82.86276256
Standard Error						499.3733939
MBv-1						
1	2896	1913	43.47727273	2852.523	0.36	471.6472763
2	6292	2619	59.52272727	6232.477	0.68	545.5599854
3	2578	1875	42.61363636	2535.386	0.44	342.9905795
4	4889	2228	50.63636364	4838.364	0.73	394.5175829
5	3080	1966	44.68181818	3035.318	0.92	196.3844579
6	4530	2566	58.31818182	4471.682	0.59	451.138198
7	4224	2591	58.88636364	4165.114	0.96	258.2535737
8	4072	2216	50.36363636	4021.636	0.71	337.1593196
9					0.55	
10					0.41	
Average						374.7063716
Standard Deviation						115.0145557
Relative Standard error						30.69458232
Standard Error						40.66378613

Table B.1 (con't)

	Int 1	Int 2	Background normalize	Net signal	weight(mg)	Sensitivity (counts/sec*gray*mg)
Mbv-2						
1	2896	1762	40.04545455	2855.955	0.42	404.7554628
2	6292	2382	54.13636364	6237.864	0.43	863.491644
3	2578	1699	38.61363636	2539.386	0.41	368.6681713
4	4889	2020	45.90909091	4843.091	0.47	613.3600442
5	3080	1817	41.29545455	3038.705	0.52	347.8370588
6	4530	2328	52.90909091	4477.091	0.44	605.6670602
7	4224	2333	53.02272727	4170.977	0.82	302.7712887
8	4072	1982	45.04545455	4026.955	0.55	435.8175915
9					0.45	
10					0.76	
Average						492.7960402
Standard Deviation						188.3077664
Relative Standard error						38.21211029
Standard Error						66.57684928
PB-1						
1	17520	8710	197.9545455	17322.05	0.84	1227.469207
2	4892	3061	69.56818182	4822.432	0.63	455.6341476
3	7091	3880	88.18181818	7002.818	0.72	578.9366883
4	3100	2141	48.65909091	3051.341	0.58	313.1507501
5	4232	2482	56.40909091	4175.591	0.27	920.544733
6	6297	3236	73.54545455	6223.455	0.96	385.8788781
7	14172	5091	115.7045455	14056.3	0.8	1045.855317
8	6196	2933	66.65909091	6129.341	0.49	744.5749404
9					0.32	
10					0.66	
Average						709.0055827
Standard Deviation						331.7729822
Relative Standard error						46.79412832
Standard Error						117.2994627
PB-2						
1	3033	1673	38.02272727	2994.977	1.14	156.379348
2	8748	4446	101.0454545	8646.955	0.45	1143.777056
3	6340	2141	48.65909091	6291.341	0.42	891.6299474
4	2938	1799	40.88636364	2897.114	0.26	663.2586164
5	1957	1757	39.93181818	1917.068	0.44	259.3436393
6	10065	6624	150.5454545	9914.455	0.61	967.4526293
7	6383	4546	103.3181818	6279.682	0.47	795.2991158
8	19219	8916	202.6363636	19016.36	0.63	1796.708582
9	10285	3895	88.52272727	10196.48	0.59	1028.70029
10					0.4	
Average						855.8388028
Standard Deviation						487.027504
Relative Standard error						56.90645276
Standard Error						162.3425013

Table B.2: Table of TL Sensitivity calculations for the sandstones in the BNR

	Int 1 (Dose)	(background)	Background Normalize	Net signal	mass (mg)	Net Sensitivity (counts/gray*mg*C)
OE1						
1	327020	702	702	326318	0.52	7470.650183
2	1845759	664	664	1845095	0.64	34320.96354
3	482290	773	773	481517	0.64	8956.789435
4	804529	708	708	803821	0.53	18055.27853
5	441669	723	723	440946	0.31	16933.41014
6	716235	721	721	715514	0.73	11668.52577
7	484204	734	734	483470	0.7	8222.278912
8	1780149	733	733	1779416	0.85	24921.79272
9	677170	730	730	676440	0.71	11342.05231
10	504300	717	717	503583	0.64	9367.243304
Average						15125.89848
Std Dev						8692.347566
Relative Std Dev						4783.229086
Std Error						2748.761652
OE2						
1	228513	753	753	227760	0.86	3152.82392
2	759006	764	764	758242	0.85	10619.63585
3	679071	751	751	678320	0.75	10766.98413
4	512543	681	681	511862	1.02	5974.112979
5	151231	744	744	150487	0.52	3445.215201
6	287458	703	703	286755	0.77	4433.441558
7	298022	779	779	297243	0.94	3764.475684
8	809638	740	740	808898	1.08	8916.424162
9	1189216	779	779	1188437	0.64	22106.34301
10	203570	756	756	202814	0.69	3499.206349
Average						7667.866284
Std Dev						5892.621176
Relative Std Dev						76.84825162
Std Error						1863.410431
MBv-1						
1	28923	704	704	28219	0.36	933.1679894
2	114481	792	18	114463	0.68	10019.52031
3	44491	747	16.97727273	44474.02273	0.44	6016.507404
4	82925	722	16.40909091	82908.59091	0.73	6760.322155
5	24091	772	17.54545455	24073.45455	0.92	1557.547525
6	75550	799	18.15909091	75531.84091	0.59	7620.242222
7	82652	746	16.95454545	82635.04545	0.96	5123.700735
8	84708	777	17.65909091	84690.34091	0.71	7100.129184
9					0.55	
10					0.41	
Average						5641.39219
Std Dev						3064.022785
Relative Standard Deviation						54.31323832
Standard Error						1083.295645

Table B.2 (Con't)

	Int 1 (Dose)	(background)	Background Normalize	Net signal	mass (mg)	Net Sensitivity (counts/gray*mg*C)
Mbv-2						
1	101074	798	798	100276	0.42	2842.290249
2	205600	685	685	204915	0.43	5673.172757
3	140649	775	775	139874	0.41	4061.382114
4	92818	782	782	92036	0.47	2331.205674
5	181903	789	789	181114	0.52	4146.382784
6	83530	748	748	82782	0.44	2239.772727
7	166813	788	788	166025	0.82	2410.351336
8	105342	702	702	104640	0.55	2264.935065
9	223373	735	735	222638	0.45	5889.89418
10	60415	791	791	59624	0.76	933.9598997
Average						3279.334679
Std Dev						1611.22518
Relative Standard Error						49.13268508
Standard Error						509.5141394
PB-1						
1	817648	694	694	816954	0.84	11578.14626
2	245842	716	716	245126	0.63	4632.010582
3	435545	793	793	434752	0.72	7188.359788
4	193001	749	749	192252	0.58	3946.059113
5	230039	725	725	229314	0.27	10110.84656
6	420284	724	724	419560	0.96	5202.876984
7	646773	693	693	646080	0.8	9614.285714
8	368923	758	758	368165	0.49	8944.727891
9					0.32	
10					0.66	
Average						7467.512143
Std Dev						2829.683501
Relative Standard Deviation						37.8932561
Standard Error						1000.444196
PB-2						
1	48375	664	15.09090909	48359.90909	1.14	505.011582
2	317401	729	16.56818182	317384.4318	0.45	41982.0677
3	144399	658	14.95454545	144384.0455	0.42	20462.59148
4	81653	759	17.25	81635.75	0.26	18689.50321
5	54795	697	15.84090909	54779.15909	0.44	7410.600526
6	512394	782	17.77272727	512376.2273	0.61	49997.68026
7	321425	754	17.13636364	321407.8636	0.47	40705.1499
8	783801	722	16.40909091	783784.5909	0.63	74053.72174
9	335322	812	812	334510	0.59	33747.98224
10					0.4	
Average						31950.47874
Std Dev						22852.08051
Relative Standard Error						71.52343695
Standard Error						7226.46237

Figure B.2: OSL Decay Curves created from CW-OSL analysis

A) OE

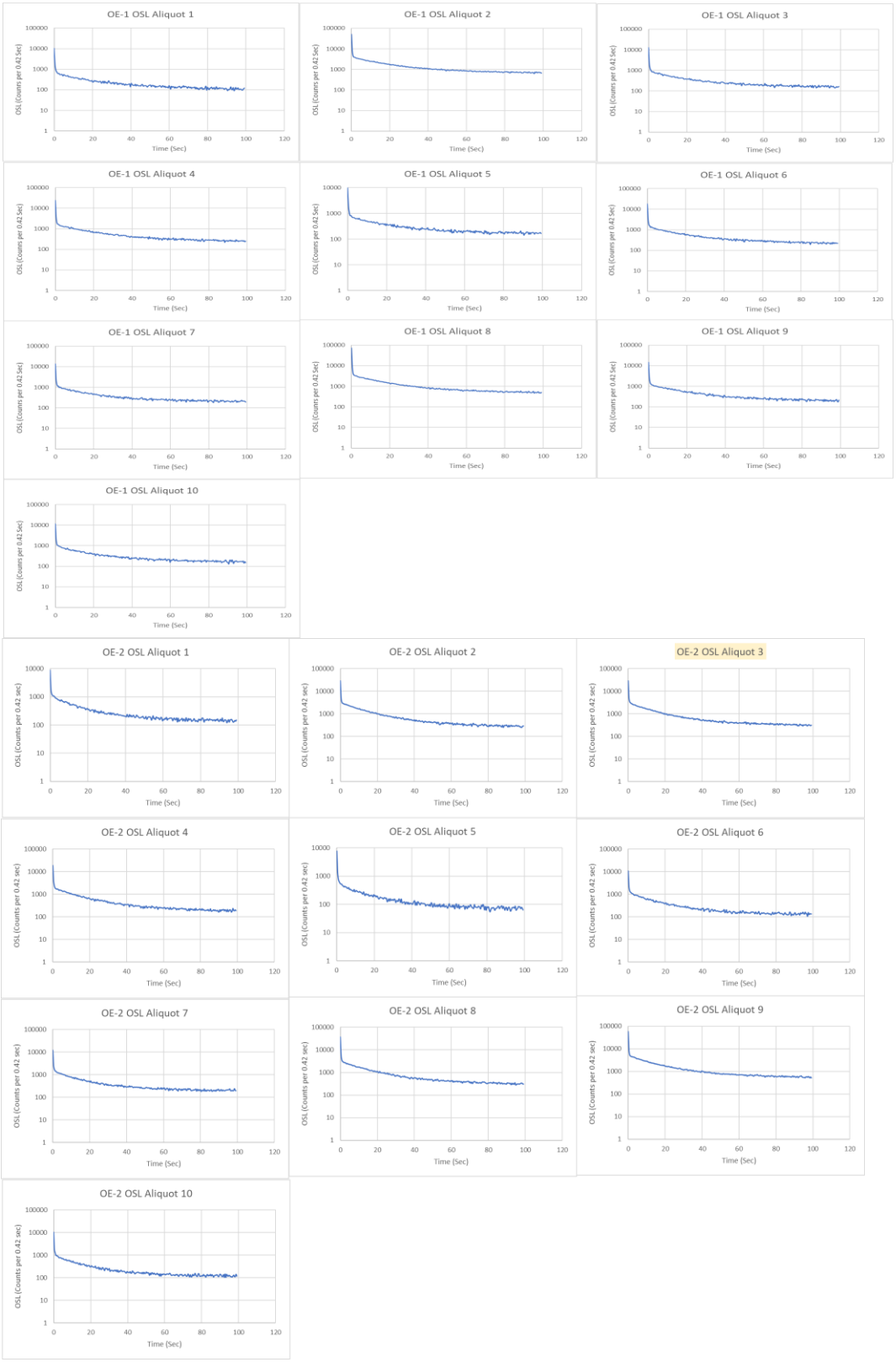

B) MBv

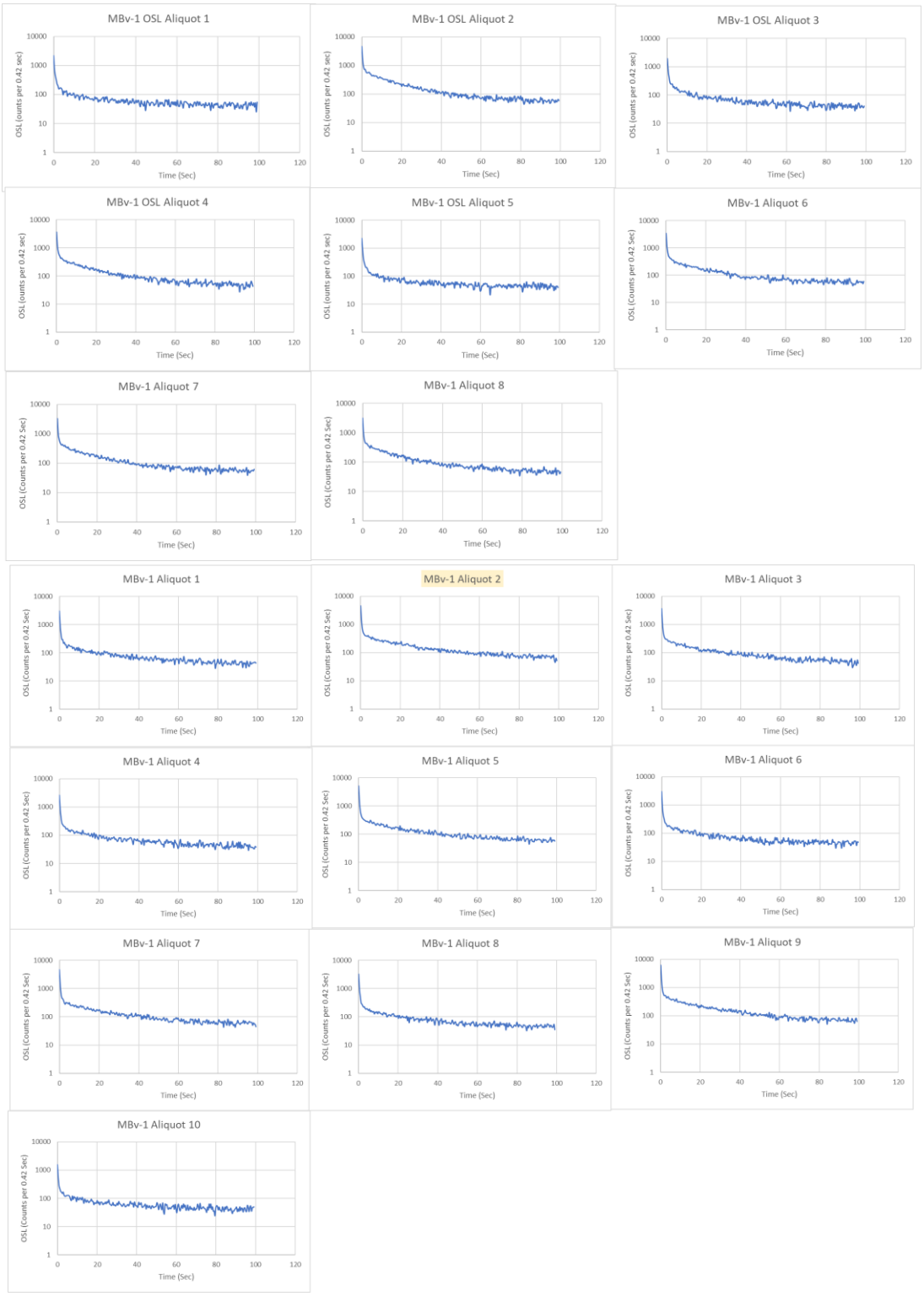
MBv-1 OSL Aliquot 1
MBv-1 OSL Aliquot 2
MBv-1 OSL Aliquot 3
MBv-1 OSL Aliquot 4
MBv-1 OSL Aliquot 5
MBv-1 Aliquot 6
MBv-1 Aliquot 7
MBv-1 Aliquot 8
MBv-1 Aliquot 1
MBv-1 Aliquot 2
MBv-1 Aliquot 3
MBv-1 Aliquot 4
MBv-1 Aliquot 5
MBv-1 Aliquot 6
MBv-1 Aliquot 7
MBv-1 Aliquot 8
MBv-1 Aliquot 9
MBv-1 Aliquot 10
OSL (counts per 0.42 sec)
OSL (Counts per 0.42 Sec)
Time (Sec)

C) PB

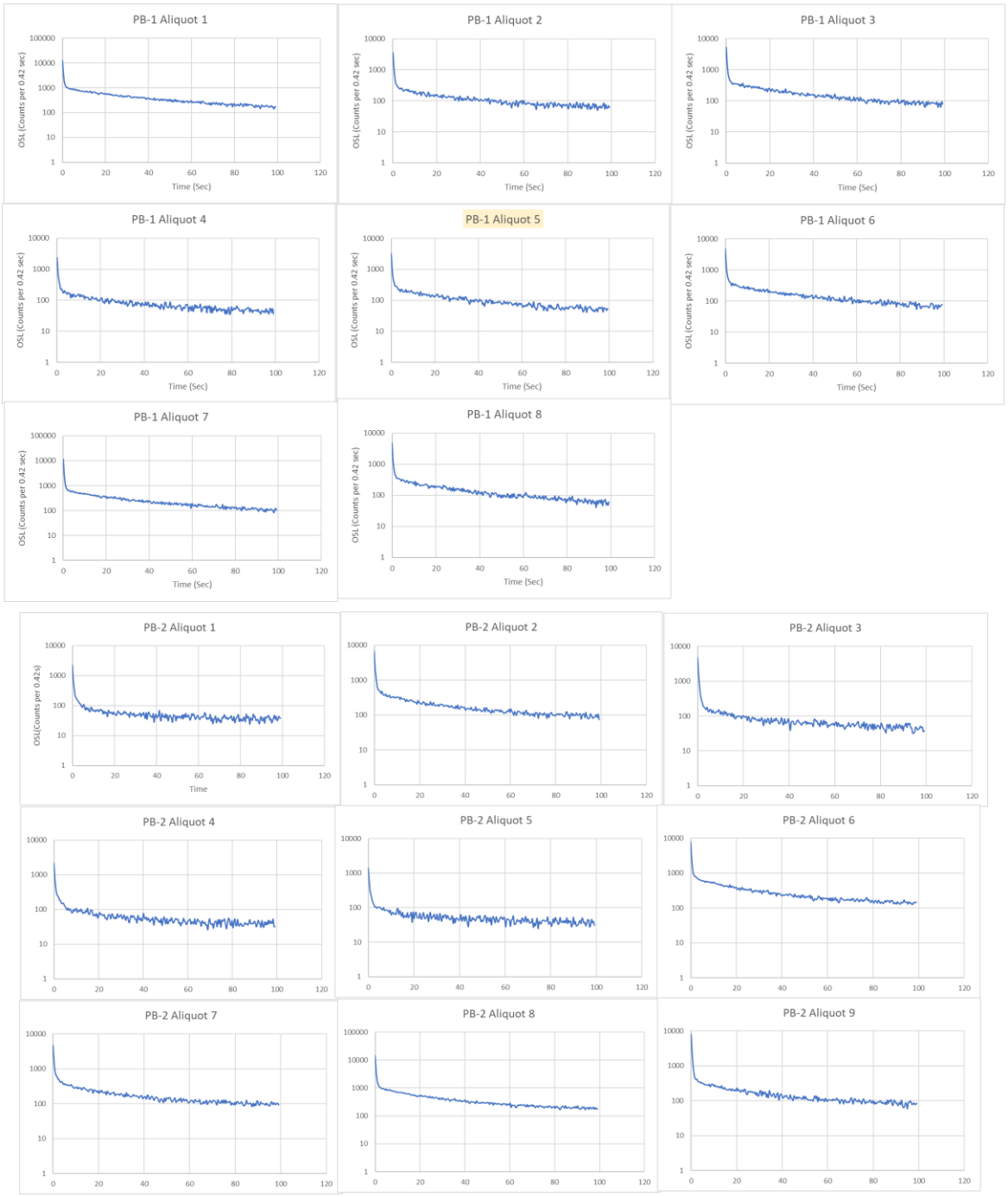
PB-1 Aliquot 1
PB-1 Aliquot 2
PB-1 Aliquot 3
PB-1 Aliquot 4
PB-1 Aliquot 5
PB-1 Aliquot 6
PB-1 Aliquot 7
PB-1 Aliquot 8
PB-2 Aliquot 1
PB-2 Aliquot 2
PB-2 Aliquot 3
PB-2 Aliquot 4
PB-2 Aliquot 5
PB-2 Aliquot 6
PB-2 Aliquot 7
PB-2 Aliquot 8
PB-2 Aliquot 9
OSL (Counts per 0.42 sec)
Time (Sec)
Time

Figure B.1: TL glow curves created from CW-OSL analysis

A) OE samples

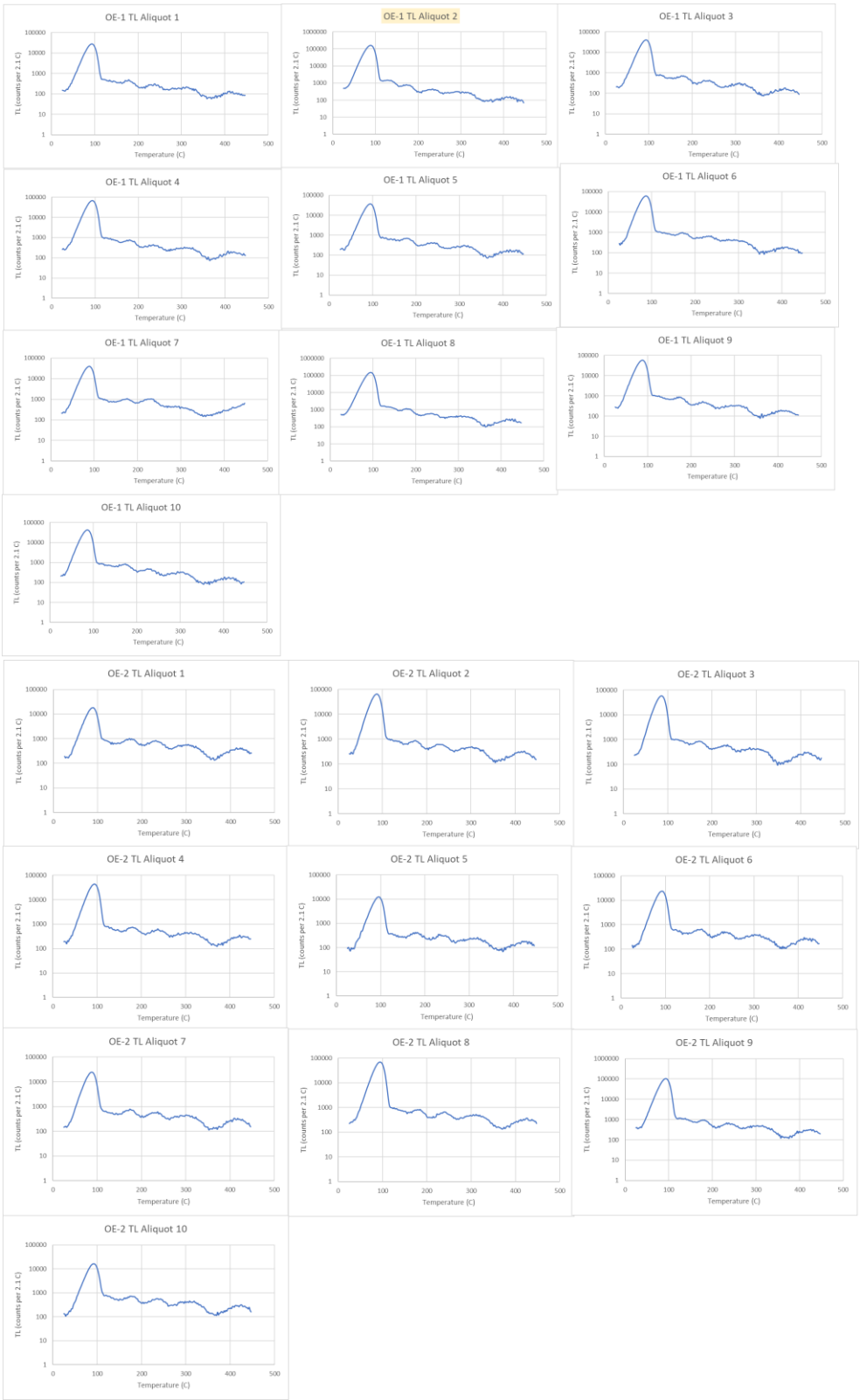

B) MBv Samples

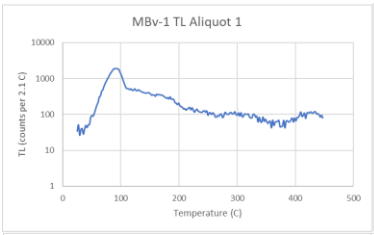

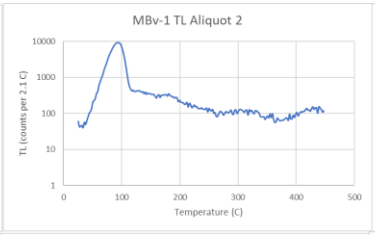

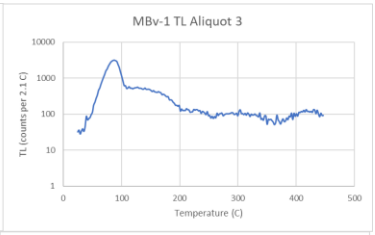

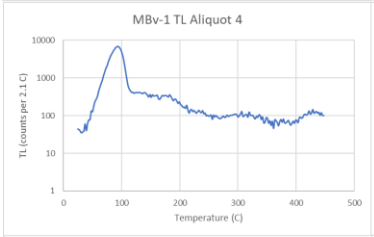

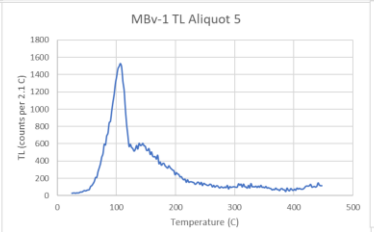

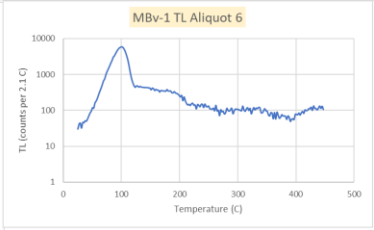

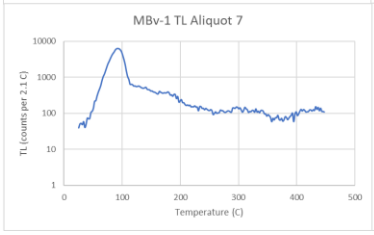

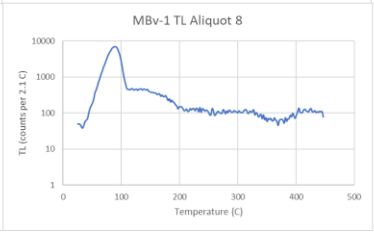

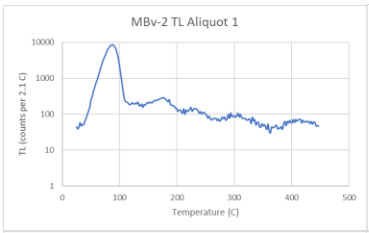

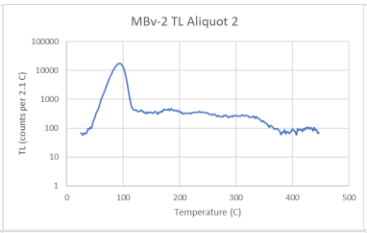

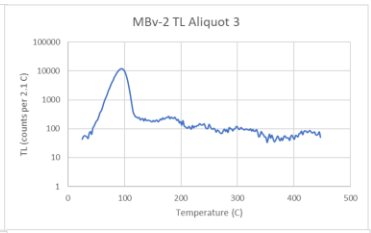

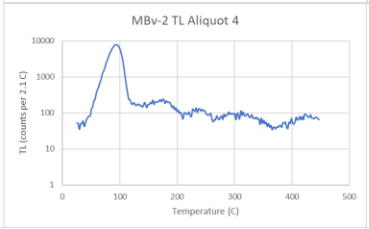

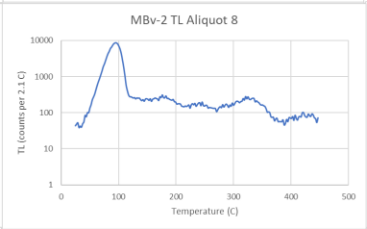

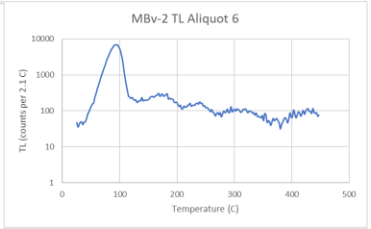

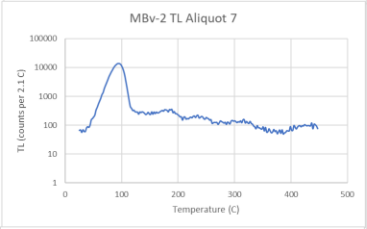

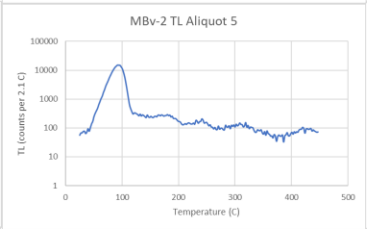

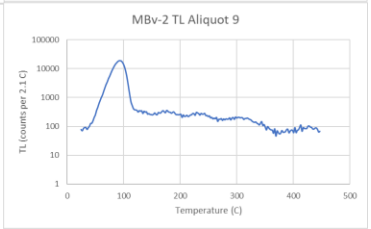

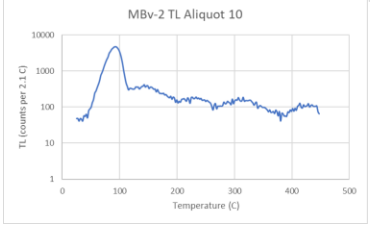

C) PB Samples

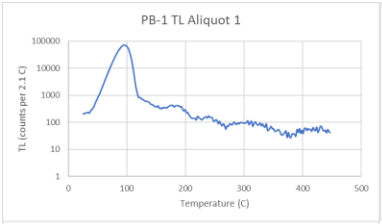
PB-1 TL Aliquot 1
TL (counts per 2.1 C)
Temperature (C)

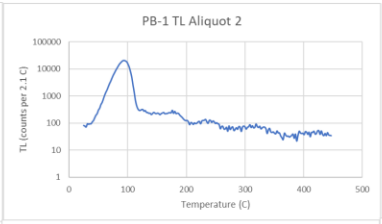
PB-1 TL Aliquot 2
TL (counts per 2.1 C)
Temperature (C)

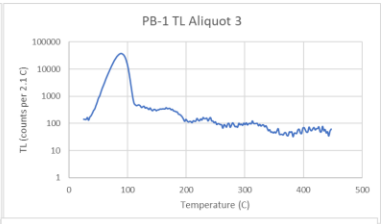
PB-1 TL Aliquot 3
TL (counts per 2.1 C)
Temperature (C)

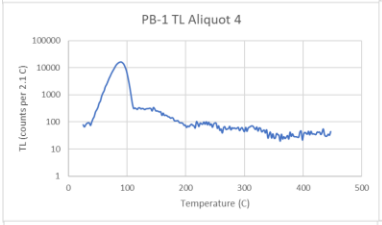
PB-1 TL Aliquot 4
TL (counts per 2.1 C)
Temperature (C)

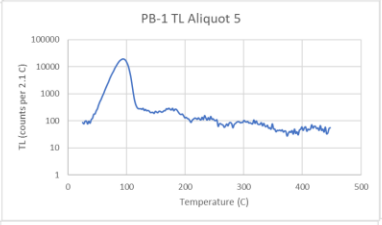
PB-1 TL Aliquot 5
TL (counts per 2.1 C)
Temperature (C)

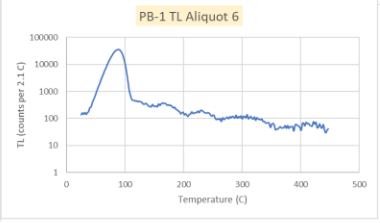
PB-1 TL Aliquot 6
TL (counts per 2.1 C)
Temperature (C)

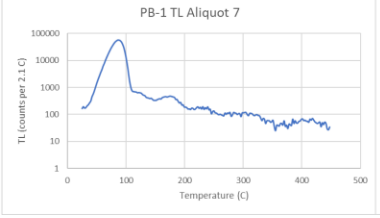
PB-1 TL Aliquot 7
TL (counts per 2.1 C)
Temperature (C)

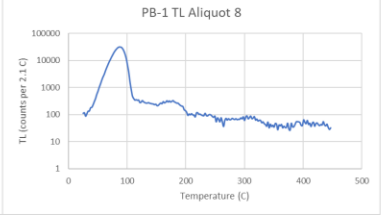
PB-1 TL Aliquot 8
TL (counts per 2.1 C)
Temperature (C)

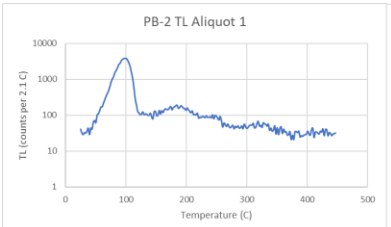
PB-2 TL Aliquot 1
TL (counts per 2.1 C)
Temperature (C)

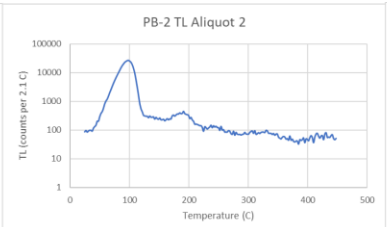
PB-2 TL Aliquot 2
TL (counts per 2.1 C)
Temperature (C)

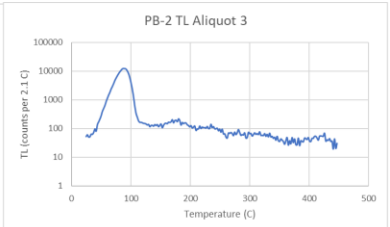
PB-2 TL Aliquot 3
TL (counts per 2.1 C)
Temperature (C)

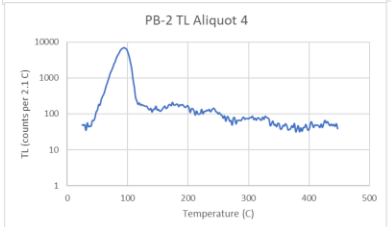
PB-2 TL Aliquot 4
TL (counts per 2.1 C)
Temperature (C)

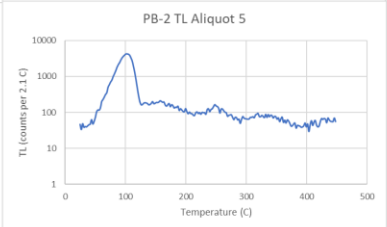
PB-2 TL Aliquot 5
TL (counts per 2.1 C)
Temperature (C)

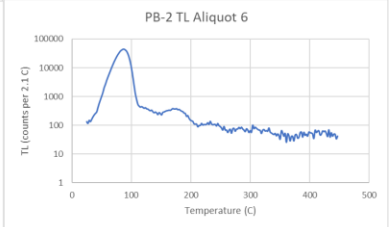
PB-2 TL Aliquot 6
TL (counts per 2.1 C)
Temperature (C)

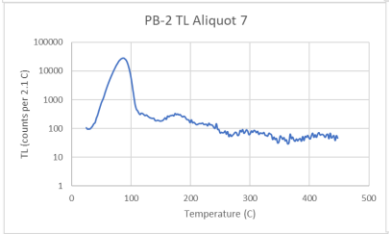
PB-2 TL Aliquot 7
TL (counts per 2.1 C)
Temperature (C)

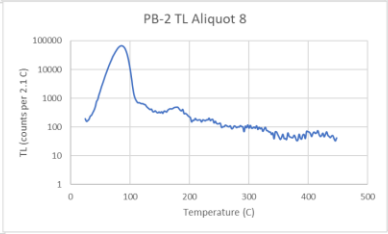
PB-2 TL Aliquot 8
TL (counts per 2.1 C)
Temperature (C)

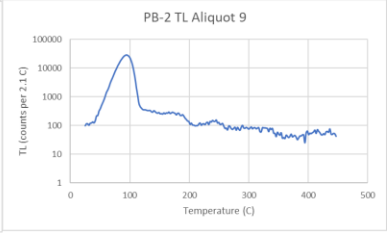
PB-2 TL Aliquot 9
TL (counts per 2.1 C)
Temperature (C)

Appendix C: LM-OSL

This appendix includes base code that was used with the Luminescence package in RStudio to create the LM-OSL component curves (Figure C.1). Table C.1 shows the number of components used to determine the best fit of the model. This appendix contains the output information that is provided by RStudio (Table C.2 (a-d)). All of the produced LM-OSL curves can also be found in this appendix (Figure C.2-C.8).

Figure C.1: image of standard code used to complete LM-OSL analysis.

```
1 fit_LMCurve(values = filename, n.components = 3, LED.power = 47, LED.wavelength = 458, log = 'x')
2
```

Table C.1: Number of components used to determine the best fit of luminescence model.

Sample	number of components	r^2
OE-1_1	5	0.8705
OE-1_2	5	0.7503
OE-1_3	4	0.9365
OE-1_4	4	0.9537
OE-2_1	4	0.9489
OE-2_2	5	0.9407
OE-2_3	5	0.8515
OE-2_4	5	0.9559
MBv-1_1	5	0.4079
MBv-1_2	6	0.6102
MBv-1_3	7	0.4707
MBv-1_4	6	0.2752
MBv-2_1	6	0.8003
MBv-2_2	5	0.4907
MBv-2_3	6	0.8266
MBv-2_4	6	0.4948
PB-1_1	5	0.5039
PB-1_2	5	0.9133
PB-1_3	4	0.6953
PB-1_4	5	0.7569
PB-2_1	6	0.5181
PB-2_2	5	0.8052
PB-2_3	6	0.6865
PB-2_4	5	0.2191

Table C.2 a) table sowing the component contribution from LM-OSL of the OE samples

Sample	OSL Components	Detrapping Probablilty	Photoionisiation Cross Section (cm2)	Relative Cross Section to Fast Component
OE-1_1	Fast	2.329	2.15E-17	1
	Slow1	0.2587	2.39E-18	0.1111
	Slow2	0.0249	2.30E-19	0.0107
	Slow3	0.0038	3.52E-20	0.0016
	Slow4	0.0003	3.10E-21	0.0001
OE-1_2	Fast	2.95	2.72E-17	1
	Slow1	0.3836	3.54E-18	0.13
	Slow2	0.0308	2.85E-19	0.0105
	Slow3	0.0044	4.09E-20	0.0015
	Slow4	0.0003	2.50E-21	0.0001
OE-1_3	Fast	2.703	2.50E-17	1
	Slow2	0.0307	2.83E-19	0.0114
	Slow3	0.0042	3.91E-20	0.0016
	Slow4	0.0005	4.71E-21	1.00E-04
OE-1_4	Fast	2.478	2.29E-17	1
	Slow2	0.0317	2.93E-19	0.0128
	Slow3	0.0053	4.89E-20	0.0021
	Slow4	0.0005	4.98E-21	1.00E-04
OE-2_1	Fast	2.702	2.49E-17	1
	Slow2	0.034	3.14E-19	0.0126
	Slow3	0.005	4.59E-20	0.0018
	Slow4	0.0003	3.29E-21	1.00E-04
OE-2_2	Fast	3.421	3.16E-17	1
	Medium	0.883	8.15E-18	0.2581
	Slow2	0.0332	3.07E-19	0.0097
	Slow3	0.005	4.59E-20	0.0015
	Slow4	0.0003	3.42E-21	0.0001
OE-2_3	Fast	2.735	2.52E-17	1
	Slow1	0.3171	2.93E-18	0.1159
	Slow2	0.0301	2.77E-19	0.011
	Slow3	0.0039	3.60E-20	0.0014
	Slow4	0.0001	1.79E-21	1.00E-04
OE-2_4	Fast	2.662	2.46E-17	1
	Slow2	0.0316	2.91E-19	0.0119
	Slow3	0.0055	5.04E-20	0.0021
	Slow4	0.0004	3.73E-21	2.00E-04

Table C.2: b) table sowing the component contribution from LM-OSL of the MBv samples

Sample	OSL Components	Detrapping Probablilty	Photoionisiation Cross Section (cm2)	Relative Cross Section to Fast Component
MBv-1_1	Fast	7.544	6.96E-17	1
	Medium	0.8794	8.12E-18	0.1166
	Slow2	0.0397	3.66E-19	0.0053
	Slow3	0.007	6.42E-20	9.00E-04
	Slow4	0.0003	3.44E-21	0
MBv-1_2	Ultrafast	17.48	1.61E-16	1
	Fast	1.506	1.39E-17	0.0862
	Slow1	0.1353	1.25E-18	0.0077
	Slow2	0.0222	2.06E-19	0.0013
	Slow3	0.0038	3.55E-20	2.00E-04
	Slow4	0.0002	2.77E-21	0
MBv1_3	Ultrafast	23.78	2.19E-16	1
	Fast	1.801	1.66E-17	0.0758
	Slow1	0.1762	1.63E-18	0.0074
	Slow2	0.0272	2.51E-19	0.0011
	Slow3	0.0054	5.02E-20	2.00E-04
	Slow4	0.0003	3.05E-21	0
MBv1_4	Ultrafast	34.68	3.20E-16	1
	Fast	2.471	2.28E-17	0.0712
	Slow1	0.2928	2.70E-18	0.0084
	Slow2	0.0342	3.16E-19	0.001
	Slow3	0.006	5.53E-20	2.00E-04
	Slow4	0.0003	3.06E-21	0
MBv-2_1	Ultrafsat	23.94	2.21E-16	1
	Fast	1.463	1.35E-17	0.0611
	Slow1	0.1846	1.70E-18	0.0077
	Slow2	0.0248	2.29E-19	0.001
	Slow3	0.0064	5.93E-20	3.00E-04
	Slow4	0.0003	3.40E-21	0
MBv-2_2	Ultrafast	9.944	9.18E-17	1
	Fast	1.063	9.81E-18	0.1069
	Slow2	0.0424	3.91E-19	0.0043
	Slow3	0.0084	7.74E-20	8.00E-04
	Slow4	0.0004	3.67E-21	0
MBv-2_3	Ultrafast	11.91	1.10E-16	1
	Fast	1.51	1.39E-17	0.1268
	Slow1	0.53	1.41E-18	0.0128
	Slow2	0.0222	2.05E-19	0.0019
	Slow3	0.0053	4.94E-20	4.00E-04
	Slow4	0.0004	3.31E-21	0
MBv-2_4	Ultrafast	38.49	3.55E-16	1
	Fast	1.987	1.83E-17	0.0516
	Slow1	0.2485	2.29E-18	0.0065
	Slow2	0.0242	2.24E-19	6.00E-04
	Slow3	0.0049	4.55E-20	1.00E-04
	Slow4	0.0003	2.84E-21	0

Table C.2: c) table sowing the component contribution from LM-OSL of the PB samples

Sample	OSL Components	Detrapping Probablilty	Photoionisiation Cross Section (cm2)	Relative Cross Section to Fast Component
PB-1_1	Ultrafast	18.49	1.71E-16	1
	Fast	1.437	1.33E-17	0.0778
	Slow1	0.231	2.14E-18	0.0125
	Slow2	0.0233	2.15E-19	0.0013
	Slow3	0.006	5.53E-20	3.00E-04
	Slow4	0.0003	3.16E-21	0
PB-1_2	Fast	2.728	2.52E-17	1
	Medium	0.8527	7.87E-18	0.3127
	Slow2	0.0283	2.62E-19	0.0104
	Slow3	0.0075	6.96E-20	0.0028
	Slow4	0.0004	3.98E-21	2.00E-04
PB-1_3	Fast	1.546	1.43E-17	1
	Slow2	0.0811	7.48E-19	0.0524
	Slow3	0.0099	9.13E-20	0.0064
	Slow4	0.0005	4.35E-21	3.00E-04
PB-1_4	Ultrafast	11.42	1.05E-16	1
	Fast	1.036	9.56E-18	0.0907
	Slow2	0.0513	4.74E-19	0.0045
	Slow3	0.0084	7.76E-20	7.00E-04
	Slow4	0.0004	3.97E-21	0
PB-2_1	Ultrafast	18.2	1.68E-16	1
	Fast	1.385	1.28E-17	0.0761
	Slow2	0.0498	4.60E-19	0.0027
	Slow3	0.0087	8.00E-20	5.00E-04
	Slow4	0.0005	4.59E-21	0
PB2_2	Ultrafast	9.971	9.20E-17	1
	Fast	1.342	1.24E-17	0.1346
	Slow2	0.0418	3.86E-19	0.0042
	Slow3	0.0089	8.21E-20	9.00E-04
	Slow4	0.0005	4.70E-21	1.00E-04
PB2_3	Ultrafast	12.16	1.12E-16	1
	Fast	1.631	1.51E-17	0.1341
	Slow1	0.1897	1.75E-18	0.0156
	Slow2	0.0231	2.14E-19	0.0019
	Slow3	0.0047	4.38E-20	4.00E-04
	Slow4	0.0004	3.69E-21	0
PB2_4	Ultrafast	14.74	1.36E-16	1
	Fast	1.16	1.07E-17	0.0787
	Slow2	0.0561	5.18E-19	0.0038
	Slow3	0.0078	7.20E-20	5.00E-04
	Slow4	0.0004	4.04E-21	0

Table C.2: d) table sowing the component contribution from aliquots in a terrace deposit

Sample	OSL Components	Detrapping Probability	Photoionization Cross Section (cm2)	Relative Cross Section to Fast Component
Terrace_1	Fast	3.534	3.26E-17	1
	Slow 3	0.0072	6.68E-20	0.002
	Slow4	0.0011	1.01E-20	3.00E-04
Terrace_2	Fast	4.232	3.91E-17	1
	Slow3	0.0057	5.30E-20	0.0014
	Slow4	0.001	8.79E-21	2.00E-04
Terrace_3	Fast	4.954	4.57E-17	1
	Slow2	0.0123	1.14E-19	0.0025
	Slow3	0.0015	1.35E-20	3.00E-04

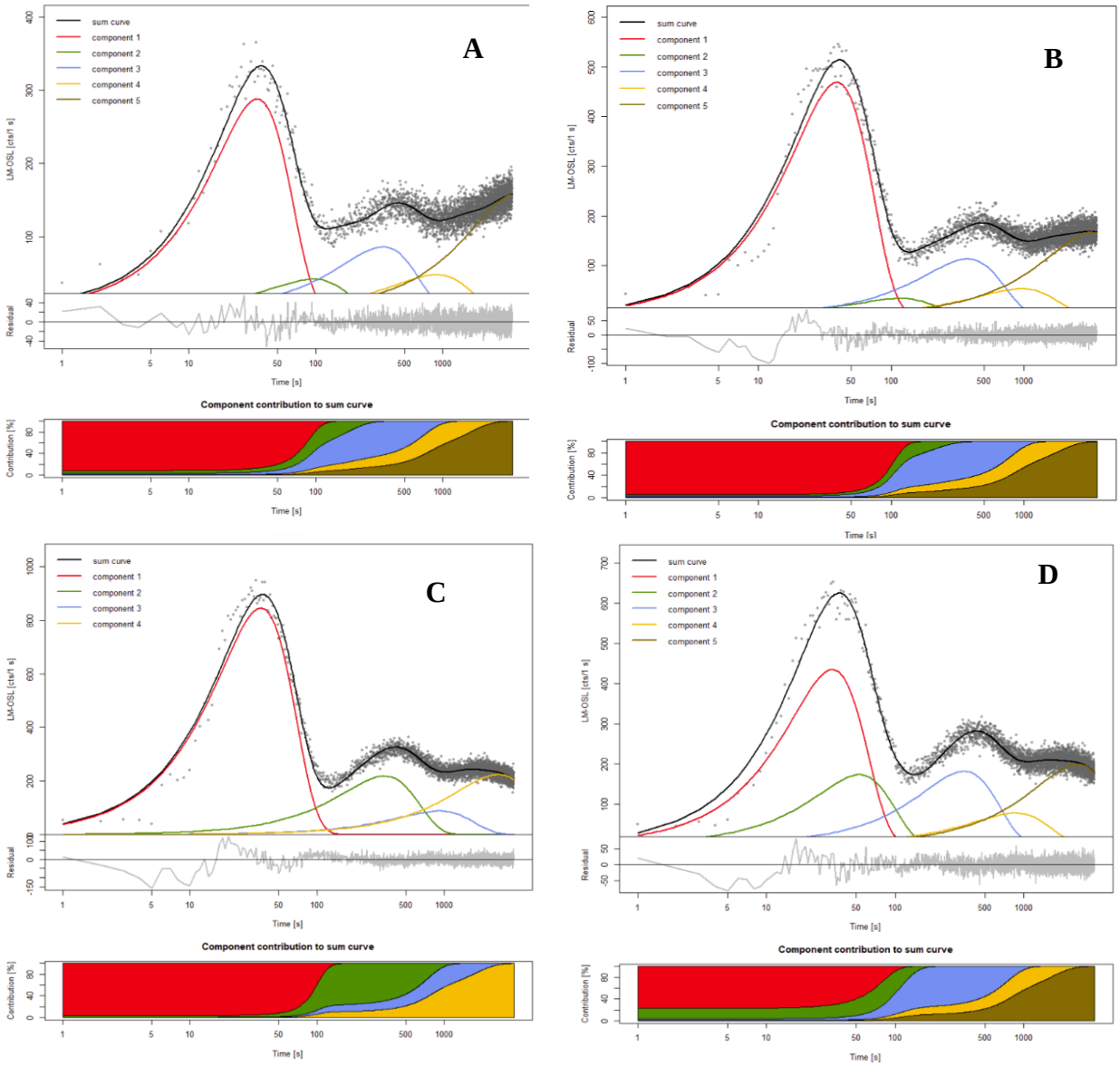

Figure C.2. LM-OSL Component curves for OE-1 A) aliquot 1, B)aliquot 2, C)aliquot 3, D) aliquot 4

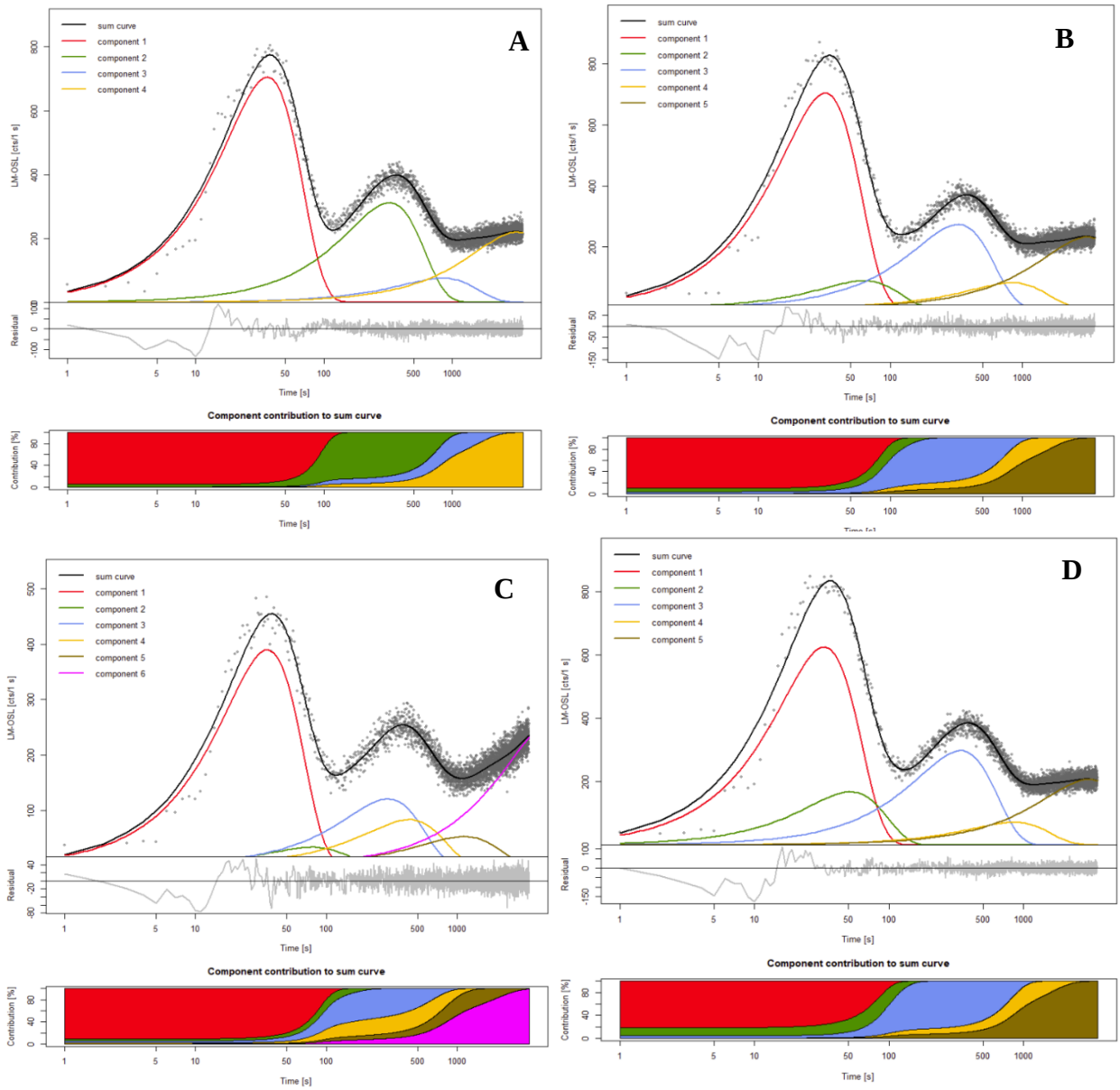

Figure C.3. LM-OSL Component curves for OE-2 A) aliquot 1, B) aliquot 2, C) aliquot 3, D) aliquot 4

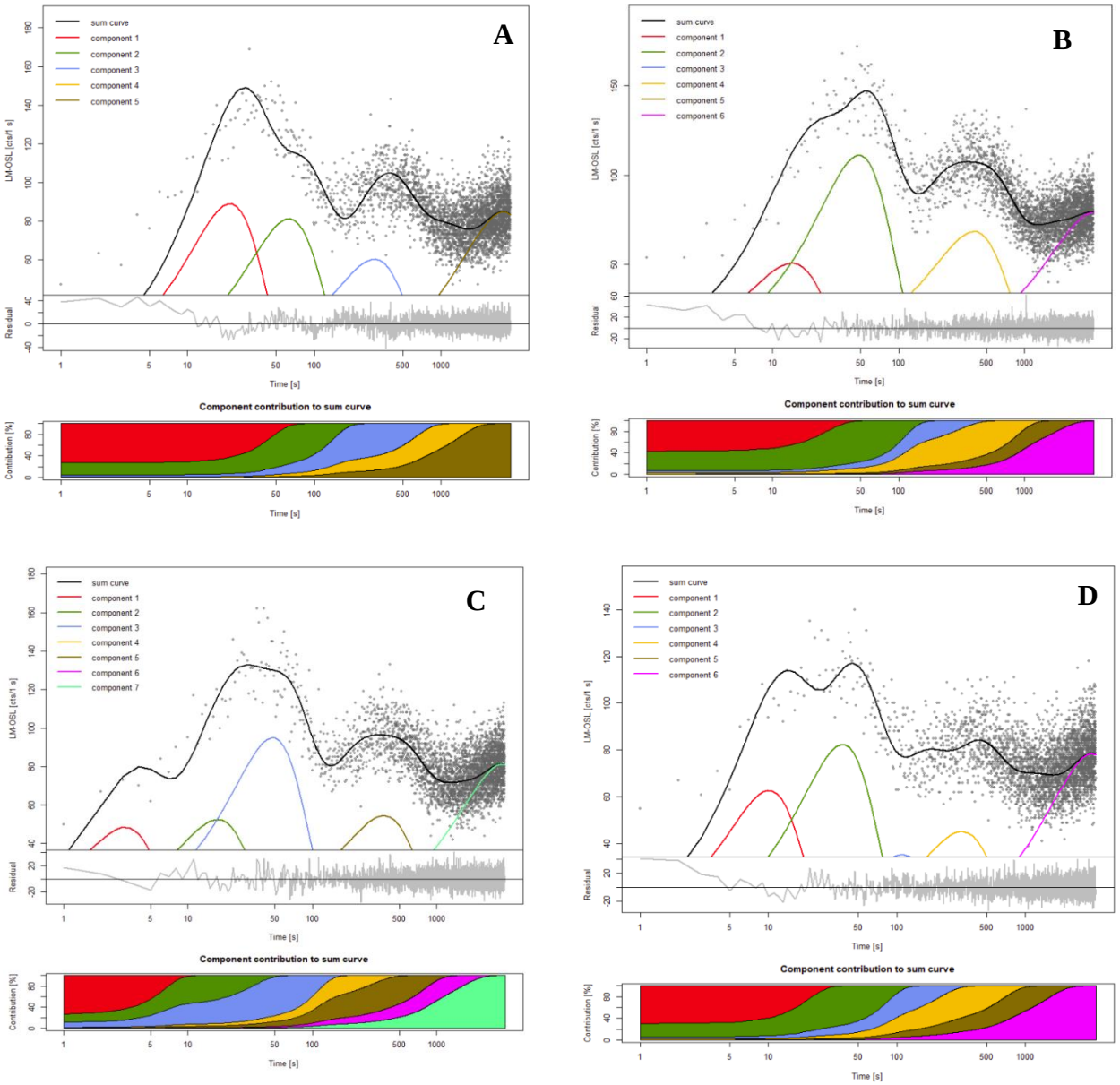

Figure C.4. LM-OSL Component curves for MBv-1 A) aliquot 1, B) aliquot 2, C) aliquot 3, D) aliquot 4

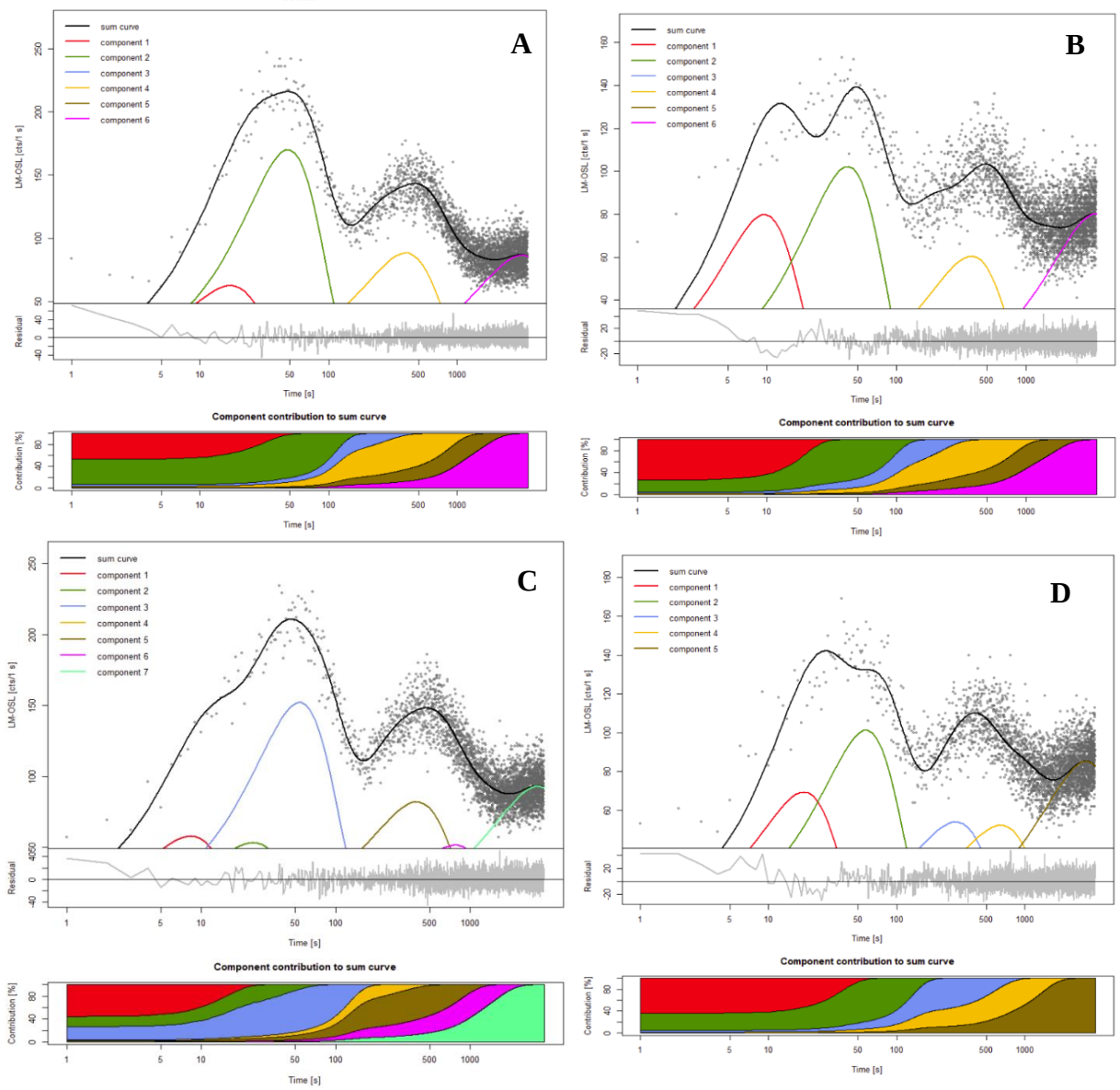

Figure C.5. LM-OSL Component curves for MBv-2 A) aliquot 1, B) aliquot 2, C) aliquot 3, D) aliquot 4

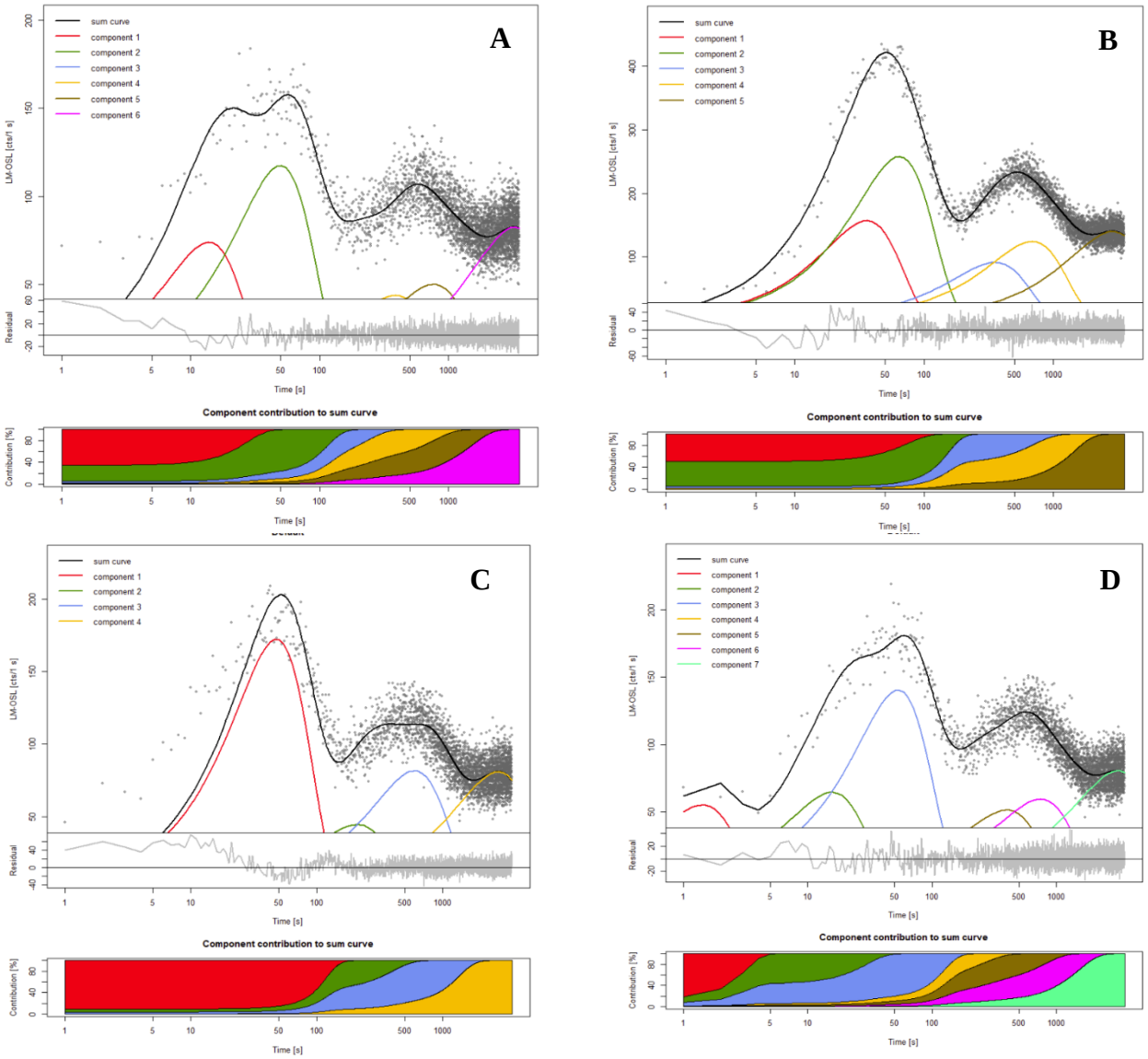

Figure C.6. LM-OSL Component curves for PB-1 A) aliquot 1, B) aliquot 2, C) aliquot 3, D) aliquot 4

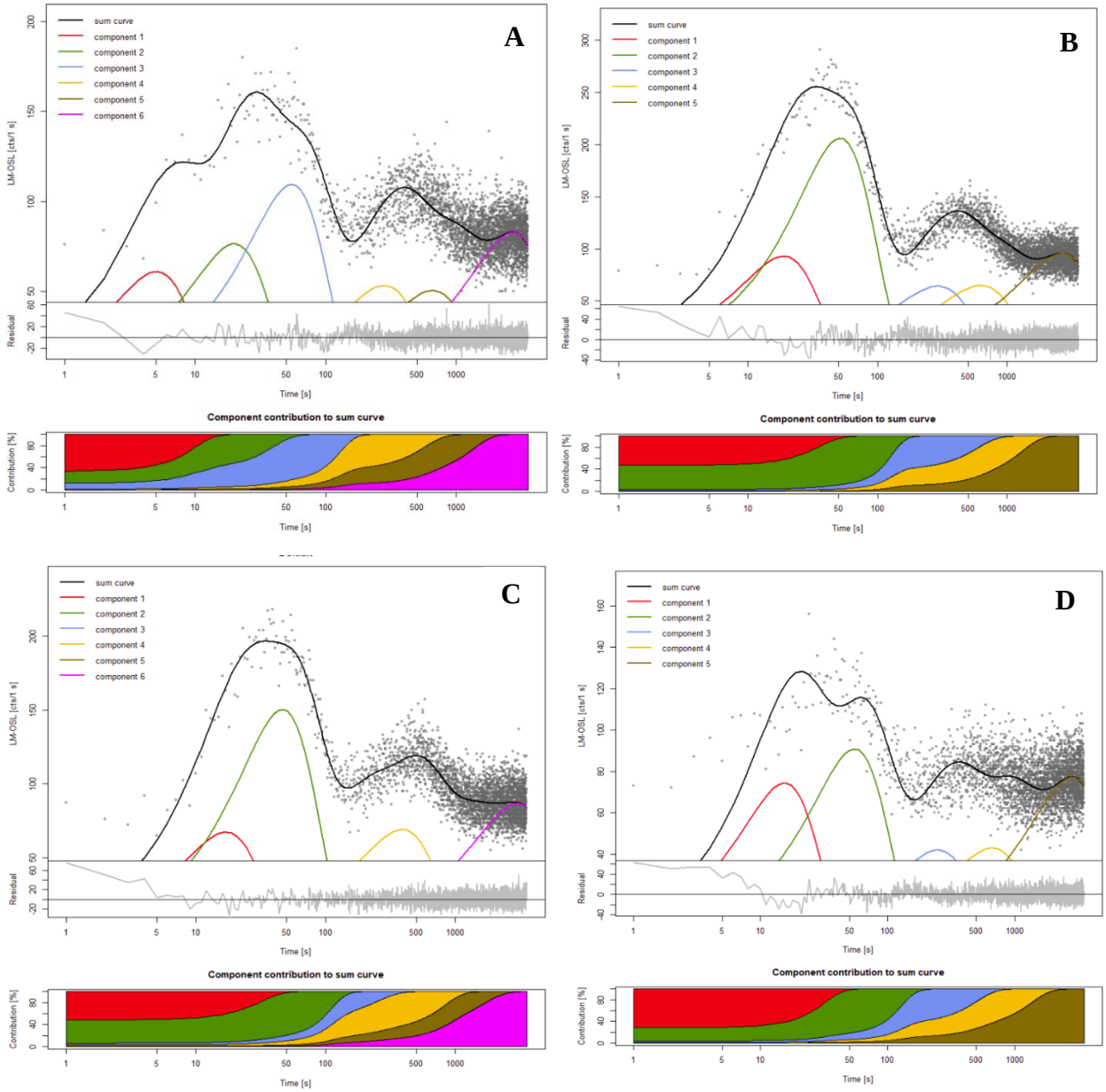

Figure C.7. LM-OSL Component curves for PB-2 A) aliquot 1, B) aliquot 2, C) aliquot 3, D) aliquot 4

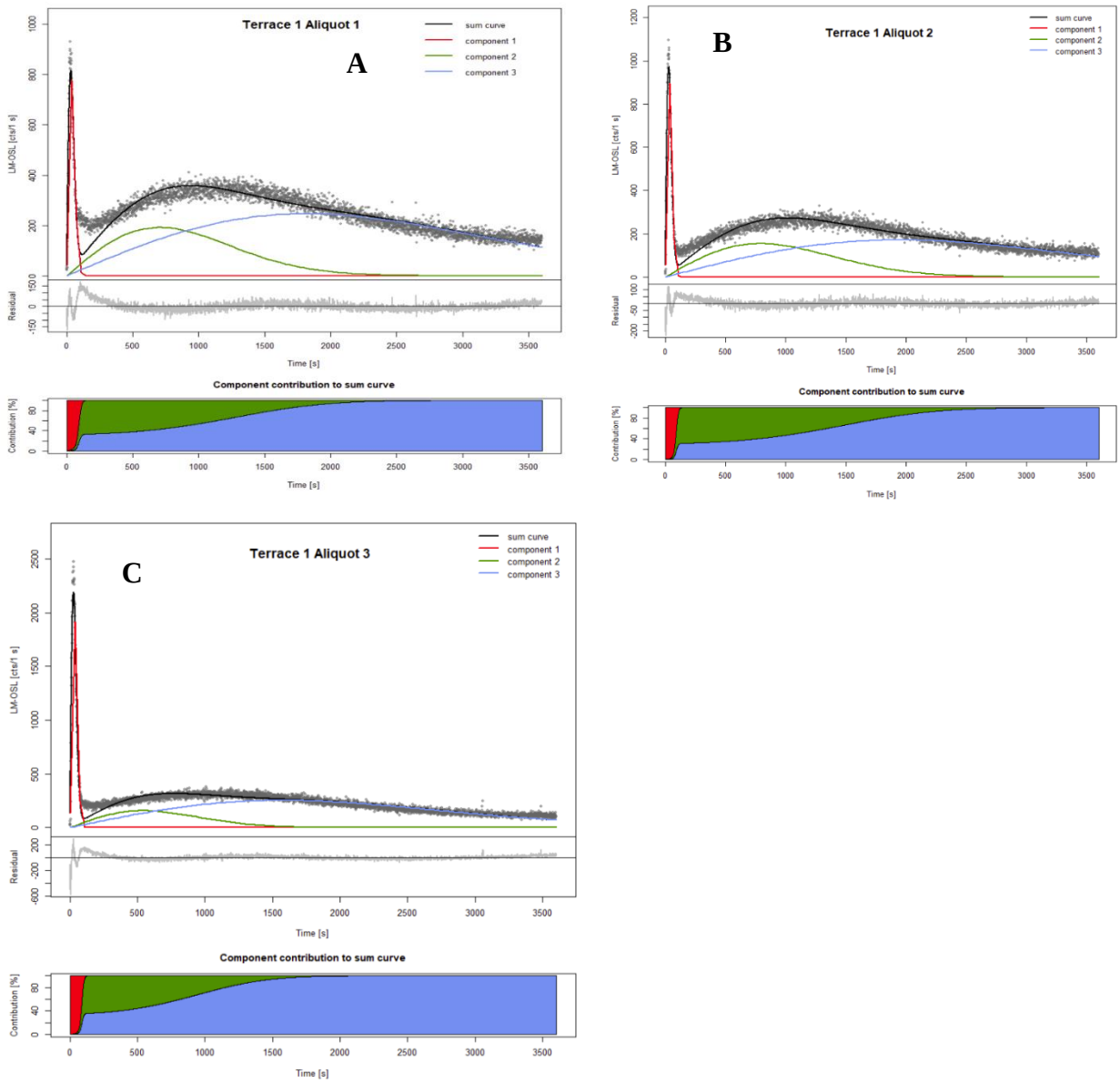

Figure C.8. LM-OSL Component curves for terrace deposit 1 A) aliquot 1, B) aliquot 2, C) aliquot 3